Comparison of three aerosol representations of NHM-Chem (v1.0) for the simulations of air quality and climate-relevant variables

Mizuo Kajino[1,2], Makoto Deushi[1], Tsuyoshi Thomas Sekiyama[1], Naga Oshima[1], Keiya Yumimoto[3,1], Taichu Yasumichi Tanaka[1], Joseph Ching[1], Akihiro Hashimoto[1], Tetsuya Yamamoto[1], Masaaki Ikegami[4], Akane Kamada[4,1], Makoto Miyashita[4], Yayoi Inomata[5,1], Shin-ichiro Shima[6], Pradeep Khatri[7], Atsushi Shimizu[8], Hitoshi Irie[9], Kouji Adachi[1], Yuji Zaizen[1], Yasuhito Igarashi[10,11], Hiromasa Ueda[12], Takashi Maki[1], and Masao Mikami[13,1]

[1]Meteorological Research Institute, Japan Meteorological Agency, Tsukuba, 305-0052, Japan
[2]Faculty of Life and Environmental Sciences, University of Tsukuba, Tsukuba, 305-8572, Japan
[3]Research Institute for Applied Mechanics, Kyushu University, Kasuga, 816-8580, Japan
[4]Japan Meteorological Agency, Chiyoda, 100-8122, Japan
[5]Institute of Nature and Environmental Technology, Kanazawa University, Kanazawa, 920-1192, Japan
[6]Graduate School of Simulation Studies, University of Hyogo, Kobe, 650-0047, Japan
[7]Center for Atmospheric and Oceanic Studies, Graduate School of Science, Tohoku University, Sendai, 980-8578, Japan
[8]National Institute for Environmental Studies, Tsukuba, 305-8506, Japan
[9]Center for Environmental Remote Sensing, Chiba University, Chiba, 263-8522, Japan
[10]Institute for Integrated Radiation and Nuclear Science, Kyoto University, Kumatori, 590-0494, Japan
[11]College of Science, Ibaraki University, Mito, 310-8512, Japan
[12]Disaster Prevention Research Institute, Kyoto University, Uji, 611-0011, Japan
[13]Japan Meteorological Business Support Center, Chiyoda, 101-0054, Japan

Correspondence to: Mizuo Kajino (kajino@mri-jma.go.jp)

Abstract. This study provides comparisons of aerosol representation methods incorporated into a regional-scale nonhydrostatic meteorology-chemistry model (NHM-Chem). Three options for aerosol representations are currently available: the 5-category nonequilibrium (Aitken, soot-free accumulation, soot-containing accumulation, dust, and sea salt), 3-category nonequilibrium (Aitken, accumulation, and coarse), and bulk equilibrium (submicron, dust, and sea salt) methods. The 3-category method is widely used in three-dimensional air quality models. The 5-category method, the standard method of NHM-Chem, is an extensional development of the 3-category method and provides improved predictions of ~~regional climate~~ variables relating to aerosol-cloud-radiation interaction processes by implementing separate treatments of light absorber and ice nuclei particles, namely, soot and dust, from the accumulation and coarse mode categories (implementation of aerosol feedback processes to NHM-Chem is still ongoing, though). The bulk equilibrium method was ~~also~~ developed for operational air quality forecasting with simple aerosol dynamics representations. The total CPU times of the 5-category and 3-category methods were 91% and 44% greater than that of the bulk method, respectively. The bulk equilibrium method was shown to be eligible for operational forecast purposes, namely, the surface mass concentrations of air pollutants such as O_3, mineral dust, and $PM_{2.5}$. The simulated surface concentrations and depositions of bulk chemical species of the 3-category method were not significantly different from those of the 5-category method. However, the internal mixture assumption of

soot/soot-free and dust/sea salt particles in the 3-category method resulted in significant differences in the size distribution and hygroscopicity of the particles. The unrealistic dust/sea salt complete mixture of the 3-category method induced significant errors in the prediction of the mineral dust-containing CCN, which alters heterogeneous ice nucleation in cold rain processes. The overestimation of soot hygroscopicity by the 3-category method induced errors in the BC-containing

5   CCN, BC deposition, and light-absorbing AOT (AAOT). Nevertheless, the difference in AAOT was less pronounced with the 3-category method because the overestimation of the absorption enhancement was compensated by the overestimation of hygroscopic growth and the consequent loss due to in-cloud scavenging. In terms of total properties, such as aerosol optical thickness (AOT) and cloud condensation nuclei (CCN), the results of the 3-category method were acceptable. ~~To evaluate the significance of separate soot and dust treatments in the 5-category method in terms of aerosol cloud radiation interaction~~

10   ~~processes, online simulation with a chemistry-to-meteorology feedback process is required.~~

1 Introduction

Atmospheric aerosols scatter and absorb solar (shortwave) and thermal (longwave) radiation and thus contribute to warming and cooling on regional to global scales. Aerosols also affect regional to global climate in various ways through aerosol-cloud-radiation interactions (Boucher et al., 2013; Oshima et al., 2020). Increases in aerosols can both decrease precipitation

15   from shallow clouds and increase precipitation from invigorated convective clouds as a result of their cloud condensation nuclei (CCN) activities. At the same time, an increase in aerosols enhances atmospheric stability and suppresses convective precipitation as a result of their radiative activities cooling the ground surface and heating the atmosphere (Rosenfeld et al., 2008). Aerosols together with the relevant gases can have negative impacts on ecosystems and health due to the production of photochemical oxidants, acid deposition, persistent organic pollutants (POPs), polycyclic aromatic hydrocarbons (PAHs),

20   radioactive nuclides, metals, and $PM_{2.5}$ (WHO, 2001; Cohen et al., 2004; Burns et al., 2011). The effect and effectiveness of aerosols on climate and pollution highly depends on their physical (size, shape, etc.) and chemical (hygroscopicity, refractive index, etc.) properties. The removal rates of aerosols, which ~~increase~~ alter atmospheric life time and earth surface contamination ~~and decrease air concentrations~~, depend highly on these properties. The nonlinear degradation effect (or positive feedback) of surface ~~and~~ air pollution (surface concentration of aerosols increases due to their enhanced atmospheric

25   stability) also depends on these properties (Kajino et al., 2017). Because these aerosol properties substantially vary in time and space and the properties change during transport, it is essential to accurately simulate aerosol physical and chemical processes for both climate and pollution modeling.

     In addition, the aerosol mixing state impacts the accuracy of the estimates of their bulk physical and chemical properties ~~of aerosols~~ (and thus their environmental impacts). Aerosols are more externally mixed near the emission source

30   regions: ~~aerosols~~ those from different emission sources exist discretely in the same air mass and in the same mode. Aerosols become more internally mixed over downwind regions: ~~aerosols~~ those from different sources coagulate, and/or gas absorption and adsorption change their chemical composition ~~of the aerosols~~. To express the high complexity of the aerosol

mixing state and the changes in the mixing state from external to internal states during transport, a variety of aerosol representation methods have been used in atmospheric models. In this context, a category approach (e.g., Jacobson, 2002) has been developed and used in both climate models (e.g., Vignati et al., 2004; Pringle et al., 2010; Aquila et al., 2011; Zhang et al., 2012; Liu et al., 2012, 2016) and chemical transport models (e.g., Riemer et al., 2003; Vogel et al., 2009;

5   Kajino and Kondo, 2011; Kajino et al., 2012a; Kajino et al., 2019a, this study). In terms of black carbon (BC), mixing state resolving models have been developed (Oshima et al., 2009a; Ching et al., 2016a; Matsui, 2017) to explicitly treat the hydrophobic to hygroscopic changes in BC-containing particles and increases in light absorption amplification and in-cloud scavenging efficiency through condensational growth during transport. The ultimate representation of the mixing state is a single particle resolving model for expressing a continuous mixing state (or an intermediate state of aerosol mixing) (Riemer

10   et al., 2009; Zaveri et al., 2010), which has been implemented in a 1-D framework (Curtis et al., 2017); 3-D implementation is currently ongoing.

Nevertheless, computational resources are limited, and there are many important processes to consider in addition to aerosol representations. Thus, it is essential to incorporate sufficiently efficient but realistic aerosol representations in coupled meteorology-chemistry models, with an awareness of the impacts of the aerosol mixing state on the bulk properties

15   of populations of aerosols, as assessed by a series of single particle-based studies (e.g., Riemer et al., 2009; Zaveri et al., 2010; Ching et al., 2012; 2016b; 2017; 2018).

From the context mentioned above, in the current study, three options for aerosol representations, namely, 5-category nonequilibrium, 3-category nonequilibrium and bulk equilibrium representations, are already implemented in a three-dimensional regional-scale meteorology-chemistry model (Kajino et al., 2019a) and are intercompared for the

20   predictions of air quality and climate-relevant variables in this study. In this study, surface concentrations and depositions are referred to as air quality variables, whereas variables involved in aerosol feedback processes such as optical properties and cloud and ice nucleation properties are referred to as climate-relevant variables. The three aerosol representations are developed for the three respective research purposes of regional climate, aerosol-cloud-radiation interaction processes (or aerosol feedback processes), air quality issues (surface air concentrations of hazardous materials including their depositions),

25   and operational forecasting (real-time forecast of hazardous materials concentrations with high computational efficiency). The 3-category method (Aitken mode, accumulation mode, and coarse mode) is a global standard method that has been widely used in various regional-scale chemical transport models (e.g., Grell et al., 2005; Byun and Schere, 2006). The 5-category method includes two additional modes: dividing the accumulation mode into soot-free and soot-containing particles to consider differences between light-absorbing and nonlight-absorbing aerosols and dividing the coarse mode into dust

30   (light-absorbing and hydrophobic) and sea salt (nonlight-absorbing and hygroscopic) particles. The bulk equilibrium method assumes instantaneous gas-aerosol partitioning and does not consider changes in the size distribution due to new particle formation, condensation, and coagulation for computational efficiency. The descriptions of the meteorological and chemical models and their coupling procedures are briefly given in Sect. 2, with the details given in Supplement 1. The descriptions of the three aerosol representation options, the highlight of this study, are given in Sect. 3, followed by the descriptions of the

simulation settings in Sect. 4 and Supplement 2 (for the volcanic emissions). ~~The model evaluations using t~~The chemical, physical, and optical observation data are presented and the model validations using the observation data are performed in Sect. 5 and Supplement 3. The differences in the model performances due to the selection of the three aerosol representation options are presented and discussed in Sect. 6 and Supplements 3-5. Conclusions are summarized in Sect. 7.

2 NHM-Chem: a regional-scale meteorology-chemistry model

NHM-Chem (v1.0) (Kajino et al., 2019a) is a chemical transport model (CTM) coupled with the Japan Meteorological Agency (JMA)'s nonhydrostatic model (NHM), either offline or online. The chemistry-to-meteorology feedback process has not yet been included and will be implemented in the near future. The online version of NHM-Chem is currently a so-called 1-way (meteorology to chemistry) online coupled model. In this study, as the first step, the simulation results obtained with the offline coupled version were presented in this paper.

NHM solves for fully compressible Navier-Stokes dynamics equations, considering major physical processes, such as atmospheric radiation, cloud microphysical processes, and planetary boundary layer, surface layer, and land surface processes (Saito et al., 2006; 2007). NHM has been developed and used for the operational weather forecasting of JMA as well as for research purposes. The research and development history of this approach and its use in ongoing projects were thoroughly reviewed by Saito (2012). Currently, the next-generation nonhydrostatic model ASUCA (Asuca is a System based on a Unified Concept for Atmosphere; JMA, 2014; Aranami et al., 2015) is operational, and the NHM is used for research purposes only.

The ~~schemes~~ configurations of the CTM and database available for NHM-Chem are summarized in Table S1. NHM-Chem was briefly described in Kajino et al. (2019a). It is described in detail in Supplement 1 that NHM-Chem considers major tropospheric chemical, dynamical, and microphysical processes, such as advection (Walcek and Aleksic, 1998), turbulent diffusion, homogeneous and heterogeneous photochemistry (Carter, 2000; Jacob 2000; Edney et al., 2007), liquid-phase chemistry (Walcek and Taylor, 1986; Carlton et al., 2007), new particle formation, condensation, coagulation, and dry deposition (Kajino et al., 2012a), fog deposition (Katata et al., 2015), in-cloud scavenging of aerosols (CCN and ice nuclei (IN) activation and subsequent cloud microphysical processes), below-cloud scavenging of aerosols (collection by settling hydrometeors), and wet deposition of gases (dissolution to cloud and rain droplets) (Kajino et al., 2012a; Kajino et al., 2019a), and subgrid-scale convective transport and deposition (Pleim and Chang, 1992).

The coupling between meteorology and chemistry is illustrated in Fig. S1-1. The offline coupled version has been used for various purposes, such as the simulation of dust vortices in the Taklimakan Desert (Yumimoto et al., 2019), the simulation of the dispersion and deposition of radionuclides due to the Fukushima nuclear accident (Kajino et al., 2019b; Sekiyama and Kajino, 2020; Kajino et al., 2021), simulation of lower-tropospheric ozone in East Asia (Kajino et al., 2019c), and the simulation of transition metals in East Asia (Kajino et al., 2020). Other meteorological models, such as the Weather Research and Forecast model (WRF; Skamarock et al., 2008), ASUCA (JMA, 2014; Aranami et al., 2015), and Scalable

Computing for Advanced Library and Environment (SCALE; Nishizawa et al., 2015, Sato et al., 2015), can be used for offline coupled simulations (Fig. S1-1). The offline NHM-Chem with WRF was used for a multi-CTM intercomparison study in Asia (e.g., Li et al., 2019; ~~Chen et al., 2019;~~ Itahashi et al., 2020~~, Kong et al., 2020; Tan et al., 2020; Ge et al., 2020~~) and a multimeteorological model study of the Fukushima nuclear accident (Kajino et al., 2019b). The offline model with

5   SCALE was used for a multi-CTM intercomparison study for the Fukushima nuclear accident (Sato et al., 2020) and that with ASUCA is currently being used by JMA to ~~produce~~ conduct an operational forecast for photochemical smog bulletins (http://www.jma.go.jp/jma/kishou/know/kurashi/smog.html; last access: 18 June 2020, in Japanese).

3 Aerosol representations

10 There are currently three options for the representations of aerosol categories (or types), namely, the 5-category nonequilibrium method, the 3-category nonequilibrium method, and the bulk equilibrium method (Fig. 1), to simulate general air quality issues (related to factors such as photochemical oxidants, $PM_{2.5}$, mineral dust, and acid deposition). Further simplified modules were developed to predict the transport of radionuclides (Kajino et al., 2019b) and transition metals (Kajino et al., 2020), which do not simulate the photochemistry and some aerosol dynamics processes, such as new

15 particle formation, condensation, and coagulation, and thus are not assessed in this study. The prognostic variables of the aerosol attributes of these three methods are listed in Table 1. Each elementary process is depicted by a colored arrow in Fig. 1. Here, the term "bulk equilibrium" indicates that the gas-aerosol partitioning of inorganic semivolatile components, such as NH_3-NH_4^+ HNO_3-NO_3^-, and HCl-Cl^-, is instantaneously attained at the equilibrium state. On the other hand, in the nonequilibrium methods, mass transfer coefficients are calculated for each category based on its size distribution, and

20 condensation and evaporation are driven by the mass transfer coefficients multiplied by the differences between the equilibrium state and the current state of each category (see Eqs. 13-16 of Kajino et al., 2012a).
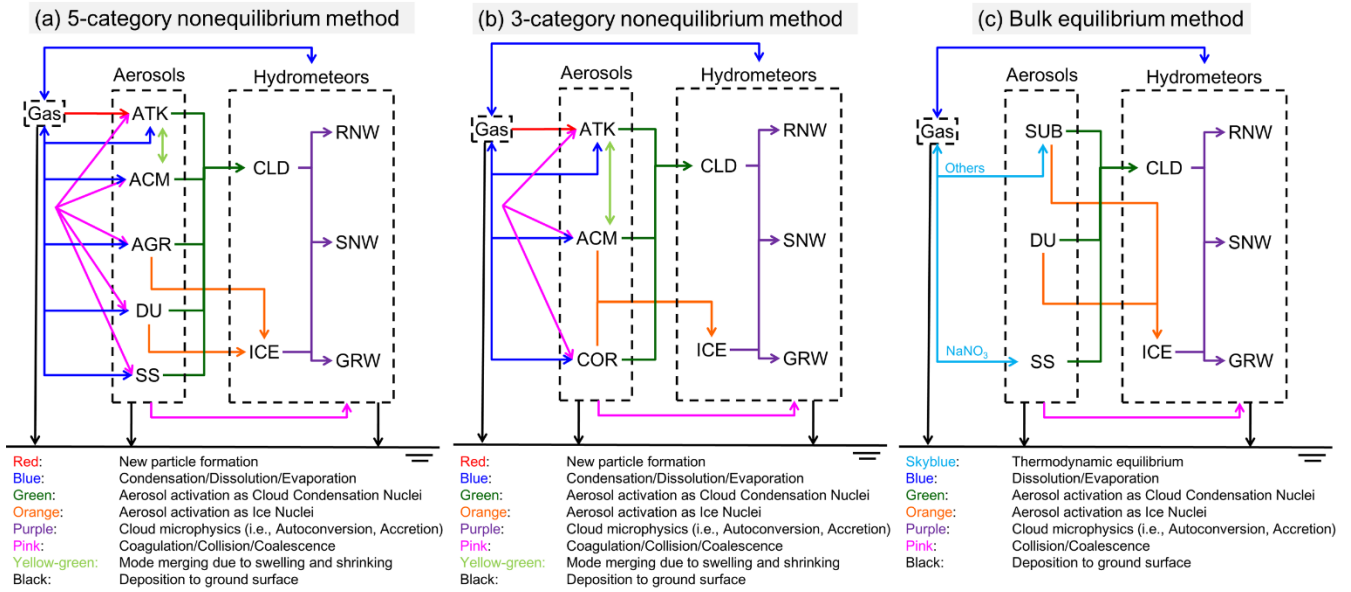
Figure 1: Schematic illustrations of gas-aerosol-cloud dynamic processes considered in (a) 5-category, (b) 3-category (global standard), and (c) bulk equilibrium methods. ATK (Aitken mode), ACM (soot-free accumulation mode, 5-category; accumulation mode, 3-category), AGR (accumulation mode, mixed with soot aggregate) DU (mixture with dust; both mineral and anthropogenic dust), SS (mixture with sea salt), COR (coarse mode), SUB (submicron), CLD (cloud), ICE (cloud ice), RNW (rain), SNW (snow), GRW (graupel). This figure is same as Fig. 1 of Kajino et al. (2019a).

Table 1: Prognostic variables of aerosol-related attributes

Aerosol options (number of tracers)	Category name	Description of category	Physical properties				Chemical compositions							
			M_0	M_2	UID	BC	OM	MD	NS	SO_4^{2-}	NO_3^-	NH_4^+	Cl^-	H_2O
5-category (50)	ATK	Aitken mode	M_0[a]	M_2[b]			OM[c]			SO_4^{2-}[d]	NO_3^-	NH_4^+	Cl^-	H_2O
	ACM	Accumulation mode, soot-free	M_0	M_2	UID[e]		OM			SO_4^{2-}	NO_3^-	NH_4^+	Cl^-	H_2O
	AGR	Accumulation mode, mixed with soot aggregate	M_0	M_2	UID	BC	OM			SO_4^{2-}	NO_3^-	NH_4^+	Cl^-	H_2O
	DU	dust	M_0	M_2	UID	BC	OM	MD[f]		SO_4^{2-}	NO_3^-	NH_4^+	Cl^-	H_2O
	SS	sea salt	M_0	M_2	UID	BC	OM	MD	NS[g]	SO_4^{2-}	NO_3^-	NH_4^+	Cl^-	H_2O
3-category (38)	ATK	Aitken mode	M_0	M_2			OM			SO_4^{2-}	NO_3^-	NH_4^+	Cl^-	H_2O
	ACM	Accumulation mode	M_0	M_2	UID	BC	OM			SO_4^{2-}	NO_3^-	NH_4^+	Cl^-	H_2O
	COR	Coarse mode	M_0	M_2	UID	BC	OM	MD	NS	SO_4^{2-}	NO_3^-	NH_4^+	Cl^-	H_2O
Bulk (20)	SUB	Bulk submicron	M_0	M_2	UID	BC	OM			SO_4^{2-}	NO_3^-	NH_4^+	Cl^-	H_2O
	DU[h]	Dust	M_0	M_2	UID			MD						
	SS[i]	Sea salt	M_0	M_2					NS		NO_3^-		Cl^-	H_2O

[a]0th moment, equal to number concentration
[b]2nd moment, proportional to surface area concentration
[c]Total (primary plus secondary) organic mass, speciation of secondary organics is treated as bulk (gas+aerosol) species. This treatment is feasible under the assumption that the molecular speeds and diffusivities of all organics are the same.
[d]Non-sea salt SO_4^{2-} only.
[e]Unidentified components, such as anthropogenic dust.
[f]mineral dust mass (natural).
[g]Nonvolatile components of pure sea salt mass (chloride is treated separately as it is volatile).
[h]Assumed to be chemically inert
[i]Only reacted with HNO_3 gas assuming instantaneous thermodynamic equilibrium

The 3-category method (ATK: Aitken mode, ACM: accumulation mode, COR: coarse mode) is a global standard method widely used in regional-scale CTMs, such as WRF-Chem and CMAQ (WRF-Chem and CMAQ provide other aerosol schemes, such as sectional methods, in addition to the standard 3 modal method, e.g., Chapman et al., 2009; Zhang et al., 2004; 2010). These models were originally developed for the purpose of air quality prediction, focusing on factors such as acid deposition, photochemical oxidants, and $PM_{2.5}$ (Byun and Schere, 2006; Grell et al., 2005); however, they have recently been used to ~~perform regional climate~~ predic~~tions considering~~ the aerosol feedback ~~cloud radiation interaction~~ processes (Chapman et al., 2009; Wong et al., 2012; Kajino et al., 2017). However, the 3-category method does not consider the two aspects that are critically important in climate simulations and are thus often resolved by climate models (e.g.,

Vignati et al., 2004; Pringle et al., 2010; Aquila et al., 2011; Zhang et al., 2012; Liu et al., 2012, 2016): (1) the differences between light-absorbing and nonlight-absorbing aerosols and (2) the differences between mineral dust and sea salt particles. To consider these two aspects, the 5-category method is implemented by dividing the accumulation mode (ACM of the 3-category method) into the ACM (soot-free accumulation mode) and AGR (accumulation mode mixed with soot aggregate) categories and by dividing the coarse mode (COR of the 3-category method) into the DU (mixture with dust; i.e., both mineral dust and anthropogenic dust) and SS (mixture with sea salt) categories.

BC is a strong light-absorbing agent and thus alters the climate by heating the air (Bond et al., 2013 and references therein). BC is usually hydrophobic when emitted and externally mixed with other aerosols to become more hygroscopic, forming an internal mixture with other components, including water-soluble inorganics, such as sulfate (SO_4^{2-}), nitrate (NO_3^-), and ammonium (NH_4^+), due to condensation and coagulation during transport (Oshima and Koike, 2013). The in-cloud scavenging of BC, which is the major removal process of BC (Kondo et al., 2011; Oshima et al., 2012), highly depends on the mixing state of BC (Ching et al., 2012; 2016b; 2018). Certainly, the 5-category method cannot resolve the mixing state of BC; however, it can simulate the bulk amounts condensed onto BC vs. non-BC particles, whereas the 3-category method cannot. Thus, the 3-category method will overestimate the condensational growth of BC and therefore overestimate its hygroscopicity, in-cloud scavenging, and subsequent heterogeneous ice nucleation (i.e., immersion ~~and condensation~~ freezing). All of the SO_4^{2-} and NO_3^- condense onto BC in the 3-category method, although major proportions of SO_4^{2-} and NO_3^- are mixed with non-BC particles in reality (Miyakawa et al., 2014). The degree of overestimation caused by the 3-category method relative to the 5-category method is presented later in Sect. 6.4.

The 3-category method assumes a completely internal mixture of dust and sea salt when the two particles coexist in the same grid box, although the chemical and physical properties of these two particles are very different. In Japan, massive transport events of mineral dust originating from Chinese arid regions, such as the Gobi and Taklimakan Deserts, often occur in the spring associated with the cold front of migrating anticyclones. Zhang and Iwasaka (2004) found that 10-20% of number fractions of coarse mode particles were mixtures of mineral dust and sea salt, with similar mass fractions, during dust events in the spring of 1996. They also found only 5-15% of pure dust particles and as much as 60-80% of mixtures of mineral dust and sea salt, including dust mixed with a small amount of sea salt and sea salt mixed with a small amount of dust. Mineral dust is hydrophobic and nonspherical when emitted and thus shows high IN activity, is light-absorbing, becomes hygroscopic during transport, and invigorates heterogeneous reactions (Kameda et al., 2016). On the other hand, sea salt is highly hygroscopic and is thus an efficient CCN. The size distributions of mineral dust and sea salt are also very different, so in this 3-category method, when the two particles coexist in the same grid box, their combined size distributions and hygroscopicity become unrealistic (i.e., the intermediate values are different from those of both particle types, as shown later in Sect. 6). This 3-category representation would be adequate for predicting air pollution over a continent, such as Europe or America. It would also be safe for global climate simulations because on average, the major global proportions of dust and sea salt exist separately in different locations, namely, over the continents and oceans, respectively. However, for cases of long-range transport over the Asian continent to Japan, mineral dust and anthropogenic pollutants travel in the sea

salt-rich boundary layer over the ocean. As discussed in Sect. 6, the 3-category method is thus not suitable for air quality and ~~regional climate~~aerosol feedback predictions in East Asia. Consequently, the 5-category method is regarded as the standard method of NHM-Chem.

The 5-category and 3-category methods ~~fully~~ solve for aerosol microphysical processes by using the triple-moment

5 modal method presented in the previous section (see red, blue, and pink arrows in Figs. 1a and 1b). Even though a modal approach, which is basically computationally efficient compared to a sectional approach, is used, it is still time-consuming because NHM-Chem explicitly models the homogeneous nucleation of sulfuric acid gas to produce 1 nm particles and their subsequent growth due to condensation and coagulation. In terms of the operational forecasts of air quality, such as photochemical oxidants, mineral dust, and $PM_{2.5}$, the surface mass concentration is of primary importance, and the detailed

10 physical and chemical properties of aerosols are of secondary importance. ~~Assessing the uncertainty in the initial and boundary conditions is critical for obtaining accurate predictions of mass concentrations; thus, data assimilation is required.~~ The operation forecast requires computational efficiency and data assimilation is applied to enhance the predication accuracy rather than solving for detailed physical and chemical processes. For the purpose of obtaining an operational forecast~~, together with data assimilation~~, the computationally efficient bulk equilibrium method is developed, which does not solve

15 aerosol microphysical processes, such as new particle formation, condensation, and coagulation (compare the sky blue arrows in Fig. 1c with the red, blue, and pink arrows in Figs. 1a and 1b). It should be noted here that the data assimilation was not applied to the simulations, because the current study focused on variations in the model performances due to the different aerosol representations. The same initial and boundary conditions were used for the all simulations. In the bulk equilibrium method, ~~Aerosols~~ aerosols are categorized into three categories, namely, SUB (submicron), DU (dust), and SS

20 (sea salt). The total dry mass of SUB can be used for the prediction of $PM_{2.5}$ and the mineral dust mass (denoted as MD) in the DU category can be used for the prediction of dust transport. As mentioned earlier in this subsection, thermodynamic equilibrium is assumed for the inorganic components, and all of the aerosol-phase components are assumed to be categorized into the SUB category, except for $NaNO_3$, which is mixed with sea salt in the SS category. Most of the SO_4^{2-} and NH_4^+ exist at the submicron size range, whereas NO_3^- in Japan is usually partitioned into both submicron and supermicron (or coarse

25 mode) size ranges because the latter is internally mixed with sea salt or mineral dust particles (Kajino et al., 2012b; Kaneyasu et al., 2012; Kajino et al., 2013; Uno et al., 2016; Uno et al., 2017). Without considering the coarse mode NO_3^-, the simulated $PM_{2.5}$ in East Asia will be significantly overestimated due to the overestimated production of NH_4NO_3. Certainly, some of the coarse mode NO_3^- should be mixed with dust, but the DU category is assumed to be inert in the bulk equilibrium method for the purposes of computational efficiency.

30 As listed in Table 1, the numbers of aerosol attributes for the 5-category, 3-category, and bulk equilibrium methods are 50, 38, and 20, respectively. In the triple-moment method, the 0th moment (number) and 2nd moment (proportional to the surface area) are the prognostic (transported) variables, and the 3rd moment (proportional to the volume) is diagnosed based on the mass concentrations of each component and their prescribed densities (i.e., 2.0, 1.77, 2.6, 2.2, 1.83, and 1.0 g cm^{-3} for UID (unidentified mass, or anthropogenic dust), carbonaceous mass (BC and OM), mineral dust (MD), sea salt

(nonvolatile components of sea salt (NS) and Cl$^-$), inorganics (SO$_4^{2-}$, NO$_3^-$, and NH$_4^+$), and water (H$_2$O), respectively). Here, note that the NS indicates the nonvolatile mass of pure sea salt particles, namely, the dry sea salt mass minus the Cl$^-$ mass.

Table 2: Rules for the transfer of moments and chemical mass concentrations from one category to another due to intercategory coagulation and mode merging

Aerosol options	Rule
5-category	*Intercategory coagulation* ATK + ACM → ACM ATK + AGR → AGR ATK + DU → DU ATK + SS → SS ACM + AGR → AGR ACM + DU → DU ACM + SS → SS AGR + DU → DU AGR + SS → SS DU + SS → SS *Mode merging[a]* ATK → ACM
3-category	*Intercategory coagulation* ATK + ACM → ACM ATK + COR → COR ACM + COR → COR *Mode merging[a]* ATK → ACM
Bulk	n.a.

[a]Transfer of moments and mass greater than 40 nm due to condensation or self-coagulation growth

The rules for the transfer of moments and mass from one category to another due to intercategory coagulation and mode merging are listed in Table 2. The intercategory coagulation rules of "from smaller to larger category" are used for the 3-category and 5-category methods; additionally, the coagulation rules of "from hydrophobic to hygroscopic category" and "from nonlight-absorbing to light-absorbing category" are used for the 5-category method. The mode merging represents the transfer of moments and mass greater than the threshold diameter of 40 nm due to condensation or self-coagulation growth. During its emission, the UID only exists in ACM and DU in the 5-category method, in ACM and COR in the 3-category method, and in SUB and DU in the bulk method. Due to intercategory coagulation, the UID is also found in AGR and SS in the 5-category method. Freshly emitted BC only exists in AGR, ACM, and SUB in the 5-category, 3-category, and bulk methods, respectively. The intercategory coagulation transfers BC to the DU and SS categories in the 5-category method and to COR in the 3-category method. OM exists in ATK, ACM, and AGR in the 5-category method, in ATK and ACM in the 3-category method, and in the SUB category in the bulk method during its emission. OM is moved to the DU and SS

categories in the 5-category method and to the COR category in the 3-category method. The MD mass only exists in the DU category for the 5-category and bulk methods, and it exists in the COR for the 3-category method. Transfer of the MD mass to the SS category is predicted only with the 5-category method. All of the secondary and semivolatile components, such as OM, SO_4^{2-}, NO_3^-, NH_4^+, and Cl^-, can exist in all of the categories in the 5-category and 3-category methods. They can exist only in SUB in the bulk method, except for NO_3^- and Cl^-, which can mix with sea salt, as mentioned earlier (Cl^- also exists in the SS category during emission). All of the aerosol categories can be hygroscopic and thus contain H_2O, except for the DU category of the bulk method. As mentioned earlier, crustal cations play an essential role in fixing acidic gases to the aerosol phase. In all three methods, the compositions of the sea salt and dust particles are defined after Song and Carmichael (2001) as follows: the MD mass contains 6.8, 1.6, 0.91, and 0.78 wt% Ca^{2+}, Na^+, K^+, and Mg^{2+}, respectively, and the NS mass contains 68.1, 17.1, 8.21, 2.58, and 2.45 wt% Na^+, SO_4^{2-}, Mg^{2+}, Ca^{2+}, and K^+, respectively. It is assumed that the UID mass does not contain any cations and is thus hydrophobic and inert.

In terms of aerosol water uptake, nonequilibrium treatment is critically important, especially for higher relative humidity conditions and coarse mode particles, because the instantaneous equilibrium assumption can cause unrealistic overestimates of aerosol diameter. For example, the equilibrium diameter of an aerosol with a dry diameter of 1.0 μm and a hygroscopicity κ value of 1.0 reaches 21.2 μm at a relative humidity RH = 100% (see κ-Köhler theory; Petters and Kreidenweis, 2007), which is equal to or greater than the initial sizes of cloud droplets. Under actual atmospheric conditions, aerosols cannot reach such a large equilibrium diameter, either because it takes too long time to reach (for low aerosol populations) or because aerosols remove too much water vapor from the air, such that the relative humidity becomes substantially lower (for high enough aerosol populations). Therefore, in the 3-category and 5-category nonequilibrium methods, aerosol water uptake is also calculated in a nonequilibrium manner: the mass transfer of water vapor is driven by the differences between the current water content and equilibrium water content, which is derived using the ZSR method (Fountoukis and Nenes, 2007). Note that the RH of air is assumed to remain unchanged due to water uptake by aerosols. In the bulk equilibrium method, instantaneous equilibrium is assumed for the aerosol water content, but a maximum threshold of an ambient RH of 98% is used to avoid the abovementioned unrealistically large aerosol size.

1. Rishiri, 2. Sado, 3. Oki, 4. Ogasawara, 5. Hedo (CHAAMS), 6. Happo, 7. Yusuhara, 8. Chiba, 9. Tsukuba, 10. Matsue, 11. Kasuga, 12. Fukue, 13. Miyako
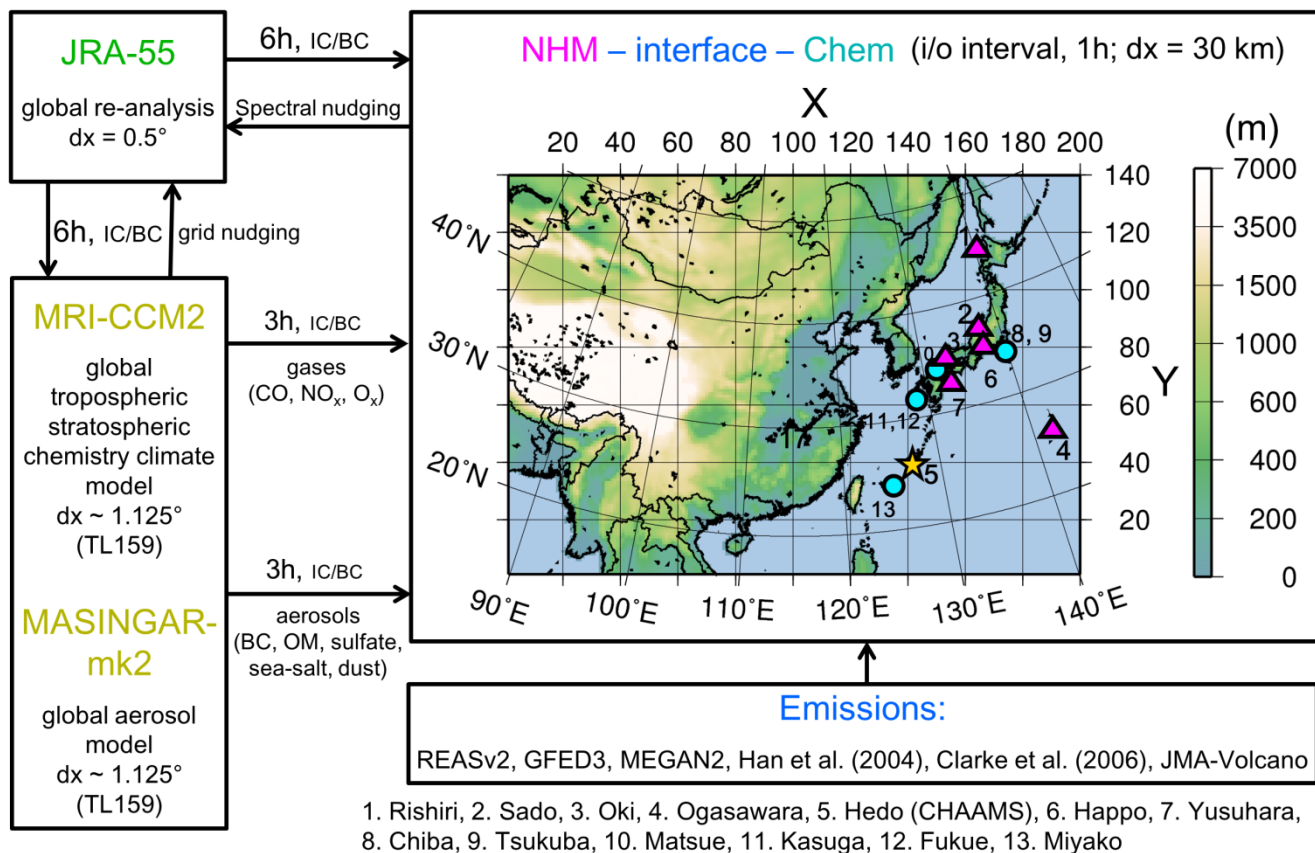
Figure 2: Current simulation settings, model domain showing terrestrial elevation (m) and observation sites. The pink triangles numbered 1-7 show the Japanese EANET sites, except site 5. Hedo (CHAAMS) is marked as the yellow start, where the SKYNET and AD-Net Hedo sites are located on the same premises. The blue circles numbered 8-13 indicate the SKYNET or AD-Net sites in Japan.

4 Experimental setup

4.1 Model domain, simulation period, and boundary conditions

The simulation settings such as the model domain and boundary conditions used in this study are presented in this section. They were the same as Kajino et al. (2019a) and thus are briefly described in this section; detailed descriptions, especially of the aerosols, are provided in Sect. 4.2. Figure 2 shows a flowchart of the simulations, including the simulation domain, which covers East Asia with 200 × 140 horizontal grid cells with a grid resolution of $\Delta x = 30$ km. The numbers of vertical grid cells in the NHM and CTM are 38 (reaching up to 22,055 m above sea level (ASL)) and 40 (reaching up to 18,000 m ASL), respectively, with terrain-following coordinates. The input/output time interval of the offline coupled NHM-Chem was 1 hour. The analysis period was the entire year of 2006, but two half-year CTM simulations were conducted and then

combined due to the initialization issue regarding the land surface model with a spin-up period of 5 days. Climatological data were used for the initial condition of the land surface model (Simple Biosphere Model, SiB) of the NHM. If the simulation started in winter, the initial climatological snow coverage could be very different from that at the actual simulation time; thus, a longer spin-up period would be required. To avoid this situation, July was selected as the initial simulation time because over a year, July corresponds to the minimum snow coverage over East Asia. Therefore, two NHM simulations were performed, from 26 JuneJuly 2005 to 1 JulyJune 2006 and from 26 JuneJuly 2006 to 1 JanuaryDecember 20067 with a spin-up period of 5 days. Then, the two CTM simulations were conducted from 27 December 2005January to 1 JulyJune 2006 and from 26 June 2006July to 1 JanuaryDecember 20067 with the 5-day spin-up. Then, the two simulation results from 1 January 2006 to 1 July 2006 and from 1 July 2006 to 1 January 2007 were combined and used in the following analysis.

The 6-hourly JRA-55 global reanalysis (Kobayashi et al., 2015) data were used to set the initial and boundary conditions of the NHM. Spectral nudging was applied to constrain the simulated meteorological field toward the global analysis, above a height of 7 km for large-scale wave components (wavelength > 1,000 km) of horizontal momentum and potential temperature, with a weighting factor of 0.06 (Nakano et al., 2012). Data assimilation was not applied to the chemical fields in this study.

The 3-hourly lateral and upper boundary concentrations of gases and aerosols were obtained from the simulation results of the global models of MRI-CCM2 (Deushi and Shibata, 2011) (TL159, $\Delta x \sim 1.125°$) and MASINGAR mk-2 (Tanaka et al., 2003; Tanaka and Ogi, 2017; Yumimoto et al., 2017) (TL159, $\Delta x \sim 1.125°$), respectively. Because the lumped mechanisms of nonmethane volatile organic compounds (NMVOCs) and aerosol representations of NHM-Chem are different from those of the two global models, only NO_x, O_3, and CO were taken from the MRI-CCM2 (in other words, the lateral boundaries should be far enough that the peroxyacetyl nitrate (PAN) and long-lived NMVOC fluxes from the boundaries are less influential on the concentrations over the targeted sites of the simulation), and the total masses of BC, OC, SO_4^{2-}, mineral dust, and sea salt were taken from MASINGAR mk-2 (although this model employs sectional methods for mineral dust and sea salt). An OM to OC ratio of 1.8 and a 100% existence of SO_4^{2-} as $(NH_4)_2SO_4$ were assumed in the boundary concentrations. The mineral dust and sea salt were treated as being externally mixed, whereas all of the BC, OM, and $(NH_4)_2SO_4$ were included in the ACM in the 3-category method and in the SUB category in the bulk equilibrium method. For the 5-category method, we assumed that 80% of the BC, OM and $(NH_4)_2SO_4$ were attributed to ACM and that the other aerosols were attributed to AGR.

4.2 Emission data sets

We used REASv2 (Kurokawa et al., 2013) with a 0.25°×0.25° resolution for the anthropogenic emissions of NO_x, SO_2, NH_3, NMVOC, BC, POC, $PM_{2.5}$ and PM_{10} with monthly variations. There is no monthly variation in NH_3. Because REASv2 does not provide hourly and vertical profiles of emissions, those of Li et al. (2017) were applied to each sector, i.e., power, industry, domestic, transport, aviation, and large point sources. We used the monthly Global Fire Emissions Database (GFED3; Giglio et al., 2010) with a 0.5°×0.5° resolution for open biomass burning emissions (NO_x, SO_2, NMVOCs, BC,

and POC) and the Model of Emissions of Gases and Aerosols from Nature (MEGAN2; Guenther et al., 2006) for biogenic emissions of isoprene, terpenes, methanol, and NO. We applied the monthly mean values of GFED3 without ~~temporal~~ daily and diurnal variations. The temporally varying biogenic emission flux was calculated by Eq. 1 of Guenther et al. (2006) using the surface solar radiation and surface air temperature, as simulated by NHM. Biogenic emissions were allocated to the

5   bottom layer. The open biomass burning emissions were uniformly allocated from the bottom layer up to 1,000 m above ground level (AGL). The lightning NO_x emission was not considered in the current simulation.

We made the following assumptions for the ratios of lumped species in the anthropogenic and biomass burning emissions. REASv2 provided speciation information about NMVOC, which was redistributed to the NMVOC speciation of SAPRC99. Because GFEDv3 does not provide NMVOC speciation information, that of Woo et al. (2003) was applied and

10   allocated to the SAPRC99 speciation. When a SAPRC99 speciation was finer than that of REASv2 or GFEDv3, the speciated NMVOC of REASv2 or GFEDv3 was equally distributed to that of SAPRC99 with equal mixing ratios. The OM to OC ratio was set to 1.8 for both emissions. The NO_x emissions were partitioned as 90% NO and 10% NO_2. Five percent of SO_2 emissions were regarded as SO_4^{2-}. The UID emissions of the fine and coarse modes were defined as $PM_{2.5}$ minus the BC minus the POM (primary organic mass; $1.8 \times POC$) and PM_{10} minus $PM_{2.5}$, respectively. The SO_4^{2-} emissions were

15   partitioned as 10% ATK and 90% ACM for the 5-category and 3-category methods. Of the POM emissions, 5%, 10%, and 85% were distributed to ATK, AGR, and ACM in the 5-category method, whereas 5% and 95% of these emissions were distributed to ATM and ACM in the 3-category method, respectively.

Hourly volcanic SO_2 emissions in Japan were developed in this study. These emissions were assumed to comprise 100% SO_2, and no volcanic SO_4^{2-} emissions were considered. JMA regularly monitors the SO_2 emission fluxes and smoke

20   heights of the six major volcanoes in Japan. Since the observation data are sporadic over time and the observation frequencies vary depending on the volcanoes and periods considered, cubic spline interpolation was applied over time to obtain hourly data, as done by Kajino et al. (2004). The details of this approach are described in Supplement 2.

The methods of Han et al. (2004) and Clarke et al. (2006) were used to predict the emissions of mineral dust and sea salt particles as functions of the friction velocity and 10-m wind speed, respectively. In addition to the formula of Han et al.

25   (2004), simulated snow coverage was applied to reduce the emission flux. Flux adjustments were made for the mineral dust and sea salt emissions by using the observed non-sea-salt (nss) Ca^{2+} (defined as $[Ca^{2+}]$ - 0.038 $\times[Na^+]$ ($\mu g/m^2$ or $\mu g/m^3$)) and PM_{10} values for the mineral dust and the observed Na^+ and PM_{10} values for the sea salt obtained at the seven Japanese Acid Deposition Monitoring Network in East Asia (EANET) stations. The adjustment ratios of the dust and sea salt emission fluxes in the simulations were 0.5 and 0.3, respectively.

Table 3: Symbols used for aerosol size parameters and their relationships

Symbol	Description	Relationship
σ_g	Geometric standard deviation	
$\rho_{p,dry}$	Particle dry density (g/cm^3)	
ρ_p	Particle density (g/cm^3)[a]	
$D_{g,n,dry}$	Number-equivalent geometric mean dry diameter	
$D_{g,m,dry}$	Mass-equivalent geometric mean dry diameter	$= D_{g,n,dry} \times \exp\left(3 \times \ln(\sigma_g)^2\right)$
$D_{g,n,aero,dry}$	Aerodynamic $D_{g,n,dry}$	$= D_{g,n,dry} \times \sqrt{\rho_{p,dry}}$ [b]
$D_{g,m,aero,dry}$	Aerodynamic $D_{g,m,dry}$	$= D_{g,m,dry} \times \sqrt{\rho_{p,dry}}$ [b]
$D_{g,n}$	Number-equivalent geometric mean diameter[a]	
$D_{g,m}$	Mass-equivalent geometric mean diameter[a]	
$D_{g,n,aero}$	Aerodynamic $D_{g,n}$	$= D_{g,n} \times \sqrt{\rho_p}$ [b]
$D_{g,m,aero}$	Aerodynamic $D_{g,m}$	$= D_{g,m} \times \sqrt{\rho_p}$ [b]

[a]When wet, or ambient
[b]For spheres

4.2 Aerosol size parameters in emission and boundary conditions

The symbols used for the aerosol parameters used in this study are summarized in Table 3. Aerosol sizes should be carefully defined because both their physical and optical measures significantly vary depending on whether their diameters are number-equivalent or mass-equivalent, wet or dry, and actual or aerodynamic. The width of the distribution σ_g, hygroscopicity κ, and aerosol density ρ_p are also key parameters because they affect the magnitudes of their physical and optical measures. Certainly, shape factors can also significantly affect these measures, as well as aerosol microphysical processes; however, all of the modeled particles are assumed to be spherical in the current version of NHM-Chem, as they are in most other CTMs.

Both Han et al. (2004) and Clarke et al. (2006) provided size-resolved emission fluxes, whereas this model assumes a log-normal size distribution. The values of the number equivalent dry D_g ($D_{g,n,dry}$) of the mineral dust and sea salt emissions were obtained by assuming the prescribed σ_g as 2.0. The $D_{g,n,dry}$ values of the mineral dust were 0.66, 1.22, and 1.22 μm for the land use category (LUC) of desert, loess, and grass, respectively. For a reference, $D_{g,n,dry}$ values of 0.66 and 1.22 μm correspond to aerodynamic $D_{g,n,dry}$ ($D_{g,n,aero,dry}$) values of 1.06 and 1.96 μm, mass-equivalent dry aerodynamic D_g ($D_{g,m,aero,dry}$)

values of 4.50 and 8.31 μm, and PM$_{2.5}$/PM$_{10}$ ratios of 0.23 and 0.068, respectively. Note that here, the simulated PM$_x$ was derived as a proportion of the dry mass in which the aerodynamic ambient (wet) diameter was smaller than x μm.

The simulated PM$_x$ was calculated using the error function (erf) as follows:

$$\mathrm{PM}_x = \sum_i \frac{M_i}{2} \, \mathrm{erf}\!\left(\frac{\ln D_x - \ln D_{g,m,aero,i}}{\sqrt{2} \ln \sigma_{g,i}} \right), \tag{1}$$

where i and M_i indicate the category and dry mass of the category, respectively.

5   We made the following assumptions for the aerosol size distributions at the boundary conditions. Because Clarke et al. (2006) proposed trimodal size distributions, they needed to be combined into a single mode. Laboratory and field experiments indicated that the major proportions of the smallest mode (i.e., 10-132 nm) should be water-insoluble organic compounds (Facchini et al., 2008; Prather et al., 2013); thus, the smallest mode was not regarded as sea salt emissions in this model. The number and volume fluxes of the sea salt emission were obtained as the summations of those of the second-

10   largest and largest modes. The surface area flux was then deduced based on the number, volume, and prescribed value of $\sigma_g =$ 2.0. The $D_{g,n,aero,dry}$ value, $D_{g,m,aero,dry}$ value, and PM$_{2.5}$/PM$_{10}$ ratio of the dry sea salt particles are 0.448 μm, 1.89 μm, and 0.66, respectively. Because sea salt particles are highly hygroscopic, at conditions of RH = 80% and 90%, the ambient diameter $D_{g,m,aero}$ values would be 2.39 and 2.88 μm, and the PM$_{2.5}$/PM$_{10}$ ratios would be 0.54 and 0.44, respectively, assuming a hygroscopicity value of $\kappa = 1.0$.

15   The prescribed size parameters were applied to the emissions of all of the species, except for the mineral dust and sea salt and are defined as follows: $(D_{g,n,aero,dry}, \sigma_g) = $ (0.01 μm, 1.3), (0.1 μm, 1.5), (0.1 μm, 1.5), and (2 μm, 1.8) for the ATK, ACM, AGR, and DU (applied to anthropogenic dust only, denoted as UID) categories of the 5-category method; (0.01 μm, 1.3), (0.1 μm, 1.5), and (2 μm, 1.8) for the ATK, ACM, and COR (applied to UID only) categories of the 3-category method; and (0.1 μm, 1.5) and (2 μm, 1.8) for the SUB and DU (applied to UID only) categories of the bulk equilibrium method,

20   respectively.

Although MASINGAR mk-2 employs a sectional model to predict changes in aerosol size distributions, the prescribed size parameters were applied to the lateral and upper boundary concentrations of NHM-Chem and are defined as follows: $(D_{g,n,aero,dry}, \sigma_g) = $ (0.01 μm, 1.3), (0.1 μm, 1.5), (0.1 μm, 1.5), (2 μm, 1.8), and (1 μm, 1.8) for the ATK, ACM, AGR, DU and SS categories of the 5-category method; (0.01 μm, 1.3), (0.1 μm, 1.5), and (1 μm, 1.8) for the ATK, ACM, and COR

25   (mineral dust and sea salt) categories of the 3-category method; and (0.1 μm, 1.5), (2 μm, 1.8), and (1 μm, 1.8) for the SUB, DU, and SS categories of the bulk method, respectively. Certainly, in the self-nesting simulations, where the boundary concentrations are taken from the outer domain simulation of NHM-Chem, the prescribed size parameters are not needed.

5 Observations and model validations

The observation data used for the evaluations of the simulation results are described in this section.

The observation sites used for the model validation are depicted in Fig. 2. The pink triangles indicate the Acid Deposition Monitoring Network in East Asia (EANET) stations (http://www.eanet.asia, last access: 18 June 2020). The blue circles indicate the ground-based international remote sensing network dedicated to aerosol-cloud-radiation interaction studies (SKYNET) stations (Takamura et al., 2004; Nakajima et al., 2007; http://atmos3.cr.chiba-u.jp/skynet, last access: 18 June 2020) and/or the Asian dust and aerosol lidar observation network (AD-Net) stations (Sugimoto et al., 2008; Shimizu et al., 2016; http://www-lidar.nies.go.jp/AD-Net/, last access: 18 June 2020). At the Japanese EANET sites, the hourly surface concentrations of gases (NO_x, SO_2, and O_3) and the aerosol mass ($PM_{2.5}$ (only Oki and Rishiri for 2006) and PM_{10}), daily wet depositions of inorganic compounds, and two or one week mean concentrations of gaseous and aerosol phases of inorganic compounds are monitored. At the SKYNET sites, sky radiometers (Prede Co. Ltd., Tokyo, Japan) are the main instruments. Aerosol optical thickness (AOT) and single scattering albedo (SSA) data in ultraviolet/visible/near-infrared regions and the Ångström exponent data are provided. We used AOT and SSA at 500 nm for the comparison. The AD-Net sites are equipped with a two-wavelength (1064 and 532 nm) polarization-sensitive (532 nm) Mie-scattering lidar system. We used the extinction coefficients for pherical (referred to as dust) and spherical aerosols for the model evaluation, derived using the attenuated backscattering coefficients and the volume depolarization ratio (Sugimoto et al., 2003; Shimizu et al., 2004). The yellow star is the Hedo site, which belongs to both EANET and SKYNET, an air quality measurement supersite called CHAAMS (Cape Hedo Atmosphere and Aerosol Monitoring Station).

The OPC (ROYCO LAS236) was equipped at CHAAMS in 2006, which measures number concentrations of aerosols with diameters larger than 0.3, 0.5, 1, 3, and 5 μm (Takamura et al., 2004). To compare the simulated number concentrations against the OPC data, a parameter NC_x is defined, the proportion of the number concentration for which the aerodynamic ambient diameter is larger than x μm, as follows:

$$NC_x = \sum_i \frac{N_i}{2} \left[1 - \mathrm{erf} \left(\frac{\ln D_x - \ln D_{g,n,aero,i}}{\sqrt{2} \ln \sigma_{g,i}} \right) \right], \tag{2}$$

where i and N_i indicate the category and total number of the category, respectively. The simulated $NC_{0.3}$ was compared against that observed by OPC.

Because aerosol optical properties are not simulated in NHM-Chem, to compare with the observation data Tthe Mie theory calculation was performed to derive the AOT and AAOT at wavelengths of 500 nm by using simulated log-normal size distribution parameters and chemical compositions. The refractive indices of the Optical Properties of Aerosols and Clouds (OPAC) database (Hess et al., 1998) were used for the Mie calculation. For the refractive indices of the model components of UID, BC, OM, MD, NS, SO_4^{2-}, NH_4^+, NO_3^-, Cl^-, and H_2O, the databases of "insoluble", "soot", "insoluble", "mineral", "sea salt", "water-soluble", "water-soluble", "water-soluble", "sea salt", and "fog" values, respectively, were used,

with some modifications for BC to 1.85-0.71i (Bond et al., 2006) and MD to 1.5-0.001i (Aoki et al., 2005) at 500 nm. To calculate the optical properties of non-light-absorbing and light-absorbing mixtures, the Maxwell-Garnett approximation was used. The BC and MD masses were regarded as light-absorbing components, and the others were regarded as non-light-absorbing (certainly, some proportions of OM are light-absorbing, i.e., brown carbon, but they are not considered in the current model). The volume-weighted refractive indices were used for the light-absorbing and non-light-absorbing components in each category.

In the current study, a model performance comparison of the aerosol representation methods was made in terms of the computational costs (Sect. 6.1), the mass concentrations of O_3, mineral dust and $PM_{2.5}$ (Sect. 6.2), the deposition of inorganics such as SO_4^{2-}, NO_3^-, and NH_4^+ (Sect. 6.3), AOT and light-absorbing AOT (AAOT) (Sect. 6.4), and CCN (Sect. 6.5). In Table 4, the statistical measures listed are the median of simulation data (*Sim. Med.*) and ~~median~~ simulation to observation median ratio (*Sim:Obs*), correlation coefficient (*R*), and fractions of simulated values within a factor of two of the observed values (*Fa2*) of the relevant variables such as O_3 and its precursor gas NO_x, dust extinction coefficient (Ext_D) and PM_{10} during the dust events of April 2006 (defined as PM_{10}_D, later in Sect. 6.2), $PM_{2.5}$, wet deposition amounts of SO_4^{2-}, NO_3^-, and NH_4^+, AOT, SSA, total (dust and spherical) extinction coefficient (Ext_T), and $NC_{0.3}$. Because the main objective of the paper is the aerosol module intercomparison, the general description of the results ~~The discrepancies between the simulations and the observations,~~ are which were already made in our previous paper (Kajino et al., 2019a), are not presented in detail here ~~discussed in Sect. 6 for each corresponding variable~~, and but are presented ~~the corresponding figures are shown~~ in Supplement 3.

Table 4: Comparative statistical analysis of observed (Obs.) and simulated (Sim.) variables

Variable	Frequency	N^a	Obs. Med.[b]	Unit	*Sim. Med (Sim:Obs)*[c]			R^d			*Fa2*[e]		
					5-ctg	3-ctg	blk	5-ctg	3-ctg	blk	5-ctg	3-ctg	blk
O_3^f	1-d	3496	42.7	ppbv	38.9 (0.91)	38.9 (0.91)	38.9 (0.91)	0.63	0.63	0.63	0.92	0.92	0.92
NO_x^f	1-d	3334	1.30	ppbv	1.22 (0.94)	1.23 (0.94)	1.21 (0.92)	0.40	0.39	0.39	0.48	0.48	0.48
Ext_D[g]	1-h	69	0.47	km⁻¹	0.22 (0.47)	n.a. n.a.	0.20 (0.42)	-0.17	n.a.	-0.17	0.61	n.a.	0.42
PM_{10}_D[h]	1-h	69	370	µg m⁻³	286 (0.77)	287 (0.77)	276 (0.74)	0.22	0.23	0.25	0.58	0.58	0.58
$PM_{2.5}^f$	1-d	695	8.83	µg m⁻³	9.55 (1.08)	10.7 (1.22)	10.1 (1.15)	0.57	0.57	0.62	0.82	0.81	0.76
$PM_{2.5}^{f,i}$	1-d	695	8.83	µg m⁻³	7.13 (0.81)	6.90 (0.78)	8.83 (0.92)	0.58	0.57	0.62	0.68	0.68	0.74
Precip.[j]	2-w	253	60.0	mm	52.9 (0.88)	52.9 (0.88)	52.9 (0.88)	0.69	0.69	0.69	0.61	0.61	0.61
W-nss-SO_4^{2-}[j]	2-w	253	0.77	mmol m⁻²	0.69 (0.90)	0.71 (0.93)	0.67 (0.87)	0.49	0.49	0.47	0.54	0.53	0.51
W-NO_3^-[j]	2-w	253	0.80	mmol m⁻²	0.69 (0.86)	0.69 (0.86)	0.65 (0.82)	0.73	0.72	0.67	0.62	0.61	0.60
W-NH_4^+[j]	2-w	253	0.67	mmol m⁻²	0.60 (0.90)	0.61 (0.91)	0.64 (0.96)	0.68	0.68	0.61	0.56	0.57	0.53
AOT[k]	1-d	566	0.30	-	0.13 (0.42)	0.14 (0.46)	0.13 (0.42)	0.39	0.40	0.38	0.44	0.47	0.46
SSA[k]	1-d	355	0.96	-	0.91 (0.95)	0.87 (0.91)	0.86 (0.90)	0.20	-0.07	-0.08	1.00	1.00	1.00
Ext_T[l]	1-d	4146	0.14	km⁻¹	0.079 (0.57)	0.078 (0.57)	0.079 (0.57)	0.31	0.32	0.28	0.55	0.55	0.52
$NC_{0.3}$[m]	1-h	1630	9.91	×10⁴ L⁻¹	11.6 (1.17)	11.4 (1.15)	14.9 (1.50)	0.36	0.33	0.29	0.64	0.63	0.55
PM_{10}[m]	1-h	1881	42.0	µg m⁻³	21.6 (0.53)	21.8 (0.53)	22.9 (0.56)	0.53	0.55	0.52	0.47	0.48	0.50

[a]Number of available data
[b]Median of observation data
[c]Median of simulation data and ~~Simulation~~ simulation to observation median ratio with brackets.
5 [d]Correlation coefficient
[e]Fraction of simulated values within a factor of two of the observed values
[f]Daily mean surface concentration
[g]Hourly mean median values below 300 m of extinction coefficient during the dust events in April 2006 at Matsue and Hedo.
[h]Hourly mean values during the dust events in April 2006 at Oki and Hedo.
10 [i]$PM_{2.5}$ but compared with simulated $PM_{2.5}$ (pile-up)
[j]Half-monthly cumulative precipitation or wet deposition amount
[k]Daily mean column amount
[l]Daily mean median values below 300 m of extinction coefficient.
[m]Hourly mean surface concentration in April and December 2006 when the OPC data are available at Hedo.

6 Model performances for various purposes

In this section, the intermodule comparisons between the bulk equilibrium, 3-category, and 5-category methods are presented in terms of their relevant purposes, i.e., simulations of variables often used for operational forecast (such as O_3, mineral dust, and $PM_{2.5}$), simulations of air quality ~~forecast~~variables (surface concentrations and depositions of pollutants), and simulations of climate-relevant variable~~s forecasts~~ (such as AOT, CCN, and ice nucleating particles (INP)) ~~of aerosols~~, respectively.

It should be noted here that the capability of the bulk equilibrium method in terms of operational forecast was not assessed by conducting forecast simulations (e.g., 3-day forecast with a data assimilation of initial conditions and post-processing for statistical bias corrections) but assessed in the hindcast simulation without data assimilations and post-processing ~~by comparing the relevant variables, which are used for operational forecasts such as surface mass concentrations of O_3, mineral dust, and $PM_{2.5}$, predicted by the bulk equilibrium method against those of the reference method, the 5-category method~~.

The main objectives of this section are itemized as follows: (1) to compare the computational efficiency of the three methods, (2) to quantify the deviations of the widely used 3-category method and the efficient bulk equilibrium method from the most realistic aerosol representation of NHM-Chem, the 5-category method, and (3) to assess the discrepancy between the simulated and observed variables and how the discrepancy varied depending on the three methods.

6.1 Computational costs

The computational costs of the three methods are listed in Table 5. $R_{CPUtime}$ and R_{aero} were measured for the earlier half-year simulations (i.e., January to June 2006). The nonequilibrium aerosol microphysics module consumed approximately half of the total CPU time for the 5-category method, while it consumed only 15% of that of the bulk equilibrium module (and the thermodynamic equilibrium model ISORROPIA2 consumed a major proportion of this 15%). The total CPU times of the 3-category and 5-category methods are 44% and 91% greater than that of the bulk equilibrium module, respectively. For these three options, the number of gaseous species is the same (58), and the numbers of their aerosol attributes are 20, 38, and 50, respectively.

Table 5: Number of transport variables (gas plus aerosol attributes) (N_{trans}) and ratios of the total CPU time to that of the bulk chemistry ($R_{CPUtime}$), as well as ratios of CPU time of the aerosol process to that of the total processes[1] (R_{aero}).

	N_{trans}	$R_{CPUtime}$	R_{aero} (%)
Bulk equilibrium method	78	1	15.0%
3-category nonequilibrium method	96	1.44	46.0%
5-category nonequilibrium method	108	1.91	54.9%

[1] Excluding the I/O and MPI communications.
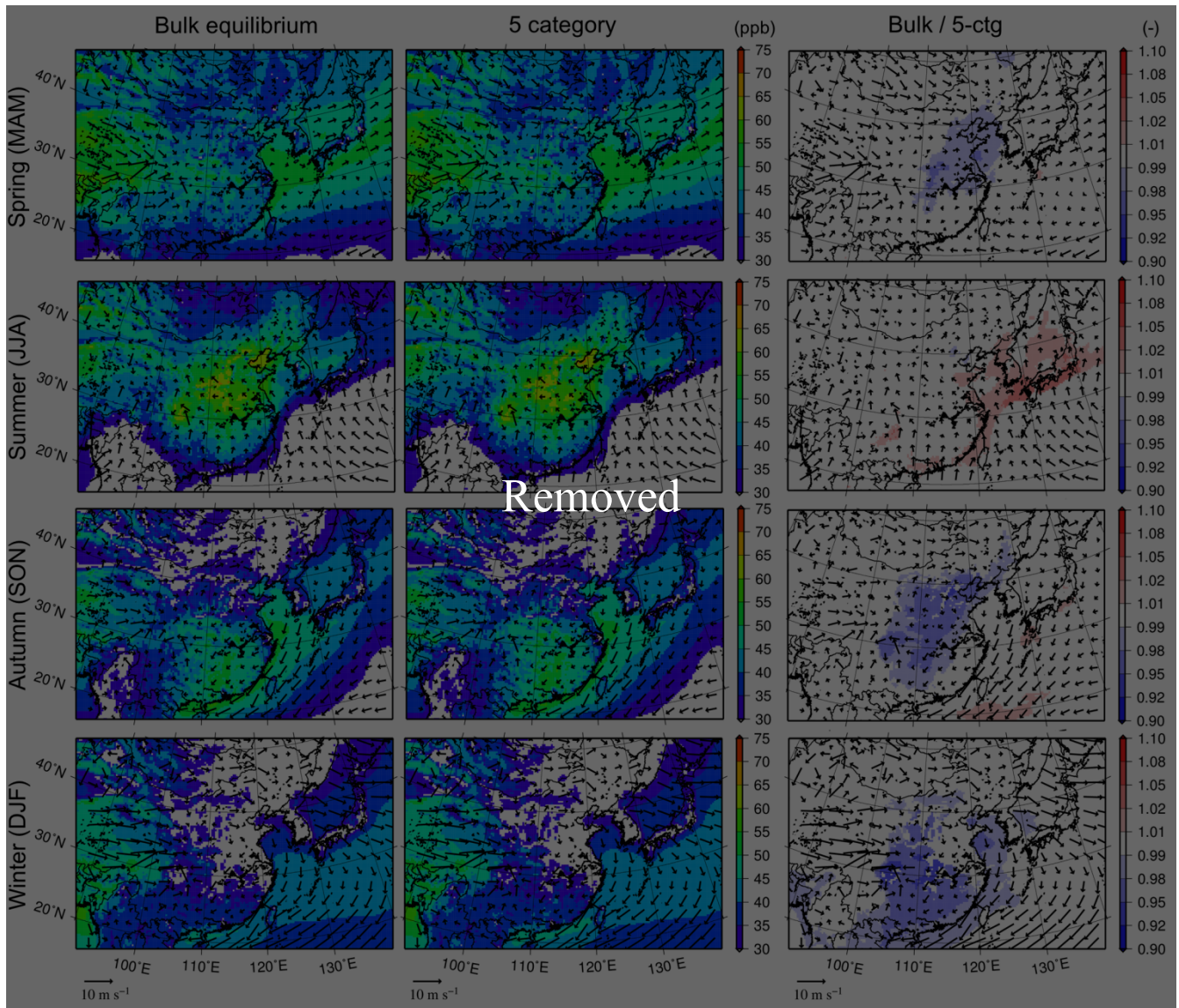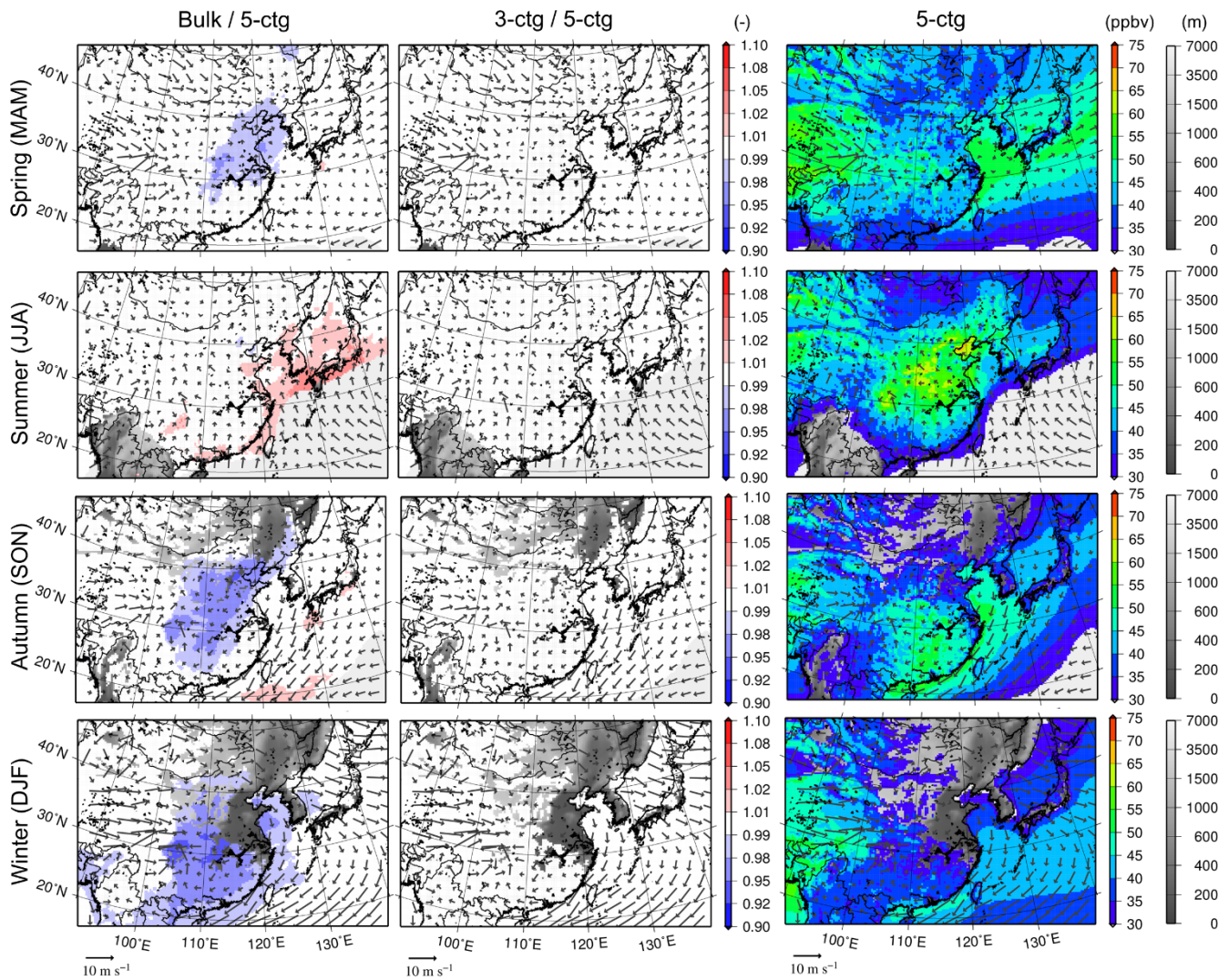
Figure 3: Seasonal mean surface concentrations of O$_3$ in (top to bottom) spring, summer, autumn, and winter of 2006 for (left to right) the ratios of the bulk to 5-category methods, the ratios of the 3-category to 5-category methods, and the ratios of the bulk to 5-category methods with surface wind vectors. The model topography is depicted in grayscale on the background of each panel. Topography is overlain by color shades for concentrations above the lower limit of the scale (in this case, 30 ppbv).

6.2 Surface mass concentration of air pollutants

Figures 3-5 present the seasonal mean surface mass concentrations of O$_3$, mineral dust, and PM$_{2.5}$, which negatively impact the health of the population and the environment and thus are often used in operational air quality forecasts. The

The mid-latitude westerlies are predominant in this region, and air pollutants are transported from west (or northwest) to east (or southeast), associated with migrating disturbances, including the cold and warm frontal transports of cyclones and anticyclonic transport throughout the year except during summer (e.g., Oshima et al., 2013). In summer, due to the Pacific high system, the transport of continental air masses is less dominant, and clean air masses of maritime origin are often transported to Japan. Northerly to northwesterly winds prevail in winter due to the Siberian high system. These seasonal wind patterns can be clearly observed in Figs. 3-5.

~~The simulated seasonal mean surface O_3 concentration over China was highest in the summer but that in Japan was highest in the spring due to the long-range transport associated with traveling disturbances (Fig. 3, Fig. S3-1). Figure S3-1 compares the observed and simulated daily O_3 concentrations with the precursor gas NO_x concentrations at the Japanese EANET stations, and the statistical scores are shown in Table 4. The simulated medians agreed well with those observed medians (Sim:Obs of O_3 and NO_x are approximately 0.9), although the correlation coefficients were not very large (approximately 0.6 and 0.4 for O_3 and NO_x, respectively). The low correlation coefficients of O_3 were due mainly to the locations of the observation sites: R at remote sites was 0.76-0.91, whereas R at rural inland sites was low (0.24-0.49) due to the complex topography that cannot be resolved by the crude resolution of the current simulation. Low correlations of NO_x were obtained mainly because it is a primary species. The uncertainty of emission flux and unresolvable heterogeneity of emission sources near the sites degraded the model performance of the primary species results more than they did for the secondary species such as O_3.~~ The difference in the horizontal distributions of O_3 between the bulk method and the other two methods was very small (Fig. 3). The differences between the bulk O_3 and 5-category O_3 were due mainly to the differences in the aerosol surface areas (different heterogeneous loss rates of NO_x, as a precursor of O_3 formation). It is inferred from Table 4 (which provides more significant digits) that the relative magnitudes of Sim:Obs of NO_x and O_3 of the three methods are consistent (Sim:Obs of NO_x of the bulk, 3-category, and 5-category methods were 0.925, 0.939, 0.938, and those of O_3 were 0.9108, 0.9115 and 0.9111, respectively). Further investigation is needed for quantitative assessment, but the errors of the bulk method were smaller than those of the other methods considered by up to 5%. Because this difference is minor compared to the difference between the simulation and observation results (especially for R), improving the model processes and/or boundary conditions will certainly improve all of the simulation results, regardless of the aerosol category methods that are selected.
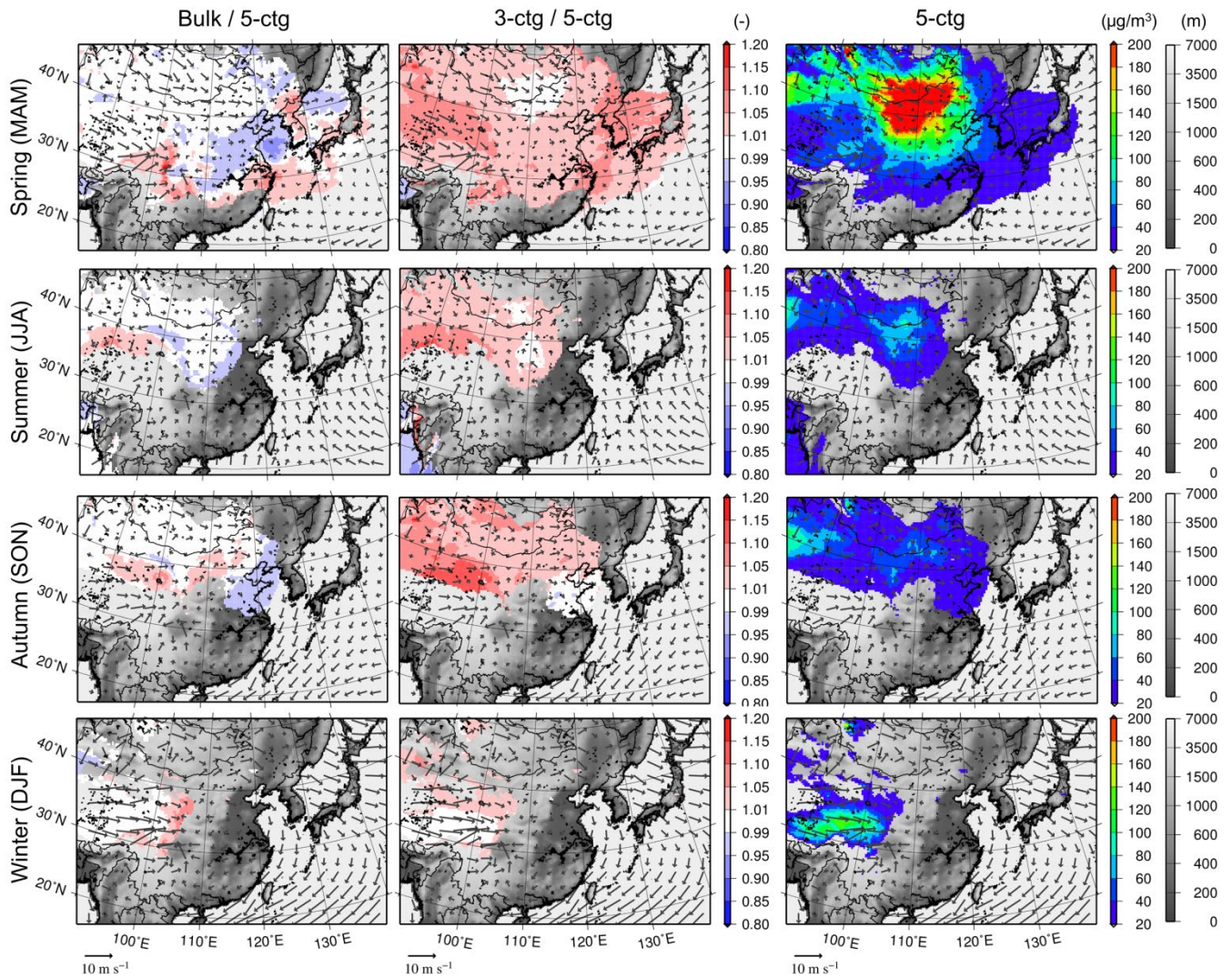
Figure 4: Same as Fig. 3 but for mineral dust ~~for (left to right) the ratios of the bulk to 5-category methods, the ratios of the 3-category to 5-category methods, and the 5-category method. The model topography is depicted in grayscale on the background of each panel. Topography is overlain by color shades for concentrations above the lower limit of the scale (in this case, 20 μg m⁻³).~~

The simulated surface mineral dust concentration was highest in the spring in the emission source regions (Taklamakan and Gobi) and the downwind regions such as Korea, and Japan (Fig. 4). ~~Figure S3-2 presents the observed and simulated hourly PM₁₀ and Ext_D at Oki/Matsue and Hedo in April 2006, when mineral dust transport events were observed. Hedo (CHAAMS) includes EANET and AD-Net, whereas Oki (Matsue) is the only EANET (AD-Net) site. The distance between Oki and Matsue is 50-60 km and there are two model grids between the nearest grids to the sites. Table 4 compares the observed and simulated PM₁₀ and Ext_D during the dust events in the month. The dust events are defined for the period~~

~~in April 2006, when Ext_D and PM₁₀ are greater than 0.1 km⁻¹ and 300 µg m⁻³ at the Oki/Matsue stations and 0.06 km⁻¹ and 150 µg m⁻³ at the Hedo station. There are no data for Ext_D of the 3-category method because sea salt and dust particles are completely internally mixed so that the extinction coefficient of dust particles cannot be isolated from the extinction coefficient of COR, which includes abundant sea salt particles at these near the coast sites.~~ The differences between the bulk and 5-category methods were generally lower than 5% and at most 10% (Fig. 4). These differences could be due mainly to the differences in the chemical aging of the mineral dust, which increases in hygroscopicity due to condensational growth during its long-range transport in the 5-category method. There are even more significant differences found between the 3-category and 5-category methods. The 3-category and 5-category methods both consider chemical aging processes, but the 3-category method assumes a complete internal mixture of dust and sea salt. Accordingly, the dust particles were more hygroscopic but smaller in the 3-category method compared to those in the 5-category method case; thus, with the 3-category method, the surface concentration was higher over the ocean in the spring by up to 10% due to the lower gravitational and dry deposition velocities. The 3-category to 5-category dust concentration ratio was higher in the regions on the continent close to the west lateral boundary due to the difference in the dust sizes; additionally, a complete dust/sea salt mixture was assumed at the boundary in the 3-category method. Because this difference (up to 10%) is minor compared to the difference between the simulation and observation (approximately 0.4-0.6 of *Fa2*, see Table 4), improving the model processes and/or boundary conditions will certainly improve all of the simulation results regardless of the aerosol category methods that are selected.
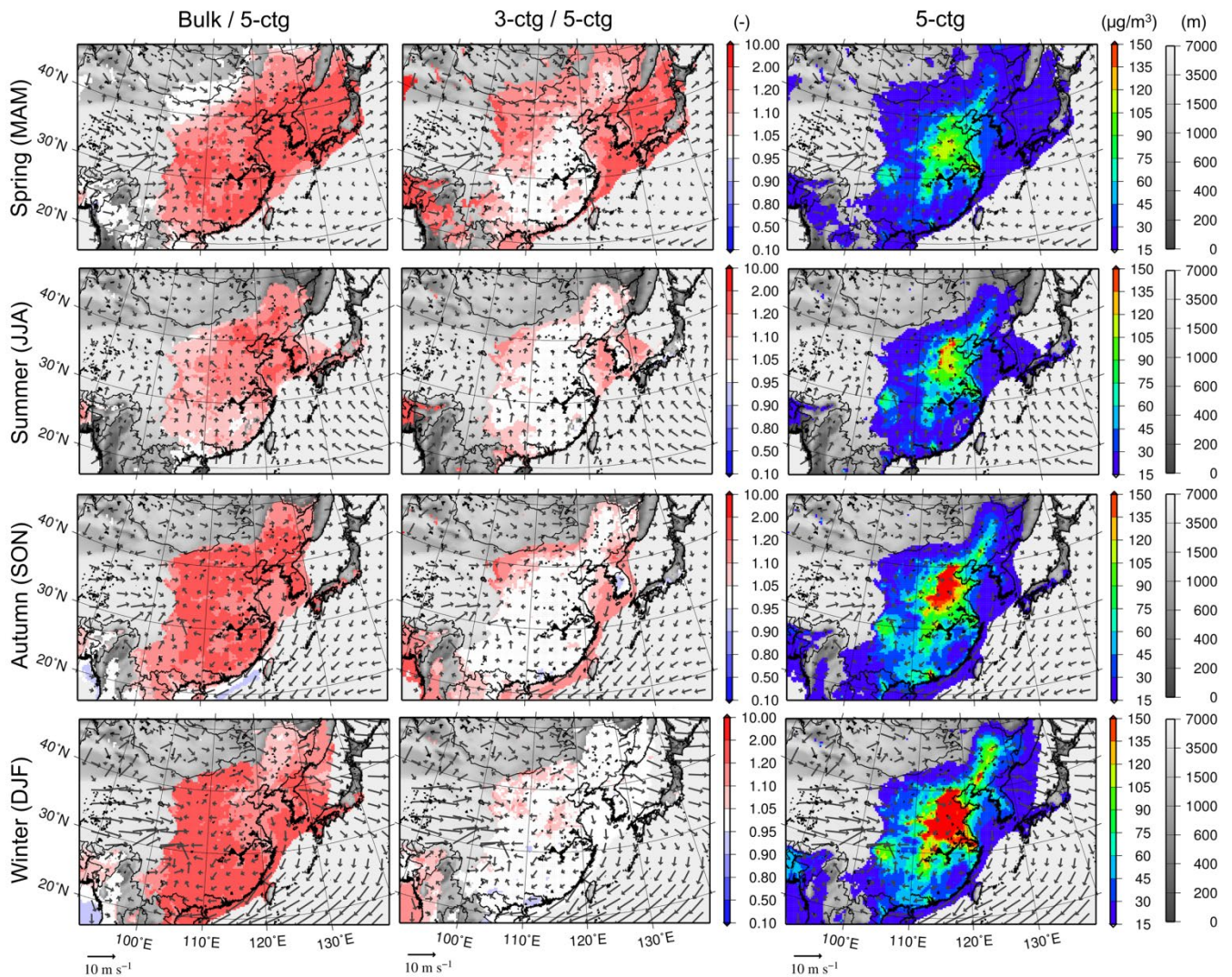
Figure 5: Same as Figs. 3 and 4 but for PM$_{2.5}$.

The differences in the model performance of the PM$_{2.5}$ prediction are shown in Fig. 5. This PM$_{2.5}$ was derived by Eq.
5   1, but the simulated PM$_{2.5}$ was sometimes defined as the pile-up of the mass concentrations of the dry components existing in the submicron categories, which is independent from the aerosol size distribution. The latter is denoted as PM$_{2.5}$ (pile-up) in the manuscript, and the horizontal distributions are shown in Fig. S4-1 in Supplement 4. The major difference between the simulated PM$_{2.5}$ and PM$_{2.5}$ (pile-up) is that PM$_{2.5}$ includes some proportion of natural aerosols, such as sea salt and dust, and can exclude proportions of submicron categories (i.e., ACM and AGR) larger than 2.5 μm, whereas PM$_{2.5}$ (pile-up)
10 completely excludes sea salt and dust particles and includes all of the submicron categories (i.e., ATK, ACM and AGR in the 5-category method, ATK and ACM in the 3-category method, and SUB in the bulk method). The simulated PM$_{2.5}$

concentration over China was highest in the spring (Fig. 5). PM$_{2.5}$ and PM$_{2.5}$ (pile-up) of the bulk method were 20-100% larger than those of the 5-category and 3-category methods due to the neglection of nitrate mixed with coarse mode dust particles by the bulk method. In the 5-cateogry and 3-category models or in reality, nitrate is mixed with mineral dust particles forming Ca(NO$_3$)$_2$ and Mg(NO$_3$)$_2$ and with anthropogenic dust by condensation of NH$_4$NO$_3$. The simulated submicron and supermicron NO$_3^-$ were comparable in the 5-category and 3-category methods over the continent for the whole seasons and over the ocean in the spring. However, all of these supermicron NO$_3^-$ were mixed with SUB in the bulk method, which caused significant overestimation of both PM$_{2.5}$ and PM$_{2.5}$ (pile-up). The overestimation was predominant in the colder seasons over the continent, because the particulate phase of NO$_3^-$ is larger as the temperature is lower. PM$_{2.5}$ of the 3-category method were 20-100% larger than those of the 5-category method especially over the ocean in the spring. It is due to the unrealistic complete internal mixing assumption of the sea salt and dust particles in the 3-category method. The sea salt and dust particles coexisted mostly as external mixtures over the ocean in the spring. As the size of sea salt is generally smaller than that of dust, mass fractions of sea salt (SS of 5-category method) smaller than 2.5 μm are larger than those of dust (DU of 5-cateogry method). However, the internal mixing assumptions resulted in smaller size of COR than DU, which resulted in overestimation of mass fractions of DU smaller than 2.5 μm and thus overestimation of PM$_{2.5}$ by the 3-category method. In contrast, the 3-category to 5-category ratio of PM$_{2.5}$ (pile-up) was negligibly small, indicating that the internal sea salt/dust mixture assumption has a minor impact of the dry mass concentrations of the submicron categories. ~~The comparison between the simulation and observation is shown in Fig. S3-3 and listed in Table 4.~~ Despite the nonnegligible differences in the predicted surface concentrations of PM$_{2.5}$ and PM$_{2.5}$ (pile-up) by the three methods, the statistical scores for the three methods are not different with each other (Table 4). It is indicated that the bulk method is eligible for operational forecasting, because the computational efficiency does not significantly deteriorate the model performance in terms of the predictions of PM$_{2.5}$ surface concentrations. ~~The performances of simulated PM$_{2.5}$ were comparable or better than those of PM$_{2.5}$ (pile-up), indicating consistent prediction of the aerosol size distributions. The *R* values of PM$_{2.5}$ and PM$_{2.5}$ (pile-up) were similar. The *Sim:Obs* of the 3-category PM$_{2.5}$ (1.22) was larger than those of the other two methods due to the complete internal mixing assumption of the sea salt and dust (both mineral and anthropogenic) particles in the 3-category method: more dust mass was included in PM$_{2.5}$ because the sea salt/dust mixture resulted in larger sea salt particles but smaller dust particles. The simulated PM$_{2.5}$ concentration over China was highest in the winter due to its higher emissions and more stable stratification, whereas in Japan, it was highest in the spring (Fig. 5). The 3-category PM$_{2.5}$ was generally lower than the bulk PM$_{2.5}$ but generally higher than the 5-category PM$_{2.5}$. Both the bulk PM$_{2.5}$ and 3-category PM$_{2.5}$ were larger than the 5-category PM$_{2.5}$, but for different reasons. The bulk PM$_{2.5}$ was higher due to larger submicron NO$_3^-$, whereas the 3-category PM$_{2.5}$ was higher due to the assumption of a complete internal dust/sea salt mixture, as mentioned above. The bulk submicron NO$_3^-$ is larger because NO$_3^-$ can mix with either submicron particles (such as ATK, ACM, or AGR) or coarse mode particles (COR or DU) over the land in the 3-category and 5-category methods, whereas NO$_3^-$ is mixed with only SUB in the bulk method in the absence of sea salt particles. As found in Fig. S3-3, the large bulk to 5-category ratio of PM$_{2.5}$ (pile-up) was consistent with that of PM$_{2.5}$ for the same reason (i.e., larger submicron NO$_3^-$). In~~

contrast, the 3-category to 5-category ratio of $PM_{2.5}$ (pile-up) was negligibly small, indicating that the internal dust/sea salt mixture assumption has a minor impact on the dry mass concentration of the submicron categories. Table 4 shows that the *Sim:Obs* of $PM_{2.5}$ was greater than that of $PM_{2.5}$ (pile-up), indicating that approximately 20% of the sea salt (and 40% of the dust/sea salt mixture) contributed to the $PM_{2.5}$ at Oki and Rishiri. It is unclear if the bulk method is eligible for operational forecasting because the bulk $PM_{2.5}$ result was generally larger than the 3- and 5-category $PM_{2.5}$ results by approximately 20-100% due to the abovementioned NO_3^- mixture assumptions. Although they have not yet been discussed, there are still large discrepancies in the simulated and observed $PM_{2.5}$ chemical compositions in Japan. Because the uncertainties in both the simulated chemical compositions and their size distributions contribute to the simulated $PM_{2.5}$, it is not necessary for the 5-category method to yield the best prediction of $PM_{2.5}$. In fact, the R value of the bulk $PM_{2.5}$ (0.62) was slightly higher than those of both the $PM_{2.5}$ and $PM_{2.5}$ (pile-up) of the 3- and 5-category methods (0.57-0.58) (Table 4). However, the current analysis is insufficient to evaluate the eligibility of the model for $PM_{2.5}$ operational forecasting because the simulated $PM_{2.5}$ was compared with observations obtained at only two stations on remote islands. Currently, relevant work is ongoing under the framework of a multimodel intercomparison study in Japan called J-STREAM (Chatani et al., 2018).
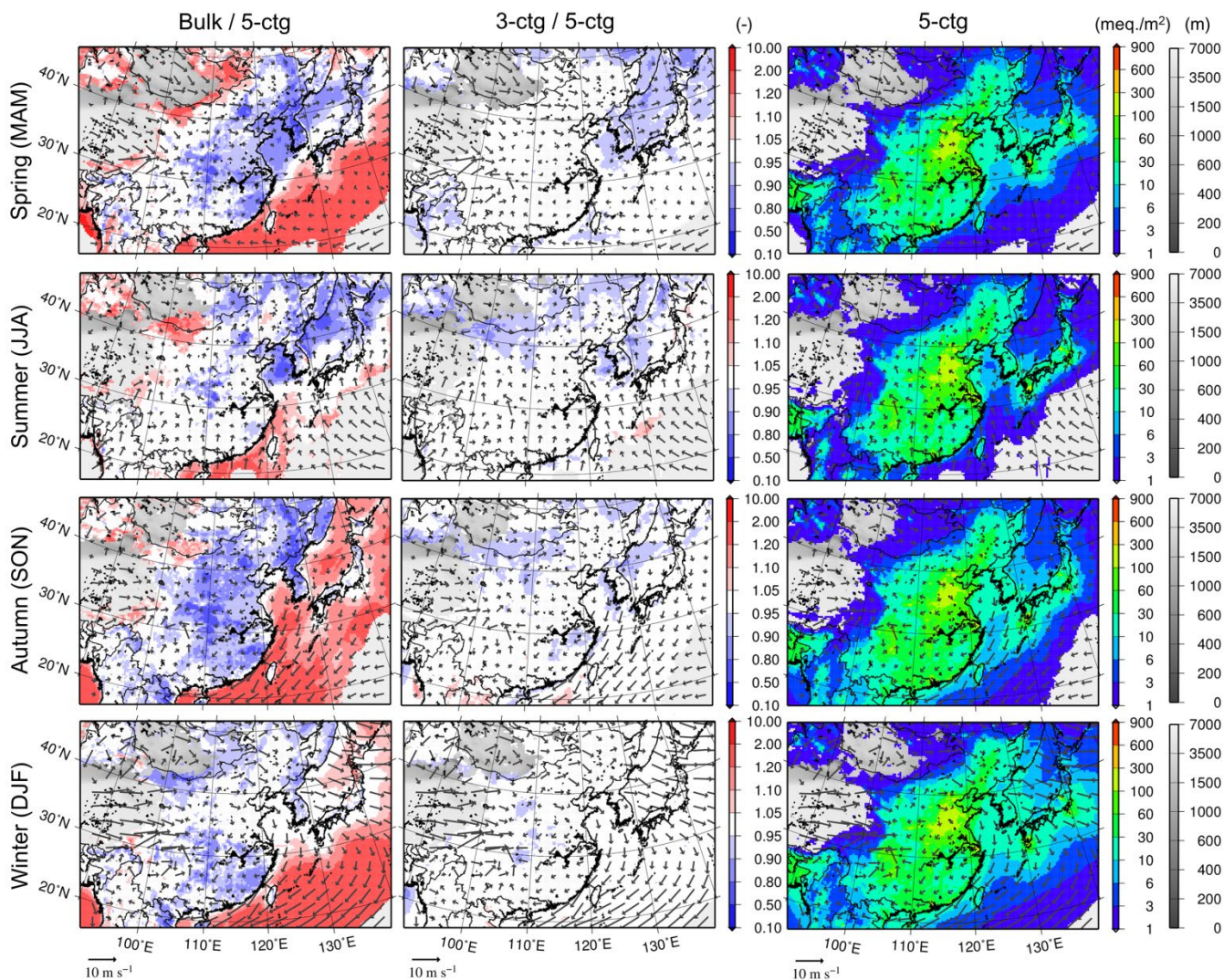
Figure 6: Same as Figs. 3-4 and 5 but for the dry deposition of sum of nss-SO$_4^{2-}$-, and T-NH$_4^+$, plusand T-NO$_3^-$.

6.3 Dry, wet, and fog deposition of acidic substances

Figs. 6 and 7 compare the predictions of the dry and wet depositions of the inorganic components of non-sea salt SO$_4^{2-}$ (nss-SO$_4^{2-}$, defined as [SO$_4^{2-}$] - 0.251 × [Na$^+$] (μg/m^2 or μg/m^3)), total (gas plus aerosol) NH$_4^+$ (T-NH$_4^+$), and T-NO$_3^-$, which are the major acidic and basic substances, obtained using the three methods. Once deposited on the ground surface, NH$_4^+$ is efficiently converted to NO$_3^-$ in the soil; thus, NH$_4^+$ is also an important agent for environmental acidification. The horizontal distribution of dry deposition was generally similar to that of surface concentration because the dry deposition flux is proportional to the surface concentration.

~~As shown in Table 4, the model precipitation predictions by NHM and the wet deposition amounts predicted by Chem are similar: 10-15% underestimation, approximately 0.7 of R, and 0.6 of $Fa2$, except 0.5 of R for wet deposition of nss-SO_4^{2-}). A similar feature, underestimation of the wet deposition amounts, is found in Fig. S3-4. Certainly, this is not likely the only reason for the lower R for nss SO_4^{2-}, which could also be due to the effect of short-lived large sea salt~~

5 ~~particles, as discussed in Kajino et al. (2012b). Because the Japanese EANET stations are located near the coasts (150-700 m from the coastline), the observed amount of W-Na^+ could be substantially affected by the short-lived (traveling distance is approximately 1 km) large sea salt particles ($D > 10$ μm), which is not considered in the model. As a result, the simulated W-Na^+ substantially underestimated the observation ($Sim:Obs = 0.26-0.27$). This discrepancy in Na^+ slightly lowered the R of nss-SO_4^{2-} compared to those of the other chemical components and precipitation ($Sim:Obs$ of total (non-sea salt plus sea~~

10 ~~salt) $SO_4^{2-} = 0.42-0.44$). SO_4^{2-} from dimethyl sulfide (DMS), which was not considered in the simulation, could be a reason for the discrepancy, but the contribution may not be large for the region of the simulation (e.g., Kajino et al., 2004).~~

The dry depositions (Fig. 6) of the 3-category and 5-category methods were very similar (the difference was lower than 5% in most of the domain) because the size distribution and gas-aerosol partitioning of the components were similar. The separation of soot/soot-free and dust/sea salt particles in the 5-category method did not substantially alter the size or gas-

15 aerosol partitioning. The difference between the bulk and 5-category methods was significant and varied by up to a factor of two. This difference is mainly due to difference in the gas-aerosol partitioning of T-NO_3^-, because. ~~t~~The differences in nss-SO_4^{2-} and NH_4^+ simulated using different methods were less significant. The dry deposition of T-NO_3^- of the bulk method was smaller over land because no coarse mode NO_3^- was formed over land, where its dry deposition velocity is much larger than that of submicron NO_3^-. Consequently, compared to the other two methods, the total (i.e., nss-SO_4^{2-}, T-NH_4^+, plus T-

20 NO_3^-) dry deposition flux of the bulk method over land was smaller. On the other hand, the total dry deposition of the bulk method is larger over the ocean, where NO_3^- mixed with sea salt was the major component of T-NO_3^-. Because the bulk method assumes instantaneous equilibrium, HNO_3 reacts immediately with sea salt particles in the bulk method, whereas HNO_3 gradually reacts with sea salt in the 5-category method. Consequently, NO_3^- fractions of sea salt mass (as well as T-NO_3^- concentrations) predicted by the bulk method are larger than those of the 5-category method, which caused larger dry

25 deposition amounts of T-NO_3^- (as well as the total dry deposition) predicted by the bulk method over the ocean areas. ~~The HNO_3 gas concentration of the bulk method was generally larger than those of the 3- and 5-category methods because the bulk method contained fewer counterpart ions of NO_3^- (i.e., mineral dust) than the other two methods. Therefore, the dry deposition amount of HNO_3 gas (and so the total amount) of the bulk method was larger than that of the other two methods, especially over the ocean, where the dry deposition velocity of HNO_3 gas was much faster than that of aerosols.~~
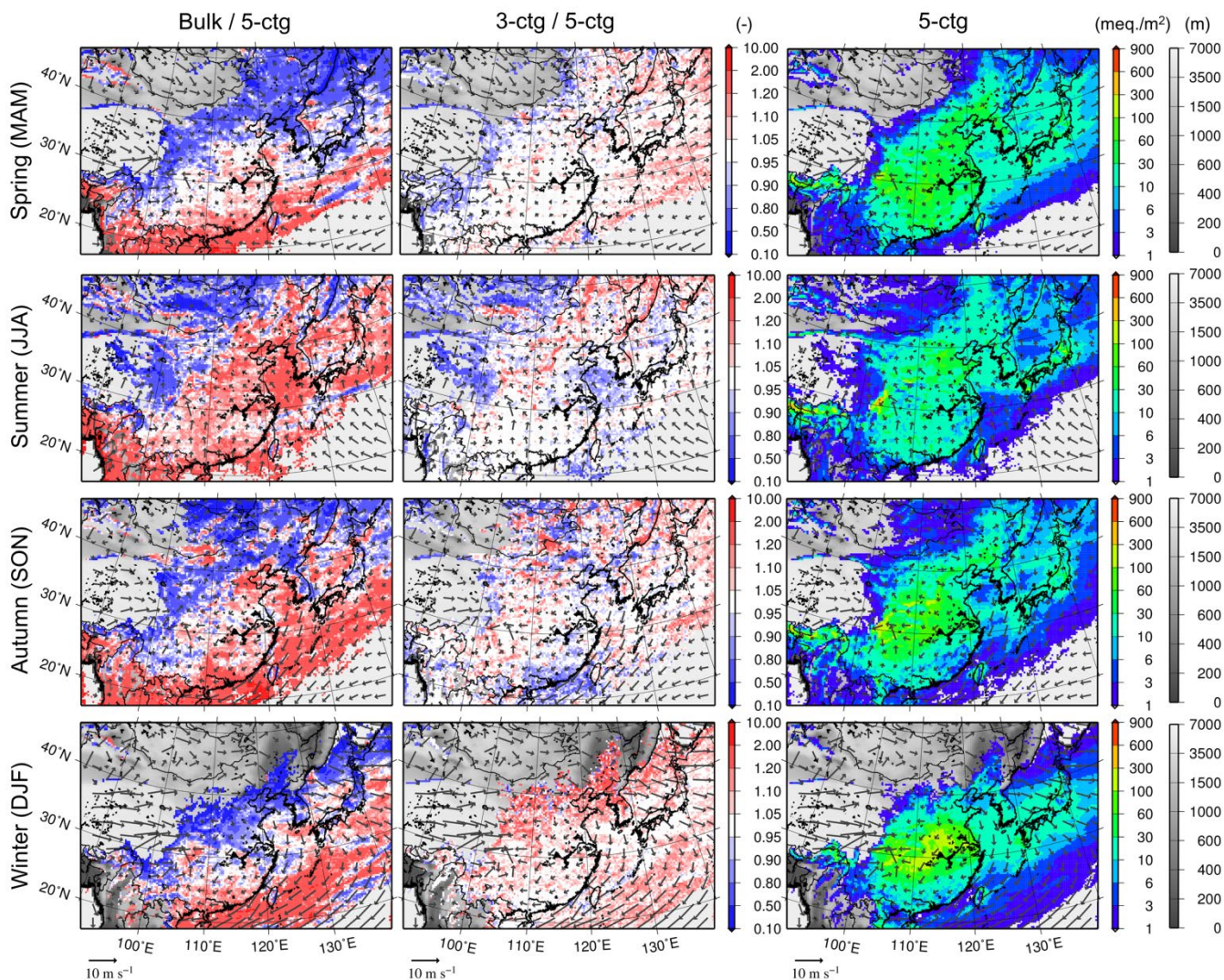
Figure 7: Same as Fig. 6 but for wet deposition.

The horizontal distribution of the wet deposition flux is patchier than that of the dry deposition flux because the horizontal distribution of precipitation is patchy, but similar patterns were found for both fluxes (Fig. 7). The difference in the fluxes between the 3-category and 5-category methods was small (lower than 10-20% in most of the domain) but larger than the difference in the dry deposition fluxes. The wet deposition of the 3-category method was generally larger than that of the 5-category method due to the overestimation of wet deposition of SO_4^{2-}, NH_4^+, and NO_3^- mixed with BC, as discussed later in Sect. 6.4.
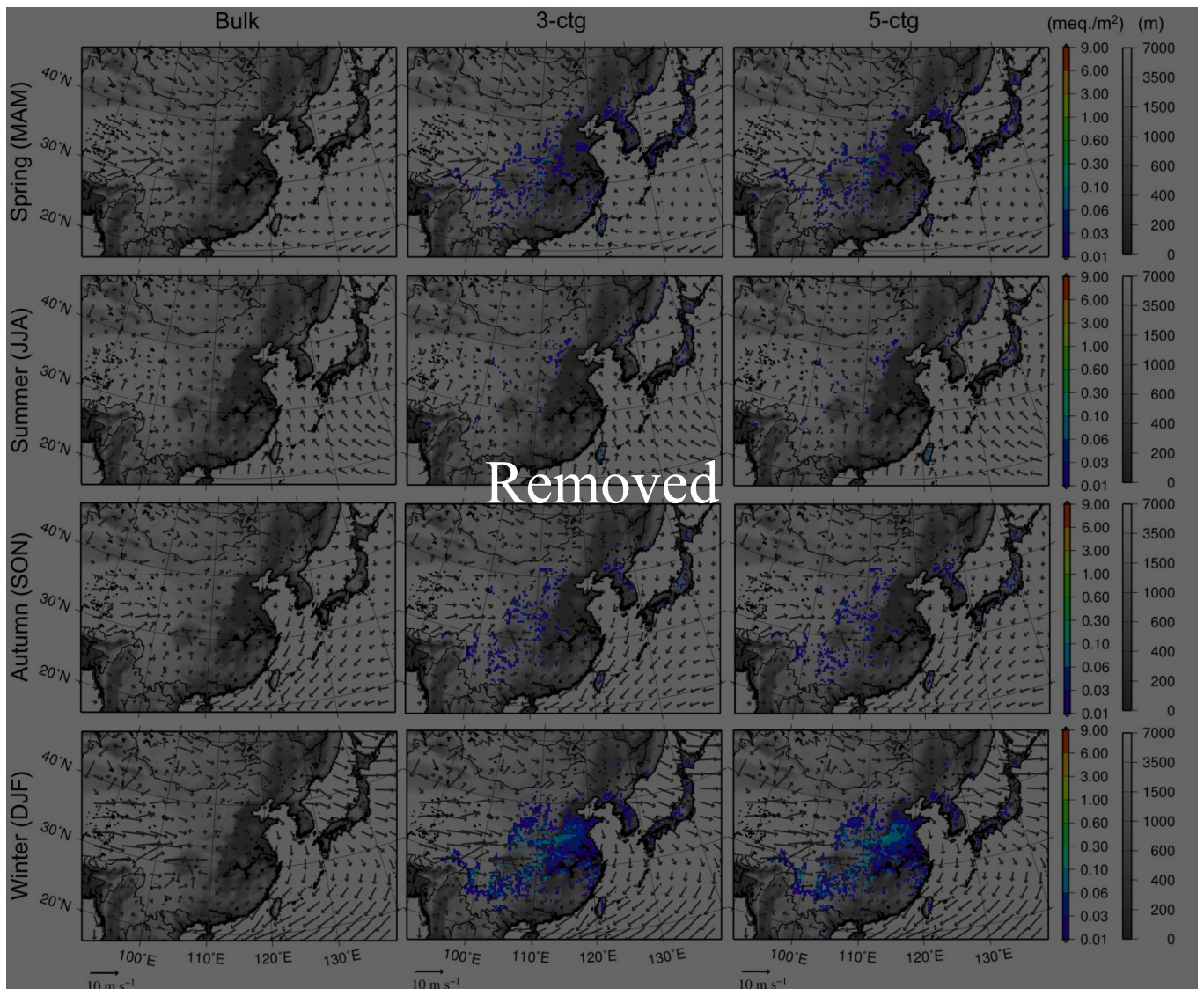
Figure 8: Same as Figs. 6 and 7 but for fog deposition for (left to right) the bulk, the 3-category, and the 5-category methods.

Fog deposition could be significantly underestimated with a crude grid resolution model, such as in the current study (Δx ~10 km), although it has been significant in local-scale simulations (Δx ~ 1 km) (e.g., Katata et al., 2011; Kajino et al., 2019b). As the grid resolution becomes cruder, the elevation and slope of the model terrain are more flattened so that the upslope fog formation is underestimated, and in many cases, the low-level clouds cannot reach the model ground surface. It is well known that fog deposition over mountain forests is proportional to elevation (e.g., Katata et al., 2011). The figures are not presented in the main text, Howeverhowever, implementation of a fog deposition scheme was a feature of the current

model; the simulated inorganic deposition due to fog is presented and discussed in Supplement 5 and Fig. 8S5-1. The fog deposition amounts were generally 1-2 orders of magnitude smaller than those of the dry and wet depositions. The fog deposition amounts of the bulk method are remarkably smaller than those of the other nonequilibrium methods. This is simply because submicron aerosols are smaller in the bulk method because the aerosol microphysical processes are not taken into account. Thus, a major proportion of the submicron aerosols of the bulk method cannot be activated as fog droplets with such low supersaturation conditions for fog formation. The fog occurrence was higher in the colder seasons, and thus, the deposition areas were smallest in the summer, except in Taiwan. In Taiwan, fog deposition was highest in the summer. Larger deposition areas are found over the high topography with highly vegetated regions in the spring, autumn, and winter. The largest deposition areas are observed over the North China Plain in the winter, associated with the increase in the radiation fog frequency and air pollution levels in winter.

Figure 98: Same as Figs. 34-7 but for AOT (at 500 nm) below approximately 1 km AGL. The wind vectors are also averaged within 1 km AGL.

6.4 Aerosol optical thickness

Figures 98 and 109 compare the three methods in terms of their predictions of AOT and AAOT at a wavelength of 500 nm integrated from the ground surface up to approximately 1 km AGL, respectively.

AOT and AAOT are both referred to as climate-relevant variables and so the simulations of the 3-category and 5-category methods are intercompared (the bulk method was not designed for the aerosol feedback studies). However, because data assimilation of AOT observed by satellites is often associated with the operational forecast of aerosol mass

concentrations, the bulk method is compared against the other two methods for AOT as presented in Fig. 8. In Figs. 9-11, only the results of the 3-category and 5-category methods are presented and compared.

The Mie theory calculation was performed to derive the AOT and AAOT at wavelengths of 500 nm by using simulated log-normal size distribution parameters and chemical compositions. The refractive indices of the Optical Properties of Aerosols and Clouds (OPAC) database (Hess et al., 1998) were used for the Mie calculation. For the refractive indices of the model components of UID, BC, OM, MD, NS, SO_4^{2-}, NH_4^+, NO_3^-, Cl^-, and H_2O, the databases of "insoluble", "soot", "insoluble", "mineral", "sea salt", "water soluble", "water soluble", "water soluble", "sea salt", and "fog" values, respectively, were used, with some modifications for BC to 1.85 0.71i (Bond et al., 2006) and MD to 1.5 0.001i (Aoki et al., 2005) at 500 nm. To calculate the optical properties of non-light-absorbing and light-absorbing mixtures, the Maxwell-Garnett approximation was used. The BC and MD masses were regarded as light-absorbing components, and the others were regarded as non-light-absorbing (certainly, some proportions of OM are light-absorbing, i.e., brown carbon, but they are not considered in the current model). The volume-weighted refractive indices were used for the light-absorbing and non-light-absorbing components in each category.

The comparisons between the simulated and observed AOT, SSA, and Ext_T are listed in Table 4, and the simulated and observed daily variations are compared in Fig. S3-5. The simulated AOT was underestimated by 50-60% (Table 4). There may be two reasons for this underestimation: the underestimation of upper atmospheric aerosol concentrations or the overestimation of the ratios of mass concentration to extinction coefficient (MEF: the mass/extinction conversion factor, as defined in Sugimoto et al., 2011). Considering that the simulated mass (PM$_{2.5}$, PM$_{2.5}$ (pile up), and PM$_{10}$) quantitatively agreed with the observed mass (PM$_{2.5}$) or slightly underestimated the observed mass by 20-30% (PM$_{2.5}$ (pile-up) and PM$_{10}$) and that the degrees of underestimations of AOT and Ext_T were similar (50-60% and 45-50%, respectively), the underestimation of Ext_T could be due to the overestimation of MEF. The simulated SSA was underestimated by 5 10%, with an observed median of 0.96 (Table 4). Therefore, the values in Fig. 9 (AOT within 1 km) could be underestimated by approximately 50%, whereas the values in Fig. 10 (AAOT within 1 km) could be overestimated by 50-100%. One of the main purposes of the development of the 5-category method was to more realistically simulate the physical and chemical properties of BC-containing particles. The statistical scores of SSA predicted by the 5-category method are better than those predicted by the other two methods, which could support consistent implementation of the 5-category method.
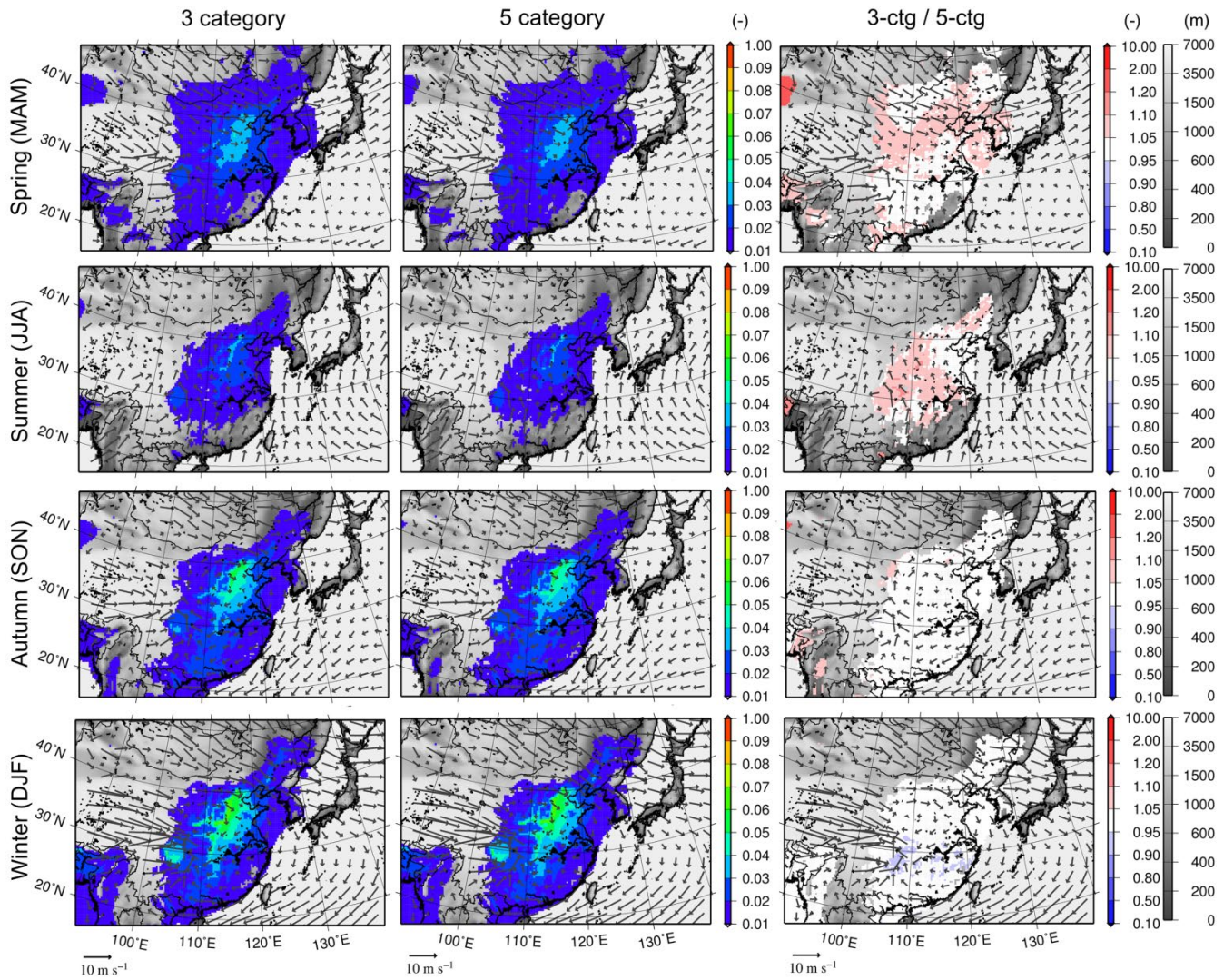
Figure 910: ~~Same as Fig. 9 but~~Seasonal mean ~~for~~ AAOT (at 500 nm) in (top to bottom) spring, summer, autumn, and winter of 2006 for (left to right) the 3-category method and the 5-category method and the corresponding ratio of the 3-category to 5-category methods.

Aerosol size distribution is an important parameter for aerosol-cloud-radiation interaction modeling, but the bulk method does not simulate aerosol microphysical processes. Therefore, the bulk method results are not discussed in detail, but the differences between the bulk method results and those from the other two methods considered are large (up to a factor of two, left panels of Fig. 89). It is only noted here that using different assumptions of size and mixing state (i.e.,

10   different settings among the three methods) could cause significant differences in the AOT simulation. This difference should be taken into account when the operational forecast of mass concentration using the bulk method is associated with the data assimilations of optical properties such as AOT. In the large emission source regions and their downwind

regions, the differences in AOT between the 3-category and 5-category methods were small, i.e., smaller than 10% in most of the domain and seasons. The large difference over the Indian Ocean near the west and south boundaries of the domain in the summer was due to differences in the internal/external mixture assumptions of soot/soot-free and dust/sea salt at the lateral boundaries. In Fig. ~~10~~9, the 3-category AAOT was slightly larger over the large emission source and their downwind regions (up to 10%). This was due to the overestimation of the so-called lensing effect (i.e., absorption enhancement by a light-absorbing agent coated by a non-light-absorbing agent; e.g., Bond et al., 2006) by the 3-category method, as the soot particles are coated by all of the soot-free components. This is also true for the bulk method. Due to the larger submicron NO_3^-, the overestimation of the lensing effect should be most significant in the bulk method. This trend is also observed in Table 4: *Sim:Obs* of SSA of the 5-category, 3-category, and bulk methods were 0.95, 0.91, and 0.90, respectively. On the other hand, the internal mixture assumption of the 3-category method caused the overestimation of the wet scavenging rates of soot and dust because the soot/soot-free and dust/sea salt particle mixture assumption could make the soot and dust particles larger and more hygroscopic. Consequently, the AAOT of the 3-category method was sometimes smaller than that of the 5-category method over the downwind regions, but this difference was small (up to 10%). Figure ~~11~~10 shows the total (dry + wet) deposition of BC and the differences between the 3- and 5-category methods. Because the dry deposition velocity of BC is very small, most BC deposition occurred due to wet deposition processes (also indicated by its patchy distribution). This difference was smaller in the spring and summer (reaching overestimation values of up to 10%) and largest in the winter (20-100%) due to the internal mixture assumption of soot and soot-free particles. Overestimation of the 3-category AAOT was more pronounced in the spring and summer than it was in the winter (Fig. ~~10~~9) because condensation of secondary pollutants to BC was larger in the warmer seasons and because overestimation of the 3-category wet deposition of BC was more significant in the winter (Fig. ~~11~~10). The differences in the total deposition of mineral dust between the 3- and 5-category methods were very small.
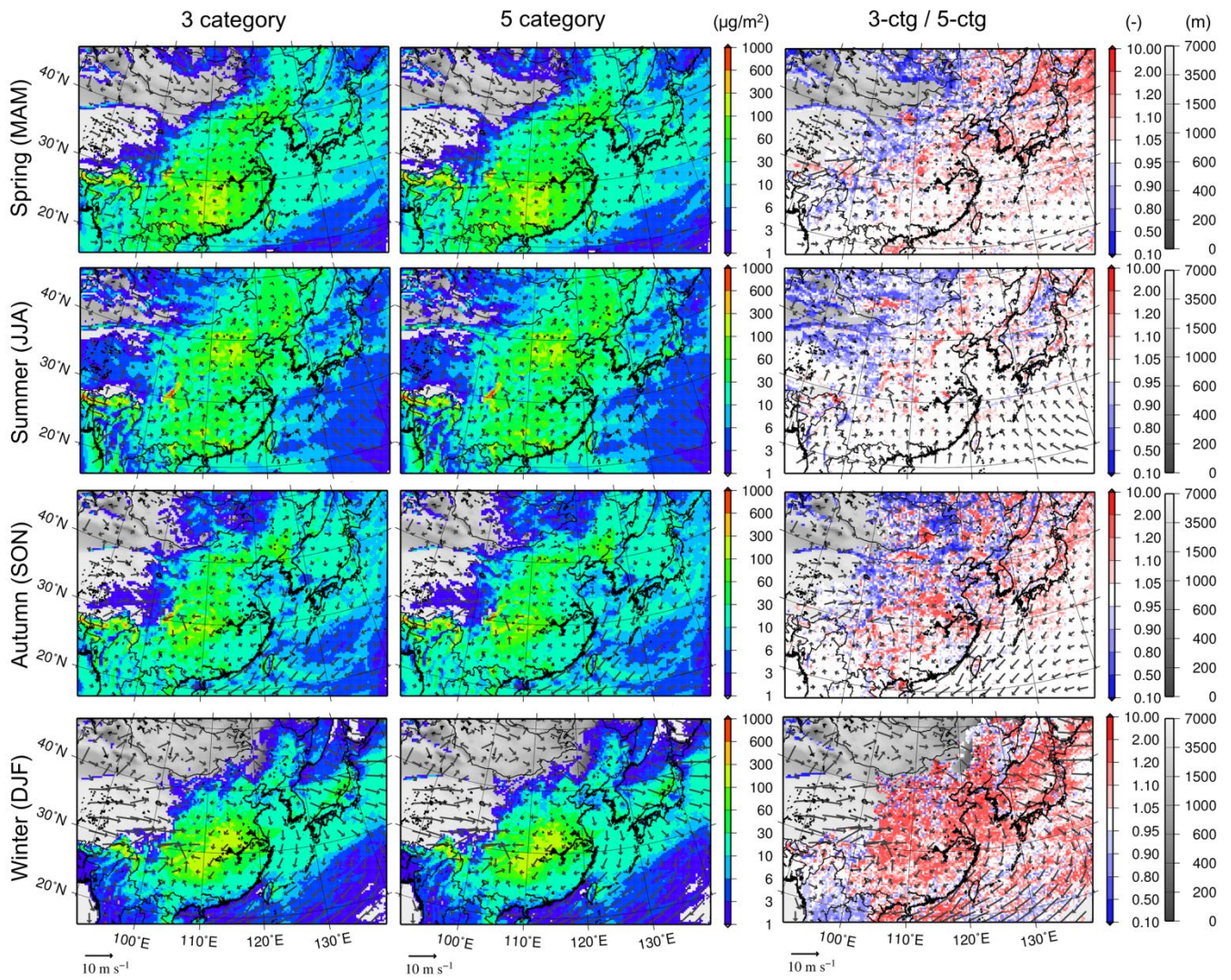
Figure 1110: Same as Figs. 6 and 79 but for the total (dry + wet) deposition of BC for (left to right) the 3-category method, the 5-category method, and the ratios of the 3-category to 5-category methods.
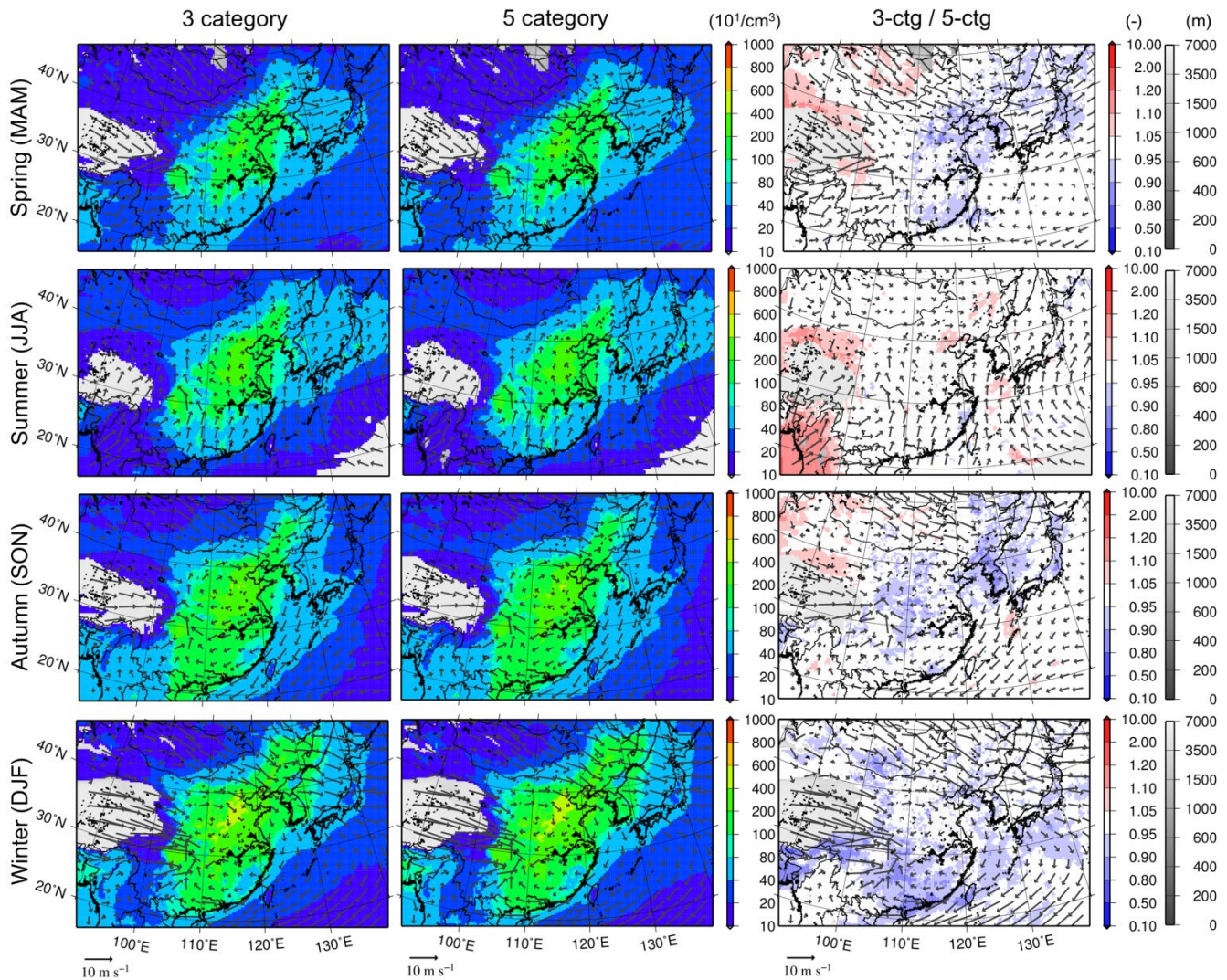
Figure ~~12~~11: Same as Figs. 9 and 10 but for the averaged CCN number concentration below approximately 1 km AGL at a supersaturation of 0.1%.

6.5 Aerosol-cloud interactions

The horizontal distributions of the averaged CCN at a supersaturation value of 0.1% below approximately 1 km AGL are compared in Fig. ~~12~~11. ~~There are no CCN observation data available for the year, but the $NC_{0.3}$ observed by OPC was used alternatively for the model evaluations of simulated CCN. The critical diameter of 0.3 μm corresponds to 0.035-0.041% of the critical supersaturations for κ of 0.3-0.4 (Petters and Kreidenweis, 2007). The OPC data are only available from March to April and November to December 2006 at Hedo. The statistical scores for $NC_{0.3}$ are listed in Table 4. Those of PM_{10} for the~~

10   Whereas the differences in the total CCN between the two methods were very small (up to 10%) (Fig. 12), significant differences were observed for some components and occasions of CCN. Figs. 123-156 illustrate the scatter diagrams of the simulated daily mean, below-1-km-AGL-averaged, CCN (of the 3- and 5-category methods and at supersaturations of 0.1% and 1%) and mass concentrations of all of the model grids, excluding 10 grids from the four lateral boundaries. The numbers of points in the scatter diagrams were randomly reduced to one-twentieth of their value to avoid too many overlaps of
15   symbols. The two supersaturation levels of 0.1% and 1% were used for this evaluation as the typical ranges of stratiform and convective clouds (Seinfeld and Pandis, 2006).
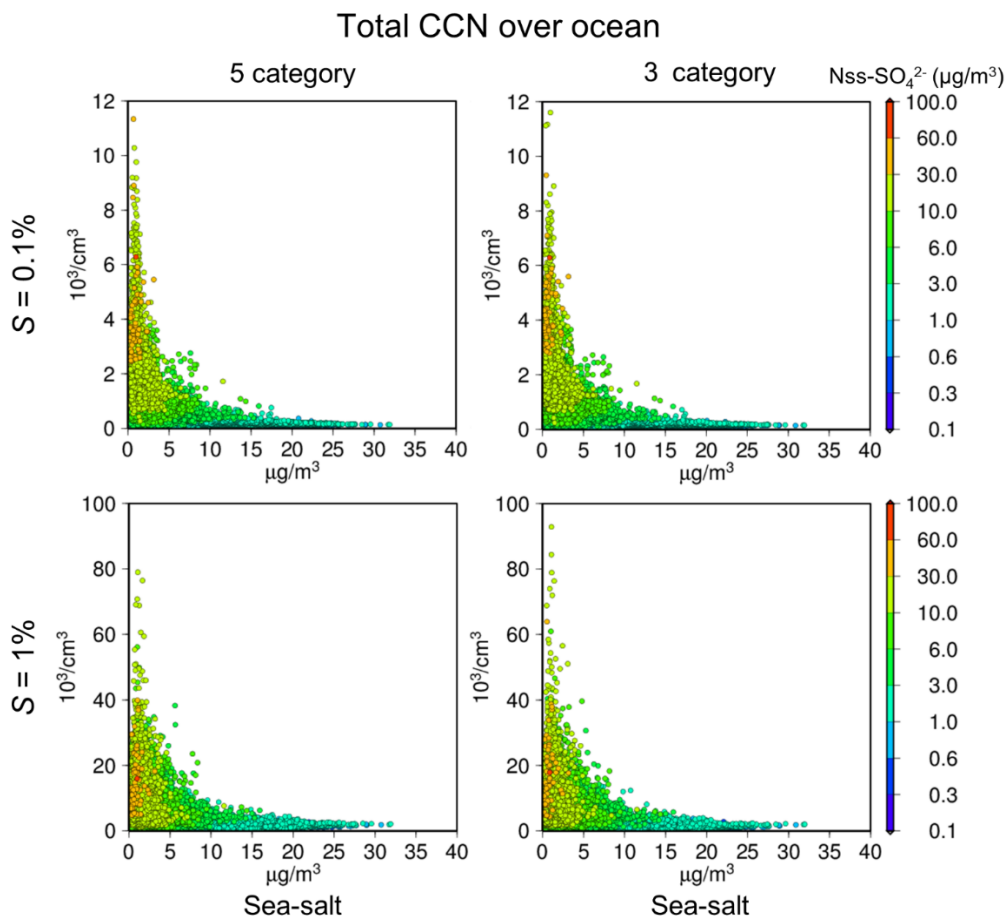
Figure 123: Scatter diagrams between the daily mean, averaged below 1 km AGL, total CCN number concentrations (y-axis) and dry mass concentrations of sea salt (x-axis) with nss-SO$_4^{2-}$ concentrations (colors) over the ocean grids for 2006. The number of data points was randomly reduced to approximately one-twentieth to avoid too much overlapping of the points at supersaturation conditions of (top) 0.1% and (bottom) 1% for (left) the 5-category and (right) 3-category methods.

Figure 132 shows the relationship between the total CCN and the sea salt mass over the ocean. In meteorological models, CCN spectra (i.e., the relationship between supersaturation and CCN) are often prescribed, and the CCN over the ocean is often assumed to be one order of magnitude lower than that over land (e.g., Rasmussen et al., 2002). However, as the ocean regions in the model domain were located downwind of the large emission source regions, the CCN could be as large as that over the land (e.g., Koike et al., 2012). The simulated total CCN over the ocean areas was up to two and three orders of magnitude larger than the simulated sea salt particles for both 0.1% and 1% supersaturations, respectively (the simulated total CCN reached up to approximately 10^4 and 10^5 cm^{-3} at 0.1 and 1%, respectively, while number concentrations of sea salt particles were approximately 100 cm^{-3} for the mass of 100 µg m^{-3}). The CCN at 1% was one order of magnitude larger than that at 0.1%. The CCN over the ocean was not correlated with the sea salt mass concentration. The CCN was proportional to the nss-SO$_4^{2-}$ concentrations, an indicator of anthropogenic secondary particles. These results indicate the

importance of considering spatiotemporal variations of CCN spectra in the meteorological models, rather than using the prescribed ones that depend only on the LUC (e.g., ocean or land). The CCN difference between the 3-category and 5-category methods was small, such that the difference in the aerosol-cloud interaction due to CCN changes predicted by the two methods over the ocean could also be small.
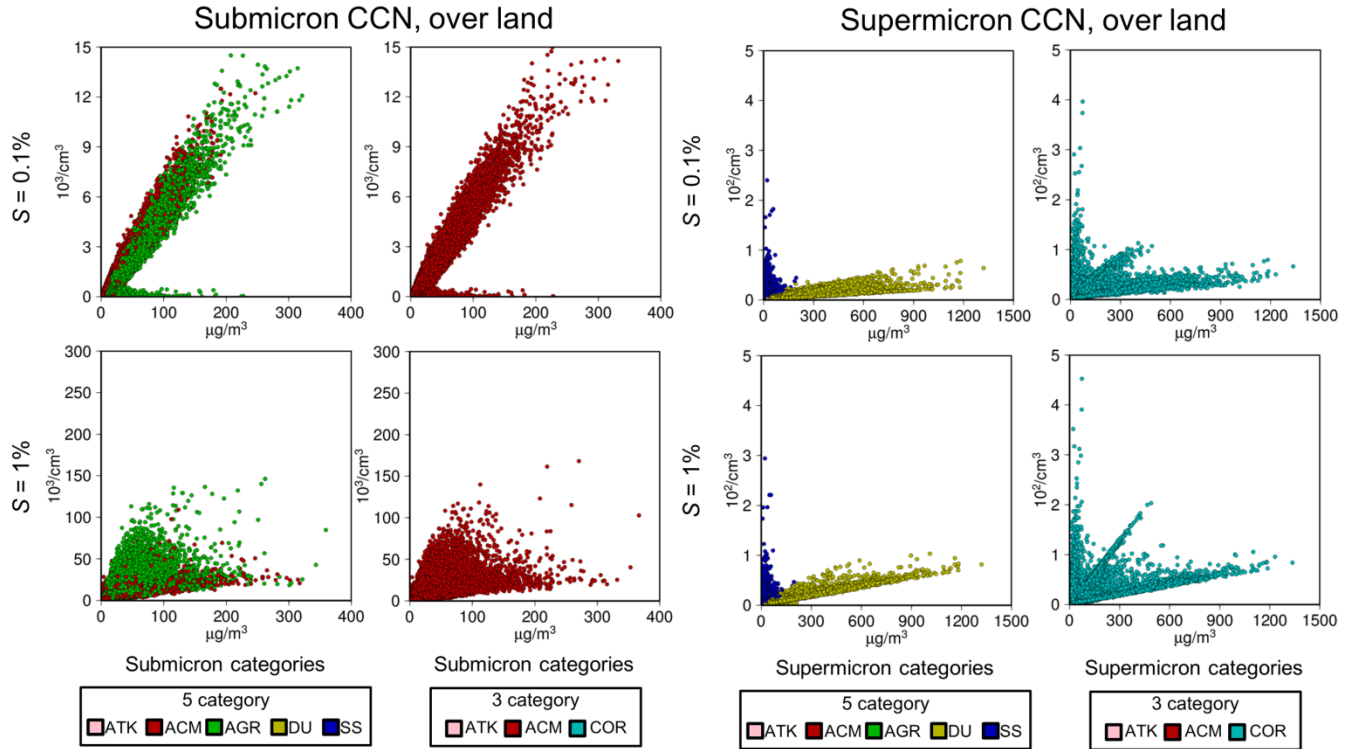
Figure ~~14~~13: Scatter diagrams between the daily mean, averaged below 1km AGL, ~~Same as Fig. 13 but for~~ CCN number concentration (y-axis) over the land grids at supersaturation of (top) 0.1% and (bottom) 1% from (left four panels) submicron categories (i.e., ATK, ACM, and AGR for the 5-category method and ATK and ACM for the 3-category method) and (right four panels) supermicron categories (i.e., DU and SS for the 5-category method and COR for the 3-category method). The x-axes are the total dry mass concentrations of the submicron (left four panels) and supermicron (right four panels) categories. The colors of the dots correspond to those of the categories in the legends with the most dominant mass concentrations of the grids.

15   Figure ~~14~~13 shows the differences in CCN over land. The submicron CCN at 1% was one order of magnitude larger than that at 0.1%. The difference in supermicron CCN between 0.1% and 1% was not very significant because the larger particles are CCN active at lower supersaturation. There was no difference for hygroscopic sea salt particles, whereas there was a slight difference for less hygroscopic dust particles. Due to the internal mixture assumption of soot and soot-free particles, the CCN at 0.1% of the 3-category method was slightly larger than that of the 5-category method. If the model assumes a constant size distribution of submicron particles, all of the points are aligned on a single line. Thus, the width of

the aggregations of points indicates the uncertainty or variability of the simulated size distribution of aerosols. The CCN at 0.1% can vary by approximately 2-fold (e.g., it ranges from 3-6 $\times 10^3$ cm^{-3} at 100 μg m^{-3} of aerosol mass). The variation (or width) was much larger at 1%, reaching approximately 1 order of magnitude (5-80 $\times 10^3$ cm^{-3} at 50 μg m^{-3}) because smaller particles can be activated and contribute less to the bulk mass concentration. The accurate prediction of the aerosol population is much more important for the submicron CCN at higher supersaturation values. For supermicron CCN, there are apparent differences in the gradients of lines originated to mineral dust and sea salt in both methods. However, there is one intermediate line in addition to the dust and sea salt lines in the 3-category method, which is the result of the unrealistic internal mixture of dust and sea salt. Overall, it is safe to presume that the difference in the aerosol-cloud interaction due to CCN changes predicted by these two methods over land could be small due to the absence of sea salt particles.
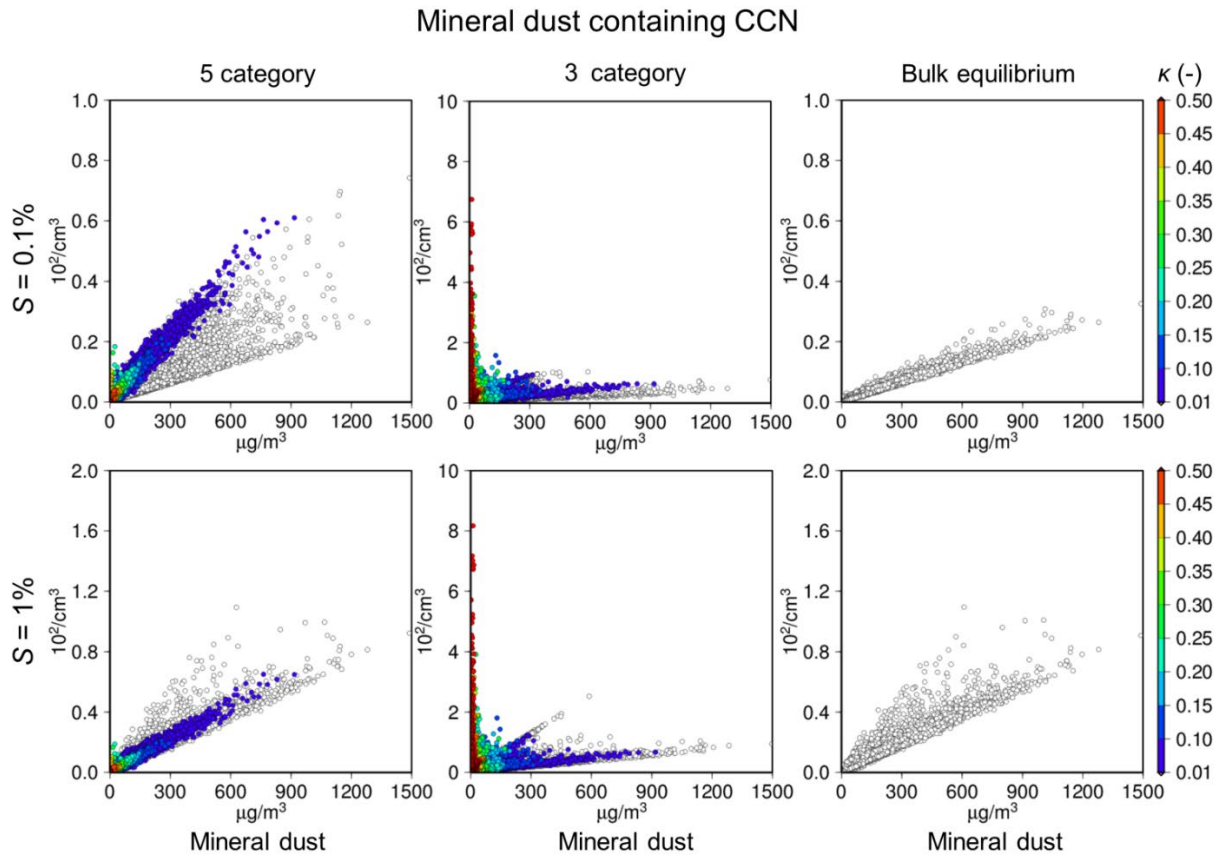
Figure 145: ~~Same as Fig. 13~~ Scatter diagrams between the daily mean, averaged below 1km AGL, ~~but for the~~ mineral dust-containing CCN (y-axis) at supersaturation of (top) 0.1% and (bottom) 1% and mineral dust dry mass concentration (x-axis) with hygroscopicity κ (colors) for (left to right) the 5-category, 3-category, and bulk methods. The circles are white if κ is smaller than 0.01.

Figure ~~15~~ 14 illustrates the relationship between mineral dust containing CCN and the mineral dust mass concentrations. Because dust is assumed to be inert and κ is assumed to be zero in the bulk method, the CCN at 0.1% is proportional to only the mineral dust mass concentration, while the variation in the size distribution is more important for the CCN at 1%. Because the hygroscopic growth of mineral dust is considered in the 5-category method, the dust-containing

5   CCN is up to several times larger than that of the bulk method (from 0.1 to 0.4 $\times 10^2$ cm^{-3} at 600 μg m^{-3}). As previously mentioned, the unrealistic internal mixture of dust and sea salt in the 3-category method caused unrealistic gradients, i.e., one that is colored in red (sea salt with tiny dust mass) and a line in between (approximately at $x = 600$ μg m^{-3} and $y = 2.5 \times 10^2$ cm^{-3}) that can be clearly seen at 1% (sea salt/dust mixture). The simulated difference in dust-containing CCN would have almost no impact on CCN-cloud-precipitation interaction processes because its number concentration was much smaller than

10   that of submicron particles. As mineral dust is an efficient IN~~P~~ (e.g., Lohmann and Diehl, 2006), it should be noted here that this difference can have significant impacts on IN~~P~~-cloud-precipitation interaction processes, especially with immersion ~~and condensation~~ freezing (i.e., the freezing of supercooled water droplets containing ~~ice nuclei~~INP).
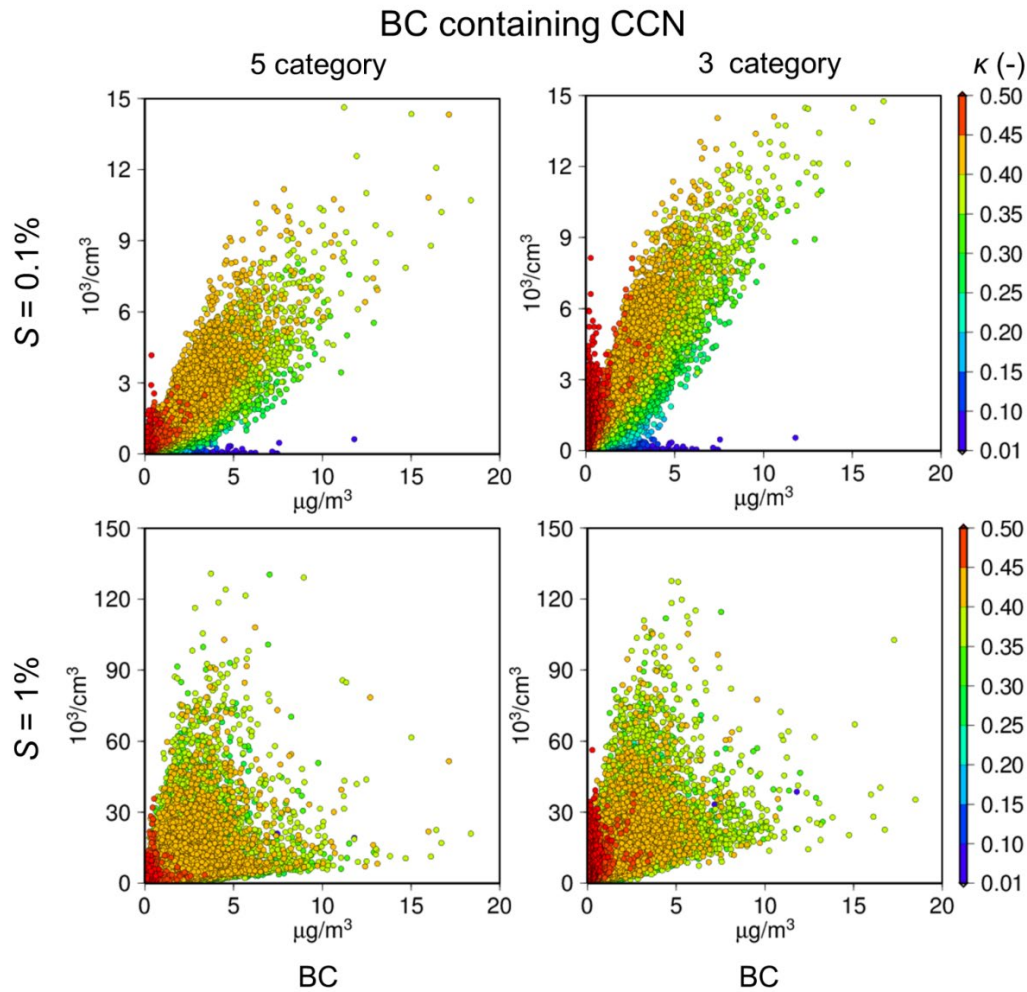
Figure 1~~5~~6: ~~Same as Fig. 15 but~~ Scatter diagrams between the daily mean, averaged below 1km AGL, ~~for the~~ BC-containing CCN (y-axis) at supersaturation of (top) 0.1% and (bottom) 1% and BC dry mass concentration (x-axis) with hygroscopicity κ (colors) for (left) the 5-category and (right) 3-category methods.

Despite the external mixture treatment of soot and soot-free particles in the 5-category method, the difference in the total submicron CCN between the 5- and 3-category methods was found to be minor (Fig. 1~~3~~4). However, the simulated BC-containing CCN values of the two methods were different, as shown in Fig. ~~16~~15. The BC-containing CCN of the 3-category method at 0.1% was generally 1.5 times larger than that of the 5-category method (e.g., up to 9 and 6 $\times 10^3$ cm^{-3} at 4 μg m^{-3}, respectively) because the absence of BC-free particles causes excess amounts of coatings on BC-containing particles (Oshima et al., 2009b). This difference caused higher BC deposition to be simulated by the 3-category method, as presented in Fig. ~~11~~10. However, the difference in the BC-containing CCN of the two methods at 1% was not as large as that at 0.1% because the CCN number concentration at higher supersaturation was not affected by hygroscopicity.

7 Conclusion and discussion

This study provides a comparison of aerosol representation methods implemented in a regional-scale meteorology-chemistry model (NHM-Chem). Three methods are currently available: the 5-category nonequilibrium (Aitken, soot-free accumulation, soot-containing accumulation, sea salt, and dust), 3-category nonequilibrium (Aitken, accumulation, and coarse), and bulk equilibrium (submicron, sea salt, and dust) methods. The three methods were intercompared for the predictions of air quality and climate-relevant variables. In this study, surface concentrations and depositions, which negatively impact the human health and environment, are referred to as air quality variables, whereas variables which can alter the earth's energy budget and water cycles through the aerosol-cloud-radiation interaction processes such as optical properties and cloud and ice nucleation properties are referred to as climate-relevant variables.

The 3-category method is widely used in three-dimensional air quality models. The 5-category method, the standard method of NHM-Chem, was an extensional development of the 3-category method to improve the predictions of ~~regional climate, including~~ aerosol-cloud-radiation interaction~~s~~ processes, by implementing separate treatments of light absorbers and ice nuclei particles, namely, soot and dust, from the accumulation and coarse mode categories (implementation of aerosol feedback processes to NHM-Chem is still ongoing). The bulk equilibrium method was developed for operational air quality forecasting with simple aerosol dynamics representations to yield the computational efficiency. The total CPU time of the 5-category and 3-category methods were 91% and 44 greater than the bulk equilibrium method, respectively. ~~The number of tracers in the 5-category, 3-category, and bulk methods are 108, 96, and 78, respectively (they each contain 58 common gases and 50, 38, and 20 aerosol attributes, respectively).~~ The main objective of the study is to quantify the deviations of the widely used 3-category method and the efficient bulk equilibrium method from the most realistic aerosol representation of NHM-Chem, the 5-category method and to discuss the magnitude of deviations.

~~The total CPU times of the 5-category and 3-category methods were 91% and 44% greater than that of the bulk method, respectively.~~

The bulk equilibrium method was evaluated for the eligibility of ~~shown to be eligible for~~ operational forecast ~~purposes~~, namely, the surface mass concentrations of air pollutants such as O_3, mineral dust, and $PM_{2.5}$. The differences in the simulated seasonal mean concentrations between the bulk method and ~~the reference method, i.e.,~~ the 5-category method, were smaller than 5% and 5-10% for O_3 and mineral dust, respectively. ~~The initial and boundary conditions should be improved before model formulation.~~ The difference in $PM_{2.5}$ was large, i.e., up to 20-100%, due to the neglection of nitrate mixed with dust particles of the bulk equilibrium method. Still, however, the statistical scores of the bulk method regarding $PM_{2.5}$ were not very different from the other methods. In order to fill the gap between observations and simulations, operational forecast is associated with data assimilation and post-process of statistical bias correction. The bulk method is not used in recent air quality models any more. Still, however, as the model performances were similar with each other, the faster bulk equilibrium method can be recommended for the use of operational forecast. ~~Improving the model formulation, as well as its initial and boundary conditions, is needed.~~

The 3-category method was shown to be eligible for air quality simulations, namely, surface concentrations and depositions of bulk chemical species. The differences in the simulated seasonal mean bulk mass concentrations ($PM_{2.5}$ (pile-up)) and dry and wet depositions of major inorganic components ($SO_4^{2-} + NH_4^+ + NO_3^-$) between the 3-category method and the reference method were smaller than 5%, 5%, and 10%, respectively. However, the internal mixture assumption of soot/soot-free and dust/sea salt particles in the 3-category method resulted in significant differences in the size distribution and hygroscopicity of the particles. The differences in $PM_{2.5}$, defined by the simulated size distribution, between the 3- and 5-category methods were 20-100%.

Although the 3-category method was not designed to simulate aerosol-cloud-radiation interaction processes, its performance in terms of total properties, such as AOT and CCN, was acceptable compared to that of the reference method (i.e., both differences were smaller than 10%). However, some specific parameters exhibited significant differences or systematic errors. For example, the unrealistic dust/sea salt complete mixture of the 3-category method induced significant errors in the prediction of mineral dust-containing CCN. The overestimation of soot hygroscopicity by the 3-category method induced errors in BC-containing CCN at a supersaturation of 0.1% (overestimation by ~50%), BC deposition (overestimation by 20-100%), and AAOT (difference of < 10%). In contrast, the difference in AAOT was less pronounced because the overestimation of the absorption enhancement was compensated by the overestimation of hygroscopic growth and the consequent loss due to in-cloud scavenging. The 5-category method requires more computational resources than the 3-category method (44% in CPU time and 12.5% in number of tracers, i.e., memory and storage). It should be case dependent which method is recommended but the 5-category method tends to be more accurate when the sea-salt and dust coexist in the same air mass (such as Gobi dust transport over the Northwest Pacific Ocean or the Saharan dust transport over the Mediterranean Sea and the Atlantic Ocean) or when concerning the light absorption and INP activity of BC and dust in the aerosol-cloud-radiation interaction system.

~~For the operational forecast, the simulation time is critical; thus, the bulk method is recommended. On the other hand, for research purposes, because the difference in the computational resources between the 5-category and 3-category methods is not very large (44% in CPU time and 12.5% in number of tracers, i.e., memory and storage), the 5-category method is regarded as the standard (default) aerosol option of NHM Chem.~~

The modal approach was used in the current aerosol microphysics module, but the same conclusion can also be inferred for the sectional (or bin) approaches in terms of the advantage of the 5-category approach, namely, the soot and dust sections should be separated from the light-scattering hygroscopic particle section for detailed investigations of aerosol-cloud-radiation interactions. There is a 12-category method that was implemented in a regional model (Glassmeier et al., 2017). This is currently the ultimate representation of the category method in 3-D CTMs. It is necessary to compare our 3- and 5-category methods to the 12-category approach as a benchmark simulation. The optimization of computational efficiency against complexity (and accuracy) of the aerosol mixing state representations should be achieved via particle analysis studies performed by electron microscopy and particle-resolved models.

There are still large discrepancies between the simulation and observation results, but the reasons are still unclear. In order to identify the reasons and improve NHM-Chem, further ~~. Furthermore, model~~ evaluations should be made ~~in the near future~~ with respect to spatial distributions (using satellites), vertical profiles (using sonde, aircraft, satellite, and lidar),

and aerosol size distributions (using such as scanning mobility particle sizer (SMPS), aerodynamic particle sizer (APS),

5   polarized optical particle counter (POPC) methods). ~~for improving NHM-Chem. In particular, model validations using the size distribution and vertical profile measurements are indispensable to identify the reason for the underestimation of AOT and Ext_T by the current model.~~ There have been tremendous advancements in new particle formation, organic chemistry, and ice nucleation studies. ~~This~~ These new knowledge~~s~~ should be ~~timely and properly~~immediately reflected in the modeling framework.

10   ~~The aerosol module comparison should be performed again in the future after substantial improvements in NHM-Chem are made, as the sensitivity could be different from the current simulations.~~ To evaluate the significance of separate soot and dust treatments in the 5-category method in terms of aerosol-cloud-radiation interaction processes, online simulation with a chemistry-to-meteorology feedback process is required. The sensitivity of aerosol-cloud-radiation interactions to the three aerosol modules will be assessed in future ~~after the installation of feedback processes to~~by the online

15   coupled NHM-Chem with the feedback processes.

Code and data availability

The NHM-Chem source code is available subject to a license agreement with the Japan Meteorological Agency. Further information is available at https://www.mri-jma.go.jp/Dep/glb/nhmchem_model/application_en.html (last access: 1 October 2020). The simulation results are free to use. The simulated and observed data used in the manuscripts are available at

20   https://mri-2.mri-jma.go.jp/owncloud/s/ASBzHdtqy9ZpbB4 (last access: 14 September 2020). The raw observation data of EANET, SKYNET, and AD-Net can be obtained from the web sites as described in Sect. 5.

Author contribution

MK designed the current research. MK mainly developed the offline coupled model with MD, who developed its online coupled version. MK and MD collaborated with TTS, NO, KY, TYT, JC, AH, MI, AK, YI, SS, KA, YZ, YI, and TM during

25   model development. MK performed the simulations, which were evaluated by the observation data provided by TY, MM (Miyashita), PK, AS, and HI. YI, HU, TM, and MM (Mikami) cosupervised this study.

Competing interests

The authors declare that they have no conflict of interest.

Acknowledgments

This work was mainly supported by the Fundamental Technology Research of MRI (M5 and P5), the Integrated Research Program for Advancing Climate Models (TOUGOU) Grant Number JPMXD0717935561 and Arctic Challenge for Sustainability II (ArCS II), Grant Number JPMXD1420318865 from the Ministry of Education, Culture, Sports, Science, and Technology Japan (MEXT), and Research Institute for Humanity and Nature (RIHN: a constituent member of NIHU) Project No.14200133 (Aakash). This work was also supported by the Japanese Society for the Promotion of Sciences (JSPS) KAKENHI Grant Numbers JP19H01155, JP16KK0018, JP19F19402, JP19H02649, JP18H03363, JP18H05292, and JP2000636) and the Environment Research and Technology Development Fund (JPMEERF20165005, JPMEERF20172003, JPMEERF14S11203, JPMEERF20202003, and JPMEERF20205001) of the Environmental Restoration and Conservation Agency of Japan and in part by a grant for the Global Environmental Research Coordination System from the Ministry of Environment, Japan (MOEJ) (MLIT1753). The authors thank Dr. Toshinori AOYAGI of the JMA, Prof. Mitsuo OHIZUMI of Meteorological College, and Drs. Hiroaki NAOE, Masashi NIWANO, and Masaya NOSAKA of the MRI for their useful comments on model developments. The authors are deeply grateful for the support of Mr. Shohei SUZUKI and Mr. Kazuki ITO of the University of Tsukuba for the visualization of simulation and observation data and Ms. Kyoko KANEBA for the comments on the manuscript. The authors also thank the Kagoshima Meteorological Office and Aso Volcano Disaster Prevention Council for providing the volcanic SO_2 emission measurement data of Mt. Sakurajima and Mt. Aso, respectively.

References

Andronache, C., Grönholm, T., Laakso, L., Phillips, V., and Venäläinen, A.: Scavenging of ultrafine particles by rainfall at a boreal site: observations and model estimations. Atmos. Chem. Phys., 6, 4739-4754, 2006.

Aquila, V., Hendricks, J., Lauer, A., Riemer, N., Vogel, H., Baumgardner, D., Minikin, A., Petzold, A., Schwarz, J. P., Spackman, J. R., Weinzierl, B., Righi, M., and Dall'Amico, M.: MADE-in: a new aerosol microphysics submodel for global simulation of insoluble particles and their mixing state, Geosci. Model Dev., 4, 325-355, https://doi.org/10.5194/gmd-4-325-2011, 2011.

Aoki, T., Tanaka, T. Y., Uchiyama, A., Chiba, M., Mikami, M., Yabuki, S., and Key, J. R.: Sensitivity experiments of direct radiative forcing caused by mineral dust simulated with a chemical transport model. J. Meteorol. Soc. Jpn., 83A, 315-331, 2005.

Aranami, K., Hara, T., Ikuta, Y., Kawano, K., Matsubayashi, K., Kusabiraki, H., Ito, T., Egawa, T., Yaashita, K., Ota, Y., Ishikawa, Y. Fujita, T., and Ishida, J.: A new operational regional model for convection-permitting numerical weather prediction at JMA, CAS/JSC WGNE Research Activities in Atmospheric and Oceanic Modelling, 5, 5-6, 2015.

Bond, T. C., Habib, G., and Bergstrom, R. W.: Limitations in the enhancement of visible light absorption due to mixing state. J. Geophys. Res., 111, D20211, 13 pp, 2006.

Bond, T. C., Doherty, S. J., Fahey, D. W., Forster, P. M., Berntsen, T., DeAngelo, B. J., Flanner, M. G., Ghan, S., Kärcher, B., Koch, D., Kinne, S., Kondo, Y., Quinn, P. K., Sarofim, M. C., Schultz, M. G., Schlz, M., Venkataraman, C., Zhang, H., Zhang, S., Bellouin, N., Guttikunda, S. K., Hopke, P. K., Jacobson, M. Z., Kaiser, J. W., Klimont, Z., Lohmann, U., Schwarz, J. P., Shindell, D., Storelvmo, T., Warren, S. G., and Zender, C. S.: Bounding the role of black carbon in the climate system: A scientific assessment. J. Geophys. Res., 118, 1-173, 2013

Boucher, O., et al.: Clouds and aerosols. In: Stocker, T.F. (Ed.), Climate Change 2013: the Physical Science Basis, Working Group I Contribution to the Fifth Assessment Report of the Intergovernmental Panel on Climate Change. Cambridge Univ. Press, New York, pp. 571-657, 2013.

Burns, D. A., Lynch, J. A., Cosby, B. J., Fenn, M. E., Baron, J. S., US EPA Clean Air Markets Div.: National Acid Precipitation Assessment Program Report to Congress 2011: An integrated assessment, National Science and Technology Council, Washington, DC, 114 pp, 2011.

Byun, D., and Schere K.: Review of the governing equations, computational algorithms, and other components of the Models-3 Community Multiscale Air Quality (CMAQ) modeling system. Appl. Mech. Rev., 59, 51-77, 2006.

Carlton, A. G., Turpin, B. J., Altieri, K. E., Seitzinger, S., Reff, A., Lim, H.-J., and Ervens, B.: Atmospheric oxalic acid and SOA production from glyoxal: Results of aqueous photooxidation experiment. Atmos. Environ., 41, 7588-7602, 2007.

Carter, W.: Documentation of the SAPRC-99 chemical mechanism for VOC reactivity assessment. Final report to California Air Resources Board, Rep. 92-329, Univ. of Calif., Riverside, 8 May, 569 pp, 2000.

Chapman, E. G., Gustafson Jr. W. I., Easter, R. C., Barnard, J. C., Ghan, S. J., Pekour, M. S., and Fast, J. D.: Coupling aerosol-cloud-radiative processes in the WRF-Chem model: Investigating the radiative impact of elevated point sources. Atmos. Chem. Phys., 9, 945-964, 2009.

Chatani, S., Yamaji, K., Sakurai, T., Itahashi, S., Shimadera, H., Kitayama, K., and Hayami, H.: Overview of Model Inter-Comparison in Japan's Study for Reference Air Quality Modeling (J-STREAM). Atmosphere, 9(1), 19, 14 pp, 2018.

Chen, L., Gao, Y., Zhang, M., Fu, J. S., Zhu, J., Liao, H., Li, J., Huang, K., Ge, B., Wang, X., Lam, Y. F., Lin, C. Y., Itahashi, S., Nagashima, T., Kajino, M., Yamaji, K., Wang, Z., and Kurokawa, J.: MICS-Asia III: multi-model comparison and evaluation of aerosol over East Asia, Atmos. Chem. Phys., 19, 11911-11937, https://doi.org/10.5194/acp-19-11911-2019, 2019.

Ching, J., Riemer, N., and West, M.: Impacts of black carbon mixing state on black carbon nucleation scavenging: Insights from a particle-resolved model. J. Geophys. Res., 117, D23209, 2012.

Ching, J., Zaveri, R.A., Easter, R. C., Riemer, N., and Fast, J. D.: A three-dimensional sectional representation of aerosol mixing state for simulating optical properties and cloud condensation nuclei. J. Geophys. Res., 121, 5912-5929, 2016a.

Ching, J., Riemer, N., West, M.: Impacts of black carbon particles mixing state on cloud microphysical properties: Sensitivity to environmental conditions. J. Geophys. Res., 121, 5990-6013, 2016b.

Ching, J., J. Fast, M. West, N. Riemer, 2017: Metrics to quantify the importance of mixing state for CCN activity. Atmos. Chem. Phys., 17, 7445-7458.

Ching, J., West, M., and Riemer, N.: Quantifying impacts of aerosol mixing state on nucleation-scavenging of black carbon aerosol particles. Atmosphere, 9, 17, 17 pp, 2018.

Clarke, A. D., Owens, S. R., and Zhou, J.: An ultrafine sea-salt flux from breaking waves: Implications for cloud condensation nuclei in the remote marine atmosphere. J. Geophys. Res., 111, D06202, 14 pp, 2006.

5   Cohen, A. J., et al.: Urban air pollution, in Comparative Quantification of Health Risks: Global and Regional Burden of Disease Attributable to Selected Major Risk Factors, 1st ed., edited by M. Ezzati et al., Vol. 2, pp. 1353-1453, World Health Organization, Geneva, 2004.

Curtis, J. H., Riemer, N., and West, M.: A single-column particle-resolved model for simulating the vertical distribution of aerosol mixing state: WRF-PartMC-MOSAIC-SCM v1.0. Geosci. Model. Dev., 10, 4057-4079, 2017.

10 Deushi, M. and Shibata, K.: Development of an MRI Chemistry-Climate Model ver.2 for the study of tropospheric and stratospheric chemistry. Papers in Meteor. Geophys., 62, 1-46, 2011.

Edney, E. O., Kleindienst, T. E., Lewandowski, M., and Offenberg, J. H.: Updated SOA chemical mechanism for the Community Multiscale Air Quality model. EPA 600/X-07/025, US Environ. Prot. Agency, Durham, NC, 2007.

Facchini, M. C., Rinaldi, M., Decesari, S., Carbone, C., Finessi, E., Mircea, M., Fuzzi, S., Ceburnis, D., Flanagan, R.,
15 Nilsson, E. D., de Leeuw, G., Martino, M., Woeltjen, J., and O'Dowd, C. D.: Primary submicron marine aerosol dominated by insoluble organic colloids and aggregates. Geophys. Res. Lett. 35, L17814, 5 pp, 2008.

Fountoukis, C. and Nenes, A.: ISORROPIA II: a computationally efficient thermodynamic equilibrium model for K^+-Ca^{2+}-Mg^{2+}-NH^{4+}-Na^+-SO_4^{2-}-NO_3^--Cl^--H_2O aerosols. Atmos. Chem. Phys., 7, 4639-4659, 2007.

Ge, B., Itahashi, S., Sato, K., Xu, D., Wang, J., Fan, F., Tan, Q., Fu, J. S., Wang, X., Yamaji, K., Nagashima, T., Li, J.,
20 Kajino, M., Liao, H., Zhang, M., Wang, Z., Li, M., Woo, J.-H., Kurokawa, J., Pan, Y., Wu, Q., Liu, X., and Wang, Z.: MICS-Asia III: Multi-model comparison of reactive Nitrogen deposition over China, Atmos. Chem. Phys. Discuss., https://doi.org/10.5194/acp-2019-1083, in review, 2020.

Giglio, L., Randerson, J. T., van der Werf, G. R., Kasibhatla, P. S., Collatz, G. J., Morton, D. C., and DeFries, R. S.: Assessing variability and long-term trends in burned area by merging multiple satellite fire products. Biogeosciences, 7,
25 1171-1186, 2010.

Glassmeier, F., Possner, A., Vogel, B., Vogel, H., and Lohmann, U.: A comparison of two chemistry and aerosol schemes on the regional scale and the resulting impact on radiative properties and liquid- and ice-phase aerosol-cloud interactions, Atmos. Chem. Phys., 17, 8651-8680, 2017.

Grell, G. A., Peckham, S. E., Schmitz, R., McKeen, S. A., Frost, G., Skamarock, W. C., and Eder, B.: Fully coupled "online"
30 chemistry within the WRF model. Atmos. Environ., 39, 6957-6975, 2005.

Guenther, A., Karl, T., Harley, P., Wiedinmyer, C., Palmer, P. I., and Geron, C.: Estimates of global terrestrial isoprene emissions using MEGAN (Model of Emissions of Gases and Aerosols from Nature). Atmos. Chem. Phys., 6 , 3181-3210, 2006.

Han, Z., Ueda, H., Matsuda, K., Zhang, R.., Arao, K., Kanai, Y., and Hasome, H.: Model study on particle size segregation and deposition during Asian dust events in March 2002. J. Geophys. Res., 109, D19205, 22 pp, 2004.

Hess, M., Koepke, P., and Schult, I.: Optical properties of aerosols and clouds: the software package OPAC. B. Am. Meteorol. Soc., 79(5), 831-844, 1998.

5   Itahashi, S., Ge, B., Sato, K., Fu, J. S., Wang, X., Yamaji, K., Nagashima, T., Li, J., Kajino, M., Liao, H., Zhang, M., Wang, Z., Li, M., Kurokawa, J., Carmichael, G. R., and Wang, Z.: MICS-Asia III: overview of model intercomparison and evaluation of acid deposition over Asia, Atmos. Chem. Phys., 20, 2667–2693, https://doi.org/10.5194/acp-20-2667-2020, 2020.

Jacob, D. J.: Heterogeneous chemistry and tropospheric ozone. Atmos. Environ., 34, 2131-2159, 2000.

10   Jacobson, M. Z.: Analysis of aerosol interactions with numerical techniques for solving coagulation, nucleation, condensation, dissolution, and reversible chemistry among multiple size distributions. J. Geophys. Res., 107, D19, 4366, 2002.

JMA: The next generation non-hydrostatic model ASUCA. Suuchi Yohoka Hokoku Bessatsu (Additonal Volume to Report of Numerical Prediction Division) 60, 151 pp., 2014 (in Japanese)

15   Kajino, M., Ueda, H., Satsumabayashi, H., and An, J.: Impacts of the eruption of Miyakejima Volcano on air quality over far east Asia. J. Geophys. Res., 109, D21204, 11 pp, 2004.

Kajino, M. and Kondo, Y.: EMTACS: Development and regional-scale simulation of a size, chemical, mixing type, and soot shape resolved atmospheric particle model. J. Geophys. Res., 116, D02303, 28 pp, 2011.

Kajino, M., Inomata, Y., Sato, K., Ueda, H., Han, Z., An, J., Katata, G., Deushi, M., Maki, T., Oshima, N., Kurokawa, J.,
20   Ohara, T., Takami, A., and Hatakeyama, S.: Development of the RAQM2 aerosol chemical transport model and predictions of the Northeast Asian aerosol mass, size, chemistry, and mixing type. Atmos. Chem. Phys., 12, 11833-11856, 2012a.

Kajino, M., Deushi, M., Maki, T., Oshima, N., Inomata, Y., Sato, K., Ohizumi, T., and Ueda, H.: Modeling wet deposition and concentration of inorganics over Northeast Asia with MRI-PM/c. Geosci. Model Dev., 5, 1363-1375, 2012b.

25   Kajino, M., Sato, K., Inomata, Y., and Ueda, H.: Source-receptor relationships of nitrate in Northeast Asia and influence of sea salt on the long-range transport of nitrate. Atmos. Environ., 79, 67-78, 2013.

Kajino, M., Ueda, H., Han, Z., Kudo, R., Inomata, Y., and Kaku, H.: Synergy between air pollution and urban meteorological changes through aerosol-radiation-diffusion feedback – A case study of Beijing in January 2013. Atmos. Environ., 171, 98-110, 2017.

30   Kajino, M., Deushi, M., Sekiyama, T. T., Oshima, N., Yumimoto, K., Tanaka, T. Y., Ching, J., Hashimoto, A., Yamamoto, T., Ikegami, M., Kamada, A., Miyashita, M., Inomata, Y., Shima, S., Takami, A., Shimizu, A., Hatakeyama, S., Sadanaga, Y., Irie, H., Adachi, K., Zaizen, Y., Igarashi, Y., Ueda, H., Maki, T., and Mikami, M., NHM-Chem, the Japan Meteorological Agency's regional meteorology – chemistry model: model evaluations toward the consistent predictions

of the chemical, physical, and optical properties of aerosols. J. Meteor. Soc. Japan, 97(2), 337-374, doi:10.2151/jmsj.2019-020, 2019a.

Kajino, M., Sekiyama, T. T., Igarashi, Y., Katata, G., Sawada, M., Adachi, K., Zaizen, Y., Tsuruta, H., Nakajima, T.: Deposition and dispersion of radio-cesium released due to the Fukushima nuclear accident: Sensitivity to meteorological models and physical modules, J. Geophys. Res., 124, 1823-1845, doi:10.1029/2018JD028998, 2019b.

Kajino, M., Hayashida, S., Sekiyama, T. T., Deushi, M., Ito, K., Liu, X.: Detectability assessment of a satellite sensor for lower tropospheric ozone responses to its precursors emission changes in East Asian summer, Sci. Rep., 9:19629, 8 pp., doi:10.1038/s41598-019-55759-7, 2019c.

Kajino, M., Hagino, H., Fujitani, Y., Morikawa, T., Fukui, T., Onishi, K., Okuda, T., and Igarashi, Y.: Modeling transition metals in East Asia and Japan toward the predictions of aerosol oxidative potential and its emission sources, GeoHealth, 4, e2020GH000259, doi:10.1029/2020GH000259, 2020. in review.

Kajino, M., Sekiyama, T. T., Igarashi, Y., Katata, G., Sawada, M., Adachi, K., Zaizen, Y., Tsuruta, H., Nakajima, T.: Deposition and dispersion of radio-cesium released due to the Fukushima nuclear accident: 2. Sensitivity to aerosol microphysical propertis of Cs-bearing microparticles (CsMPs), J. Geophys. Res., 126, e2020JD033460, doi:10.1029/2020JD033460, 2021.

Kameda, T., Azumi, E., Fukushima, A., Tang, N., Matsuki, A., Kamiya, Y., Toriba, A., and Hayakawa, K.: Mineral dust aerosols promote the formation of toxic nitropolycyclic aromatic compounds. Sci. Rep., 6, 24427, 10 pp, 2016.

Kaneyasu, N., Ohashi, H., Suzuki, F., Okuda, T., and Ikemori, F.: Sulfate aerosol as a potential transport medium of radiocesium from the Fukushima nuclear accident. Environ. Sci. Technol., 46(11), 5720-5726, doi:10.1021/es204667h, 2012.

Katata, G., Kajino, M., Hiraki, T., Aikawa, M., Kobayashi, T., and Nagai, H.: A method for simple and accurate estimation of fog deposition in a mountain forest using a meteorological model. J. Geophys. Res., 116, D20102, 2011.

Katata, G., Chino, M., Kobayashi, T., Terada, H., Ota, M., Nagai, H., Kajino, M., Draxler, R., Hort, M. C., Malo, A., Torii, T., and Sanada. Y.: Detailed source term estimation of the atmospheric release for the Fukushima Daiichi Nuclear Power Station accident by coupling simulations of an atmospheric dispersion model with an improved deposition scheme and oceanic dispersion model. Atmos. Chem. Phys., 15, 1029-1070, 2015.

Kobayashi, S., Ota, Y., Harada, Y., Ebita, A., Moriya, M., Onda, H., Onogi, K., Kamahori, H., Kobayashi, C., Endo, H., Miyaoka, K., and Takahashi, K.: The JRA-55 Reanalysis: General specifications and basic characteristics. J. Meteor. Soc. Japan, 93, 5-48, 2015.

Koike, M., Takegawa, N., Moteki, N., Kondo, Y., Nakamura, H., Kita, K., Matsui, H., Oshima, N., Kajino, M., and Nakajima, T. Y.: Measurements of regional-scale aerosol impacts on cloud microphysics over the East China Sea: Possible influences of warm sea surface temperature over the Kuroshio ocean current. J. Geophys. Res., 117, D17205, 21 pp, 2012.

Kondo, Y., Oshima, N., Kajino, M., Mikami, R., Moteki, N., Takegawa, N., Verma, R. L., Kajii, Y., Kato, S., and Takami, A.: Emissions of black carbon in East Asia estimated from observations at a remote site in the East China Sea. J. Geophys. Res., 116, D16201, 14 pp, 2011.

Kong, L., Tang, X., Zhu, J., Wang, Z., Fu, J. S., Wang, X., Itahashi, S., Yamaji, K., Nagashima, T., Lee, H. J., Kim, C. H., Lin, C.-Y., Chen, L., Zhang, M., Tao, Z., Li, J., Kajino, M., Liao, H., Wang, Z., Sudo, K., Wang, Y., Pan, Y., Tang, G., Li, M., Wu, Q., Ge, B., and Carmichael, G. R.: Evaluation and uncertainty investigation of the NO2, CO and NH3 modeling over China under the framework of MICS-Asia III, Atmos. Chem. Phys., 20, 181-202, https://doi.org/10.5194/acp-20-181-2020, 2020.

Kurokawa, J., Ohara, T, Morikawa, T., Hanayama, S., Janssens-Maenhout, G., Fukui, T., Kawashima, K., and Akimoto, H.: Emissions of air pollutants and greenhouse gases over Asian regions during 2000-2008: Regional Emission inventory in ASia (REAS) version 2. Atmos. Chem. Phys., 13, 11019-11058, 2013.

Li, J., Nagashima, T., Kong, L., Ge, B., Yamaji, K., Fu, J. S., Wang, X., Fan, Q., Itahashi, S., Lee, H.-J., Kim, C.-H., Lin, C.-Y., Zhang, M., Tao, Z., Kajino, M., Liao, H., Li, M., Woo, J.-H., Kurokawa, J., Wu, Q., Akimoto, H., Carmichael, G. R., and Wang, Z.: Model evaluation and inter-comparison of surface-level ozone and relevant species in East Asia in the context of MICS-Asia phase III Part I: overview.. Atmos. Chem. Phys., 19, 12993-13015, doi:10.5194/acp-19-12993-2019, 2019.

Li, M., Zhang, Q., Kurokawa, J.-I., Woo, J.-H., He, K., Lu, Z., Ohara, T., Song, Y., Streets, D. G., Carmichael, G. R., Cheng, Y., Hong, C., Huo, H., Jiang, X., Kang, S., Liu, F., Su, H., and Zheng, B.: MIX: a mosaic Asian anthropogenic emission inventory under the international collaboration framework of the MICS-Asia and HTAP, Atmos. Chem. Phys., 17, 935-963, 2017.

Liu, X., Easter, R. C., Ghan, S. J., Zaveri, R., Rasch, P., Shi, X., Lamarque, J.-F., Gettelman, A., Morrison, H., Vitt, F., Conley, A., Park, S., Naele, R., Hannay, C., Ekman, A. M. L., Hess, P., Mahowald, N., Collins, W., Iacono, M. J., Bretherton, C. S., Flanner, M. G., and Mitchell, D.: Toward a minimal representation of aerosols in climate models: description and evaluation in the Community Atmosphere Model CAM5. Geosci. Model Dev., 5, 709-739, 2012.

Liu, X., Ma, P.-L., Wang, H., Tilmes, S., Singh, B., Easter, R. C., Ghan, S. J., and Rasch, P. J.: Description and evaluation of a new four-mode version of the Modal Aerosol Module (MAM4) within version 5.3 of the Community Atmosphere Model. Geosci. Model Dev., 9, 502-522, 2016.

Lohmann, U. and Diehl, K.: Sensitivity studies of the importance of dust ice nuclei for the indirect aerosol effect on stratiform mixedphase clouds. J. Atmos. Sci., 63, 968-982, 2006.

Matsui, H.: Development of a global aerosol model using a two-dimensional sectional method: 1. Model design. J. Adv. Model. Earth Syst., 9, 1921-1947, 2017.

Miyakawa, T., Takeda, N., Koizumi, K., Tabaru, M., Ozawa, Y., Hirayama, N., and Takegawa, N.: A new lase induced incandescence – mass spectrometric analyzer (LII-MS) for online measurement of aerosol composition classified by black carbon mixing state. Aerosol Sci. Tech., 48, 853-863, 2014.

Nakajima, T., Yoon, S. C., Ramanathan, V., Shi, G. Y., Takemura, T., Higurashi, A., Takamura, T., Aoki, K., Sohn, B. J., Kim, S. W., Tusuruta, H., Sugimoto, N., Shimizu, A., Tanimoto, H., Sawa, Y., Lin, N. H., Lee, C. T., Goto, D., and Schutgens, N.: Overview of the Atmospheric Brown Cloud East Asian Regional Experiment 2005 and a study of the aerosol direct radiative forcing in east Asia. J. Geophys. Res., 112, D24S91, 2007.

5   Nakano, M., Kato, T., Hayashi, S., Kanada, S., Yamada, Y., and Kurihara, K.: Development of a 5-km-Mesh Cloud-System-Resolving Regional Climate Model at the Meteorological Research Institute. J. Meteorol. Soc. Jpn., 90A, 339-350, 2012.

Nishizawa, S., Yashiro, H., Sato, Y., Miyamoto, Y., and Tomita, H.: Influence of grid aspect ratio on planetary boundary layer turbulence in large-eddy simulations, Geosci. Model Dev., 8, 3393-3419, doi:10.5194/gmd-8-3393-2015, 2015.

Oshima, N., Koike, M., Zhang, Y., Kondo, Y., Moteki, N., Takegawa, N., and Miyazaki, Y.: Aging of black carbon in

10   outflow from anthropogenic sources using a mixing state resolved model: Model development and evaluation. J. Geophys. Res., 114, D06210, 2009a.

Oshima, N., Koike, M., Zhang, Y., and Kondo, Y.: Aging of black carbon in outflow from anthropogenic sources using a mixing state resolved model: 2. Aerosol optical properties and cloud condensation nuclei activities, J. Geophys. Res., 114, D18202, 2009b.

15   Oshima, N., Kondo, Y., Moteki, N., Takegawa, N., Koike, M., Kita, K., Matsui, H., Kajino, M., Nakamura, H., Jung, J. S., and Kim, Y. J.: Wet removal of black carbon in Asian outflow: Aerosol Radiative Forcing in East Asia (A-FORCE) aircraft campaign, J. Geophys. Res., 117, D03204, doi:10.1029/2011JD016552, 2012.

Oshima, N. and Koike, M.: Development of a parameterization of black carbon aging for use in general circulation models, Geosci. Model Dev., 6, 263–282, https://doi.org/10.5194/gmd-6-263-2013, 2013.

20   Oshima, N., Koike, M., Kondo, Y., Nakamura, H., Moteki, N., Matsui, H., Takegawa, N., and Kita, K.: Vertical transport mechanisms of black carbon over East Asia in spring during the A-FORCE aircraft campaign, J. Geophys. Res. Atmos., 118, 13175–13198, doi:10.1002/2013JD020262, 2013.

Oshima, N., Yukimoto, S., Deushi, M., Koshiro, T., Kawai, H., Tanaka, T. Y., and Yoshida, K.: Global and Arctic effective radiative forcing of anthropogenic gases and aerosols in MRI-ESM2.0, Prog. Earth. Planet. Sci., 7, 38,

25   https://doi.org/10.1186/s40645-020-00348-w, 2020.

Petters, M. D. and Kreidenweis, S. M.: A single parameter representation of hygroscopic growth and cloud condensation nucleus activity. Atmos. Chem. Phys., 7, 1961-1971, 2007.

Pleim, J. E. and Chang, J. S.: A non-local closure model for vertical mixing in the convective boundary layer. Atmos. Environ., 26A, 965-981, 1992.

30   Prather, K. A., Bertram, T. H., Grassian, V. H., Deane, G. B., Stokes, M. D., Demott, P. J., Aluwihare, L. I., Palenik, B. P., Azam, F., Seinfeld, J. H., Moffet, R. C., Molina, M. J., Cappa, C. D., Geiger, F. M., Roberts, G. C., Russel, L. M., Ault, A. P., Baltrusaitis, J., Collins, D. B., Corrigan, C. E., Cuadra-Rodriguez, L. A., Ebben, C. J., Forestieri, S. D., Guasco, T. L., Hersey, S. P., Kim, M. J., Lambert, W. F., Modini, R. L., Mui, W., Pedler, B. E., Ruppel, M. J., Ryder, O. S., Schoepp,

N. G., Sullivan, R. C., and Zhao, D.: Bringing the ocean into the laboratory to probe the chemical complexity of sea spray aerosol. Proc. Natl. Acad. Sci., 110(19), 7550-7555, 2013.

Pringle, K. J., Tost, H., Message, S., Steil, B., Giannadaki, D., Nenes, A., Fountoukis, C., Stier, P., Vignati, E., and Lelieveld, J.: Description and evaluation of GMXe: a new aerosol submodel for global simulations (v1), Geosci. Model Dev., 3, 391-412, https://doi.org/10.5194/gmd-3-391-2010, 2010.

Rasmussen, R. M., Geresdi, I., Thompson, G., Manning, K., and Karplus, E.: Freezing drizzle formation in stably stratified layer clouds: The role of radiation cooling of cloud droplets, cloud condensation nuclei, and ice initiation. J. Atmos. Sci., 59, 837-860, 2002.

Riemer, N., Vogel, H., Vogel, B., and Fiedler, F.: Modeling aerosols on the mesoscale-γ: Treatment of soot aerosol and its radiative effects. J. Geophys. Res., 108, D19, 4601, 2003.

Riemer, N., West, M., Zaveri, R. A., and Easter, R. C.: Simulating the evolution of soot mixing state with a particle-resolved aerosol model. J. Geophys. Res., 114, D09202, 2009.

Rosenfeld, D., Lohmann, U., Raga, G. B., O'Dowd, C. D., Kulmala, M., Fuzzi, S., Reissell, A., and Andreae M. O.: Flood or drought: how do aerosols affect precipitation?, Science, 321, 1309-1313, 2008.

Saito, K., Fujita, T., Yamada, Y., Ishida, J., Kumagai, Y., Aranami, K., Ohmori, S., Nagasawa, R., Kumagai, S., Muroi, C., Kato, T., Eito, H., and Yamazaki, Y.: The operational JMA nonhydrostatic mesoscale model. Mon. Wea. Rev., 134, 1266-1298, 2006.

Saito, K., Ishida, J., Aranami, K., Hara, T., Segawa, T., Narita, M., and Honda, Y.: Nonhydrostatic atmospheric models operational development at JMA. J. Meteor. Soc. Japan, 85B, 271-304, 2007.

Saito, K.: Chapter 5. The JMA nonhydrostatic model and its application to operation and research. *Atmospheric Model Applications*, Ed. Ismail Yucel, InTech Open Access Publisher, 85-110, 2012.

Sato, Y., Nishizawa, S., Yashiro, H., Miyamoto, Y., Kajikawa, Y., and Tomita, H.: Impacts of cloud microphysics on trade wind cumulus: which cloud microphysics processes contribute to the diversity in a large eddy simulation?, Prog. Earth Planet. Sci., 2, 23, doi:10.1186/s40645-015-0053-6, 2015.

Sato, Y., Sekiyama, T. T. , Fang, S. , Kajino, M., Quérel, A., Quélo, D., Kondo, H., Terada, H., Kadowaki, M., Takigawa, M., Morino, Y., Uchida, J., Goto, D., and Yamazawa, H.: A Model intercomparison of atmospheric ^{137}Cs concentrations from the Fukushima Daiichi Nuclear Power Plant accident, Phase III: Simulation with an identical source term and meteorological field at 1 km resolution, *Atmos. Environ X*, in review.

Seinfeld, J. H. and Pandis, S. N.: Atmospheric Chemistry and Physics: From Air Pollution to Climate Change, 2nd Edition, 1203 pp., John Wiley, New York, 2006.

Sekiyama, T. T., and Kajino, M.: Reproducibility of surface wind and tracer transport simulations over complex terrain using 5-, 3-, and 1-km-grid models, J. Appl. Meteor. Climatol., 59(5), 937-952, doi:10.1175/JAMC-D-19-0241.1, 2020.

Shimizu, A., Sugimoto, N., Matsui, I., Arao, K., Uno, I., Murayama, T., Kagawa, N., Aoki, K., Uchiyama, A., and Yamazaki, A.: Continuous observations of Asian dust and other aerosols by polarization lidar in China and Japan during ACE-Asia. J. Geophys. Res., 109, D19S17, 2004.

Shimizu, A., Nishizawa, T., Jin, Y., Kim, S.-W., Wang, Z., Batdorj, D., and Sugimoto, N.: Evolution of a lidar network for tropospheric aerosol detection in East Asia. Optical Engineering, 56(3), 03219, 2016.

Skamarock, W. C., Klemp, J. B., Dudhia, J., Gill, D. O., Barker, D. M., Duda, M. G., Huang, X. Y., Wang, W., and Powers, J. G.: A description of the advanced research WRF version 3. Tech. Note, NCAR/TN~475+STR, 125 pp., Natl. Cent. for Atmos. Res., Boulder, Colo, 2008.

Song, C. H. and Carmichael, G. R.: A three-dimensional modeling investigation of the evolution processes of dust and sea-salt particles in east Asia. J. Geophys. Res., 106(D16), 18,131-18,154, 2001.

Sugimoto, N., Uno, I., Nishikawa, M., Shimizu, A., Matsui, I., Dong, X., Chen, Y., and Quan, H. Record heavy Asia dust in Beijing in 2002: Observations and model analysis of recent events. Geophys. Res. Lett., 30(12), 1640, 2003.

Sugimoto, N., Matsui, I., Shimizu, A., Nishizawa, T., Hara, Y., Xie, C., Uno, I., Yumimoto, K., Wang, Z., Yoon, S.-C. Lidar network observations of tropospheric aerosols. SPIE, Vol. 7153, 2008.

~~Sugimoto, N., Hara, Y., Shimizu, A., Yumimoto, K., Uno, I., and Nishikawa, M. Comparison of surface observations and a regional dust transport model assimilated with lidar network data in Asian dust event of March 29 to April 2, 2007. *SOLA*, 7A, 13-16, 2011.~~

Takamura, T., Nakajima, T., and SKYNET community group.: Overview of SKYNET and its activities. Opt. Pura Apl., 37, 3303-3308, 2004.

~~Tan, J., Fu, J. S., Carmichael, G. R., Itahashi, S., Tao, Z., Huang, K., Dong, X., Yamaji, K., Nagashima, T., Wang, X., Liu, Y., Lee, H. J., Lin, C. Y., Ge, B., Kajino, M., Zhu, J., Zhang, M., Hong, L., and Wang, Z.: Why models perform differently on particulate matter over East Asia? — A multi-model intercomparison study for MICS Asia III, Atmos. Chem. Phys. Discuss., https://doi.org/10.5194/acp-2019-392, accepted.~~

Tanaka, T. Y., Orito, K., Sekiyama, T. T., Shibata, K., Chiba, M., and Tanaka, H.: MASINGAR, a global tropospheric aerosol chemical transport model coupled with MRI/JMA98 GCM: Model description. Pap. Meteor. Geophys., 53(4), 119-138, 2003.

Tanaka, T. Y. and Ogi, A.: Update of Japan Meteorological Agency's global mineral dust operational forecast model. Sokkou-Jihou, 84, 109-128, 2017 (in Japanese).

Uno, I., Nagata, K., Yumimoto, K., Itahashi, S., Kuwata, S., Pan, X., Hara, Y., and Yamamoto, S.: Numerical analysis of trans-boundary transport of dust-nitrate during the long-lasting yellow sand episode observed over the Northern Kyushu Area in late May-early June 2014, J. Jpn. Soc. Atmos. Environ., 51, 181-189, 2016 (in Japanese).

Uno, I., Osada, K., Yumimoto, K., Wang, Z., Itahashi, S., Pan, X., Hara, Y., Kanaya, Y., Yamamoto, S., and Fairlie, T. D.: Seasonal variation of fine- and coarse-mode nitrates and related aerosols over East Asia: synergetic observations and chemical transport model analysis. Atmos. Chem. Phys., 17(23), 14,181-14,197, 2017.

Vignati, E., Wilson, J., Stier, P.: M7: An efficient size-resolved aerosol microphysics module for large-scale aerosol transport models. J. Geophys. Res., 109, D22202, 2004.

Vogel, B., Vogel, H., Bäumer, D., Bangert, M., Lundgren, K., Rinke, R., and Stanelle, T.: The comprehensive model system COSMO-ART – Radiative impact of aerosol on the state of the atmosphere on the regional scale, Atmos. Chem. Phys., 9, 8661-8680, 2009.

Walcek, C. J. and Aleksic, N. M.: A simple but accurate mass conservative peak-preserving, mixing ratio bounded advection algorithm with fortran code. Atmos. Environ., 32, 3863-3880, 1998.

Walcek, C. J. and Taylor, G. R.: A theoretical method for computing vertical distributions of acidity and sulfate production within cumulus clouds. J. Atmos. Sci., 43, 339-355, 1986.

WHO: IARC monographs on the evaluation of carcinogenic risks to humans, Ionizing radiation, part 2: Some internally deposited radionuclides, Vol. 78, 595 pp, 2001.

Wong, D. C, Pleim, J., Mathur, R., Binkowski, F., Otte, T., Gilliam, R., Pouliot, G., Xiu, A., Young, J. O., and Kang, D.: WRF-CMAQ two-way coupled system with aerosol feedback: software development and preliminary results. Geosci. Model Dev., 5, 299-312, 2012.

Woo, J.-H., Streets, D. G., Carmichael, G. R., Tang, Y., Yoo, B., Lee, W.-C., Thongboonchoo, N., Pinnock, S., Kurata, G., Uno, I., Fu, Q., Vay, S., Sachse, G. W., Clake, D. R., Fried, A., and Thornton, D. C.: Contribution of biomass and biofuel emissions to trace gas distributions in Asia during the TRACE-P experiment. J. Geophys. Res., 108(D21), 8812, 2003.

Yumimoto, K. Tanaka, T. Y., Oshima, N., and Maki, T.: JRAero: the Japanese Reanalysis for Aerosol v1.0. Geosci. Model Dev., 10, 3225-3253, 2017.

Yumimoto, K., Kajino, M., Tanaka, T. Y., and Uno, I.: Dust vortex in the Taklimakan desert by Himawari-8 high frequency and resolution observation, Sci. Rep., 9:1209, 7 pp., doi:10.1038/s41598-018-37861-4, 2019.

Zaveri, R. A., Barnard, J. C., Easter, R. C., Riemer, N., and West, M.: Particle-resolved simulation of aerosol size, composition, mixing state, and the associated optical and cloud condensation nuclei activation properties in an evolving urban plume. J. Geophys. Res., 115, D17210, 2010.

Zhang, D., and Iwasaka, Y.: Size change of Asian dust particles caused by sea salt interaction: Measurements in southwestern Japan. Geophys. Res. Lett., 31, L15102, 4 pp, 2004.

Zhang, K., O'Donnell, D., Kazil, J., Stier, P., Kinne, S., Lohmann, U., Ferrachat, S., Croft, B., Quaas, J., Wan, H., Rast, S., and Feichter, J.: The global aerosol-climate model ECHAM-HAM, version 2: sensitivity to improvements in process representations, Atmos. Chem Phys. 12, 8911-8949, 2012.

Zhang, Y., Pan, B., Vijayaraghavan, K., Wu, S.-Y., Seigneur, C., Pandis, S. N., Jacobson, M. Z., Nenes, A., and Seinfeld, J. H.: Development and application of the Model of Aerosol Dynamics, Reaction, Ionization, and Dissolution (MADRID). J. Geophys. Res., 109, D01202, 2004.

Zhang, Y., Pan, Y., Wang, K., Fast, J. D., and Grell, G. A.: WRF/Chem-MADRID: Incorporation of an aerosol module into WRF/Chem and its initial application to the TexAQS20000 episode. J. Geophys. Res., 115, D18202, 2010.

Supplement 1

Supplement 1 includes the description of the NHM (the Japan Meteorological Agency's Non-Hydrostatic Model)-Chem model. *Originally, the previous version of current manuscript was published in Geoscientific Model Development Discussion as a model description paper (Kajino et al., 2018; https://doi.org/10.5194/gmd-2018-128), but the revision was not accepted. The current version is a resubmission of Kajino et al. (2018), but as a model evaluation paper this time, based on the referees' comments. Thus, the model description part is separately written in this section.*

Table S1-1 summarizes the schemes of the chemical transport model (CTM) and database available for NHM-Chem. The advection algorithm (Walcek and Aleksic, 1998) was used to determine advection by mean wind. The turbulent diffusion calculation utilized the forward-time central-space method using turbulent diffusivities predicted by meteorological models or calculated as a function of predicted turbulent kinetic energy (TKE) and mixing length, depending on the selection of the turbulence scheme of the meteorological models. The SAPRC99 gas-phase chemistry mechanism (Carter, 2000) was used with the photolysis rates predicted by Madronich (1987). The three heterogeneous chemical reactions of N_2O_5, HO_2, and NO_2 from Jacob (2000) were included in SAPRC99. The heterogeneous reaction rates were formulated as a function of aerosol surface area and independent of their substrates; same rates used for different aerosol surfaces composed of ammonium sulfate, organics, or mineral dust. The secondary organic aerosol (SOA) chemistry was predicted by Edney et al. (2007), and the liquid phase chemistry was predicted by Walcek and Taylor (1986) for inorganics and Carlton et al. (2007) for organics.

For the aerosol microphysics calculations, the triple-moment modal method (Kajino, 2011) was used. A log-normal size distribution was assumed for the aerosol populations. There are three parameters used to identify the log-normal function, namely, the number concentration, geometric mean diameter D_g, and geometric standard deviation σ_g. The three moments of the number, surface area, and mass concentrations of aerosols are selected to fix the log-normal parameters and are transported in the simulation. The variations in these three moments represent how the log-normal parameters of aerosol populations are changed in a physically consistent manner throughout the simulation. Although Kajino (2011) accounted for the fractal shapes of particles (as implemented by Kajino and Kondo, 2011 in the 3-D CTM framework), currently, all particles are assumed to be spherical for aerosol microphysics. A spherical shape is also assumed for the calculations of the optical and radiation properties of the aerosols. The aerosol microphysics calculation algorithm to calculate condensation, evaporation, and Brownian coagulation was described in detail by Kajino et al. (2012a). Kuang et al. (2008) was used to calculate the new particle formation as a function of sulfuric acid vapor. ISORROPIA2 (Fountoukis and Nenes, 2007) and Edney et al. (2007) were used to calculate the surface equilibrium vapor pressures of inorganic and organic compounds, respectively. The dry deposition velocities of gases were calculated by Zhang et al. (2003), and those of aerosols were calculated by a scheme developed based on Zhang et al. (2001) with modifications by Katata et al. (2008, 2011a) and Kajino et al. (2012a). The in-cloud scavenging process is composed of several elementary processes, namely, cloud condensation

nuclei (CCN) activation (Abdul-Razzak and Ghan, 2000), ice nuclei (IN) activation (Lohmann and Diehl, 2006), and subsequent cloud microphysical processes (Lin et al., 1983). The subgrid-scale convection and scavenging were calculated by Pleim and Chang (1992).

Table S1-1: List of models, schemes, and databases available for NHM-Chem

Scheme/data	Name/reference
Meteorological model[a]	Nonhydrostatic model (NHM; Saito et al., 2006, 2007, Saito 2012)
Mascon model[b]	MCWCM (Ishikawa, 1994)
Boundary concentrations	Climatological value or 3-hourly field obtained from MRI-CCM2 (Deushi and Shibata, 2011) and MASINGAR mk-2 (Tanaka et al., 2003, Tanaka and Ogi 2017, Yumimoto et al., 2017)
Emission	Anthropogenic (REASv2, Kurokawa et al., 2013; EAGrid, Kannari et al., 2007, Fukui et al., 2014), Biomass burning (GFED3, Giglio et al., 2010), Biogenic (MEGAN2, Guenther et al., 2006), Asian dust (Han et al., 2004), Sea-salt (Clarke et al., 2006)
Advection	MPMAA (Walcek and Aleksic, 1998)
Photolysis rate	Madronich (1987) with TOMS O_3 column data
Gas chemistry	SAPRC99 (Carter, 2000) (72 species and 214 reactions) + Jacob (2000) heterogeneous reactions (3 reactions)
SOA chemistry	Edney et al. (2007)
Liquid chemistry	Walcek and Taylor (1986), Carlton et al. (2007)
New particle formation[c]	Kuang et al. (2008)
Aerosol microphysics[c]	Kajino (2011), Kajino et al. (2012a)
Aerosol representations	5-category nonequilibrium method, 3-category nonequilibrium method, bulk equilibrium method (This study)
Surface gas-aerosol equilibrium of inorganic compounds	ISORROPIA2 (Fountoukis and Nenes, 2007)
Dry deposition	Zhang et al. (2001, 2003), Katata et al. (2008, 2011a), and Kajino et al. (2012a)
Fog deposition	Katata et al. (2015)
In-cloud scavenging	CCN activation (Abdul-Razzak and Ghan, 2000), IN activation (Lohmann and Diehl, 2006), and subsequent cloud microphysical processes (i.e., autoconversion and accretion; Lin et al., 1983)
Below-cloud scavenging	Kajino and Kondo (2011), Slinn (1984), Murakami (1985), Andronache et al. (2006)
Subgrid-scale convection and wet deposition	ACM (Pleim and Chang, 1992)

[a]Other models such as the Weather Research and Forecasting model (WRF; Skamarock et al., 2008), Asuca is a System based on a Unified Concept for Atmosphere (ASUCA; JMA, 2014; Aranami et al., 2015), and Scalable Computing for Advanced Library and Environment (SCALE; Nishizawa et al., 2015, Sato et al., 2015) can also be used for the offline coupled version. [b]The mascon model is needed only for the offline coupled version after the vertical interpolation is made because the vertical coordinates of the NHM and CTM are different, so that the number of vertical levels or model top height can be reduced in the CTM. The mascon model is not needed for the online coupled version, as the vertical coordinates of the meteorological and chemical variables are the same. The model top height can also be reduced for the online version. [c]Not used in the bulk method. Used in the 5-category and 3-category methods.

Most of the above processes are similar to those used by Kajino et al. (2012a), whereas the fog deposition parameterization of Katata et al. (2015) and a detailed below-cloud scavenging scheme are also incorporated in this study, as described below.

Katata et al. (2015) developed a parameterization to calculate the fog deposition velocity as a function of the land use category (LUC), leaf area index (LAI), atmospheric stability, and 10-m wind speed. Fog deposition is calculated only in the bottom layer of the model when the cloud water content is greater than 10^{-5} kg kg^{-1} (Kajino et al., 2019). In island countries, such as Japan in the western Pacific, ground surfaces are often covered with humid mountain forests, and the contribution of fog deposition is ubiquitous.

The large discrepancy between the theoretical and experimental rates of below-cloud scavenging has been a critical issue and has not yet been resolved (Wang et al., 2010; Zhang et al., 2013). The theoretical rates are sometimes one to two orders of magnitude smaller than the empirical rates, especially for aerosols that are in the diameter ranges of approximately 1 μm, where Brownian motion and an inertial force are both small. In the current implementation, we proposed two options for below-cloud scavenging, namely, the conventional modal method developed by Kajino and Kondo (2011) and a newly implemented method using detailed size-resolved parameterizations. The latter size-resolved option requires a longer computational time, but the Gauss-Hermite quadrature method is used to minimize the computational time (however, it is still computationally expensive). Slinn's (1984) parameterization, which considers thermophoresis, diffusiophoresis, and electrostatic forces (Andronache et al., 2006), is used for the derivation of the collection efficiencies of aerosols by rain droplets. There are two options to calculate the efficiencies collected by snow and graupel particles, i.e., those of Slinn (1984) and Murakami (1985). In this study, we used the approach presented by Kajino and Kondo (2011) because of its computational efficiency.

Many of the schemes are similar or almost equivalent to those implemented in widely used regional community models, such as CMAQ (Byun and Schere, 2006; Wong et al., 2012) and WRF-Chem (Grell et al., 2005; Chapman et al., 2009), as seen from the result of a multi-CTM intercomparison study (Li et al., 2019; Chen et al., 2019; Itahashi et al., 2020; Kong et al., 2020; Tan et al., 2020; Ge et al., 2020): NHM-Chem behaved similarly to the other models, including CMAQ and WRF-Chem. The advantage of the current model is not considerable, except for the detailed fog deposition and below-cloud scavenging parameterizations. In fact, the fog deposition scheme for liquid water is already implemented in WRF (Katata et al., 2011b) but not in WRF-Chem to simulate the fog deposition of various chemical compositions. The resulting disadvantage is the underestimation of SOA formation in the current model. Although their formation mechanisms are still unknown, a volatility-based set SOA formation model (Donahue et al., 2006) was developed to improve the significant underestimation of conventional models already implemented in CMAQ and WRF-Chem, but not in NHM-Chem.

The source code structure of NHM-Chem was designed for the seamless development of online and offline coupling, as presented in Fig. S1-1. The codes are written in Fortran 90. The offline and online NHM-Chem share common subroutines (or physical/chemical schemes). The chemistry-to-meteorology feedback process has not been included and will be implemented in the near future. The online version of NHM-Chem is currently a so-called 1-way (meteorology to chemistry) online coupled model.
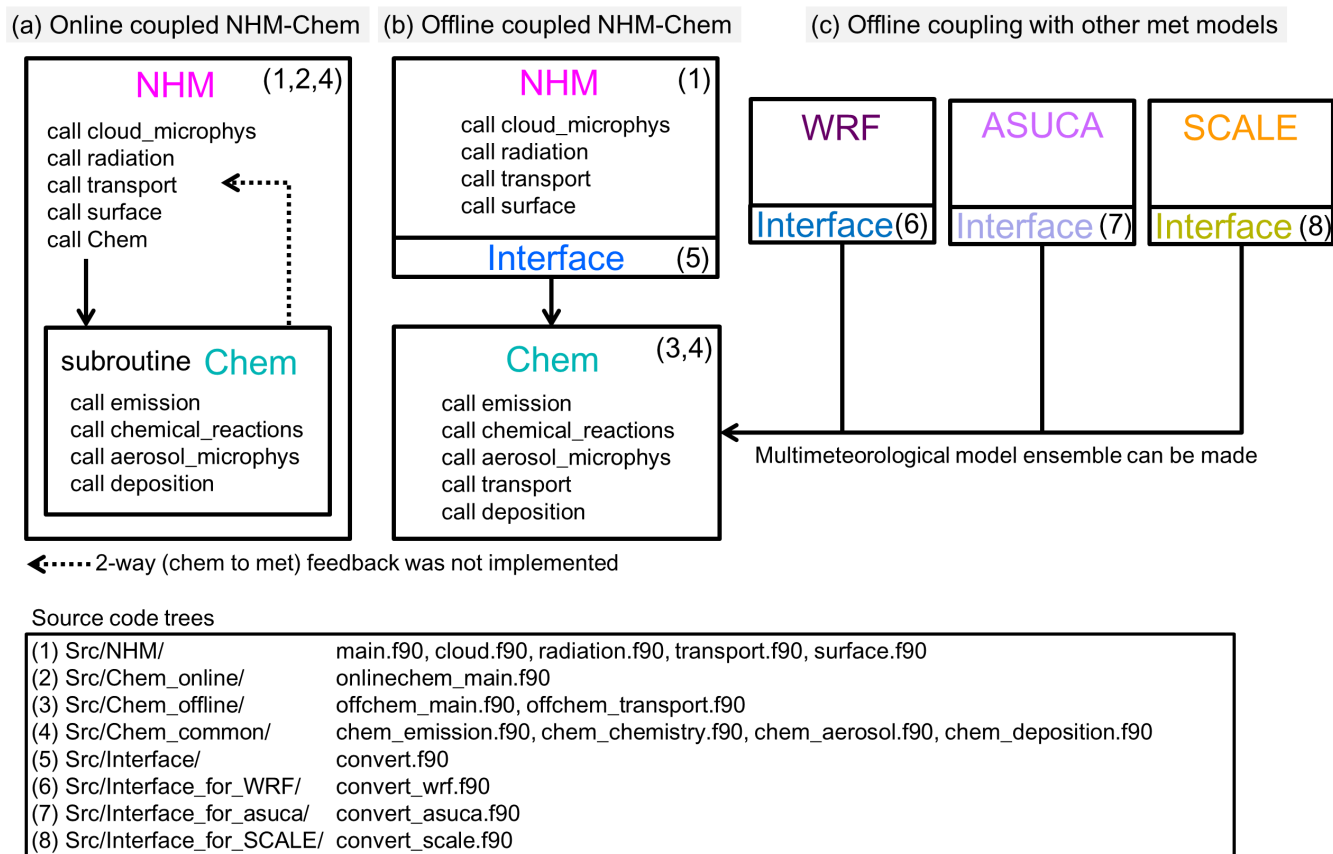
Figure S1-1. Online/offline coupling framework of NHM-Chem v1.0.

Online and offline coupling have different advantages and disadvantages. In online coupling, changes in meteorological fields affect chemical fields at small time steps (a few seconds) (e.g., Grell et al., 2005), whereas in offline coupling, changes in meteorological fields are interpolated between crude input/output time steps (an hour to a few minutes) (e.g., Byun and Schere, 2006). Certainly, chemistry-to-meteorology feedback processes cannot be readily implemented in the offline coupled framework but has been implemented in many of the online models (so-called 2-way (meteorology to chemistry/chemistry to meteorology) online coupled models, e.g., Chapman et al., 2009; Vogel et al., 2009; Wong et al.,

2012). Online coupling is slightly more time consuming if sensitivity tests in chemical fields are conducted: meteorology simulations are conducted for every sensitivity simulation in online coupling, whereas meteorological simulations are needed only once for offline coupling.

In the offline-coupling framework, a multimeteorological model intercomparison can be readily performed: we only need an interface to convert a meteorological model output to a chemical model input. Currently, interfaces with WRF, ASUCA, and SCALE are available in NHM-Chem. Kajino et al. (2019) evaluated the impact of the uncertainty in meteorological simulations on the modeling of chemical transport and deposition by using NHM, NHM-LETKF (Local Ensemble Transform Kalman Filter data assimilation method coupled with NHM; Kunii, 2014; Sekiyama et al., 2015), and WRF with several combinations of turbulence and cloud microphysics modules. For the offline coupled NHM-Chem, the horizontal grid of the CTM is identical to that of meteorological models, but the vertical coordinate is different; thus, users can reduce the number of vertical layers or the model top height for the computational efficiency, or they can use different meteorological models that use different vertical coordinates. To reduce the mass divergence due to vertical interpolation to approximately 10^{-5} to 10^{-6} (s^{-1}), the mass continuity model (Ishikawa, 1994) is incorporated into the meteorology-chemistry model interface of the offline coupled NHM-Chem, as shown in Table S1-1. For the online coupled NHM-Chem, the mass continuity model is not needed because the vertical coordinates of the CTM and NHM are common, but the model top layers of the CTM can be reduced for computational efficiency.

Supplement 2

Supplement 2 includes the locations of the six major SO_2-emitting volcanoes and the time series of the temporally smoothed and raw SO_2 emission flux and smoke height data measured by the JMA and used in the NHM-Chem model. The locations and periods of the volcanic data are summarized in Table S2-1.

Table S2-1: Availability of volcanic emission data in Japan and time-averaged continuous SO_2 emissions from the 1970s to 1997, with the maximum values of the emissions since the 2000s provided in brackets.

Volcano	Longitude (E)	Latitude (N)	Height (m MSL)	SO_2 emission (ton d^{-1})[a]	Period (SO_2 emission, smoke height)
Miyakejima (Mt. Oyama)	139°31′	34°05′	775[b]	270 (82,200)	August 26, 2000 –August 16, 2018 January 1, 2008 – February 29, 2016
Mt. Asama	138°31′	36°24′	2,568	370 (8,700)	July 4, 2002 – August 20, 2018 January 1, 2008 – February 29, 2016
Mt. Aso	131°06′	32°53′	1,592	27 (15,000)[d]	March 22, 2007 – August 16, 2018 January 1, 2008 – February 29, 2016
Mt. Kirishima (Shinmoedake)	130°52′	31°56′	1,420	-[e] (34,100)[f]	January 27, 2011 – June 1, 2018 January 1, 2008 – February 29, 2016
Mt. Sakurajima	130°39′	31°35′	1,117	1,900[e] (7,400)	May 23, 2007 – July 26, 2018 January 1, 2008 – February 29, 2016
Kuchinoerabujima	130°11′	30°28′	649	570 (3,100)	October 4, 2008 – July 13, 2018 January 1, 2008 – February 29, 2016

[a]Time-averaged SO_2 emissions from 1970s to 1997 (Andres and Kasgnoc, 1998) and maximum values since the 2000s (this study).
[b]Previously 814 m, before a large eruption occurred in 2000.
[c]Andres and Kasgnoc (1998) also provide the sporadic emission amount for Mt. Aso.
[d]The maximum value is not shown in Fig. S2-2 but it was observed on October 7, 2016.
[e]Andres and Kasgnoc (1998) does not separate emissions from the two volcanoes, but the emission amount is supposed to be associated with Mt. Sakurajima.
[f]The maximum value is not shown in Fig. S2-2 but was observed on March 7, 2018.

The locations of the volcanoes are depicted in Fig. S2-1. The time series of the smoothed volcanic SO_2 emissions and smoke height data, together with the raw data, are illustrated in Figs. S2-2 and S2-3, respectively. The spline interpolation failed for the Kirishima volcano case, as its emissions were considerable but sporadic. The linear interpolation or periodical average should be used for the case. The volcanic emissions from other volcanoes worldwide are taken from Andres and Kasgnoc (1998). The volcanic emissions were uniformly allocated from the bottom layer to the smoke height or to 1,000 m AGL when smoke height information was not available.
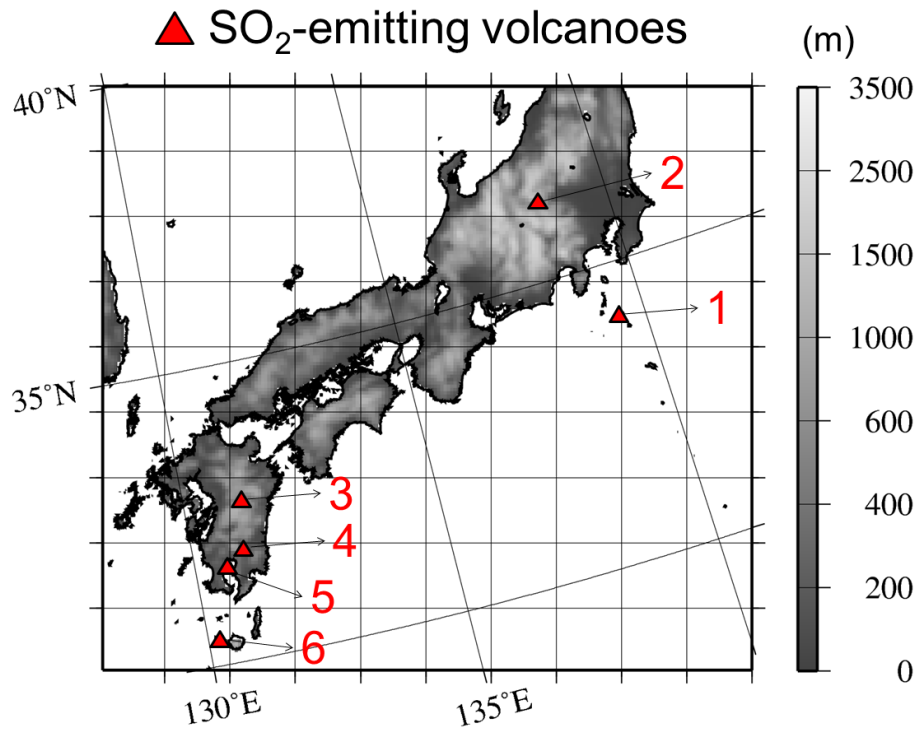
1. Miyakejima (Mt. Oyama), 2. Mt. Asama, 3. Mt. Aso,
4. Mt. Kirishima (Shinmoedake), 5. Mt. Sakurajima,
6. Kuchinoerabu-jima (Shindake)

Figure S2-1: Locations of the six SO$_2$-emitting volcanoes in Japan monitored by the JMA.
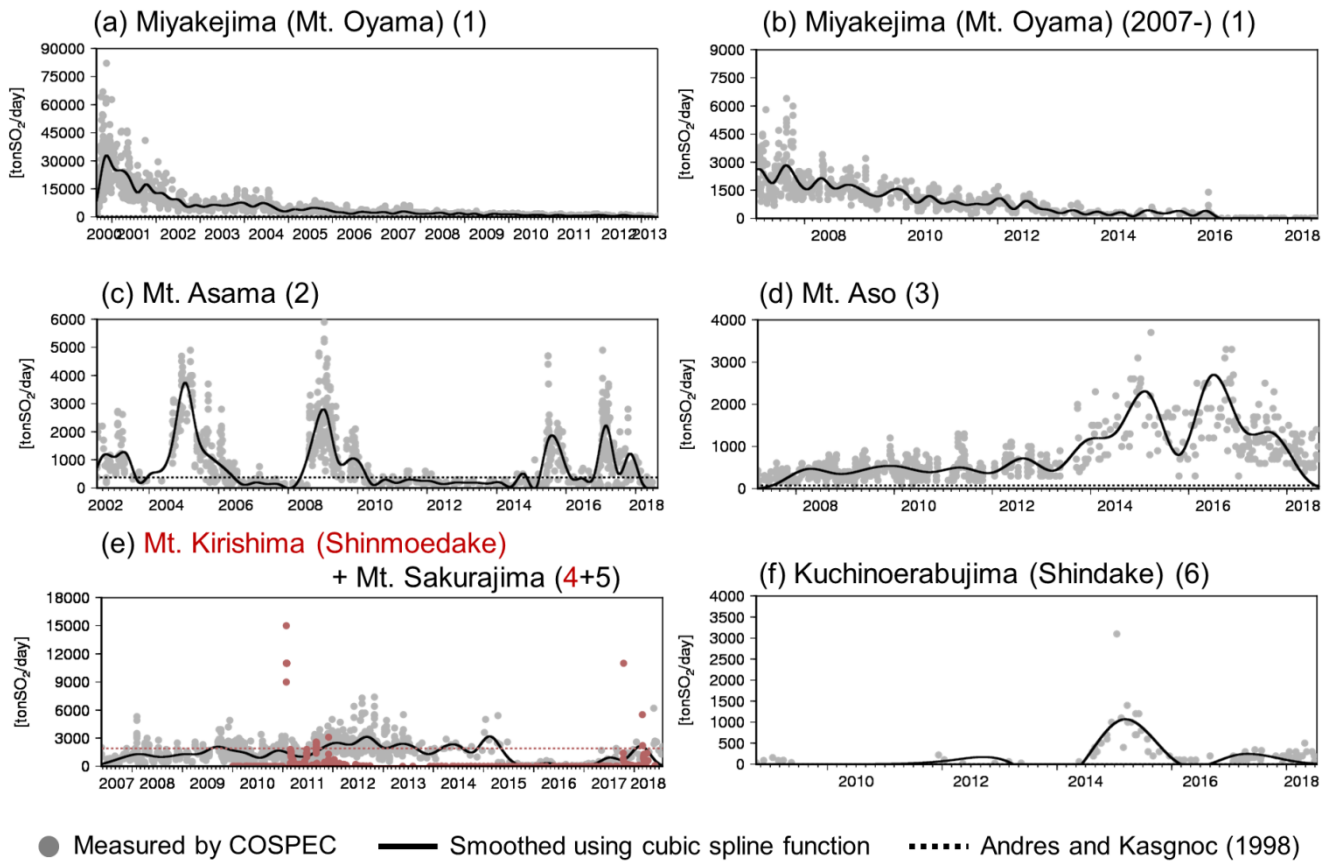
Figure S2-2: The time series of temporally smoothed data (solid line), with the raw data (gray dots) and estimations of Andres and Kasgnoc (1998) (dotted line), of the SO$_2$ emission flux, measured by the JMA and used in the NHM-Chem model. The red dot in Fig. S2-2e is the sum of Mt. Kirishima and Mt. Sakurajima because Andreas and Kasgnoc (1998) do not differentiate emissions from the two volcanoes (associated with the eruption of Mt. Sakurajima). The smoothed interpolation for Mt. Kirishima is not shown in Fig. S2-2e because the time variation is sporadic; thus, spline smoothing failed and linear interpolation was used.
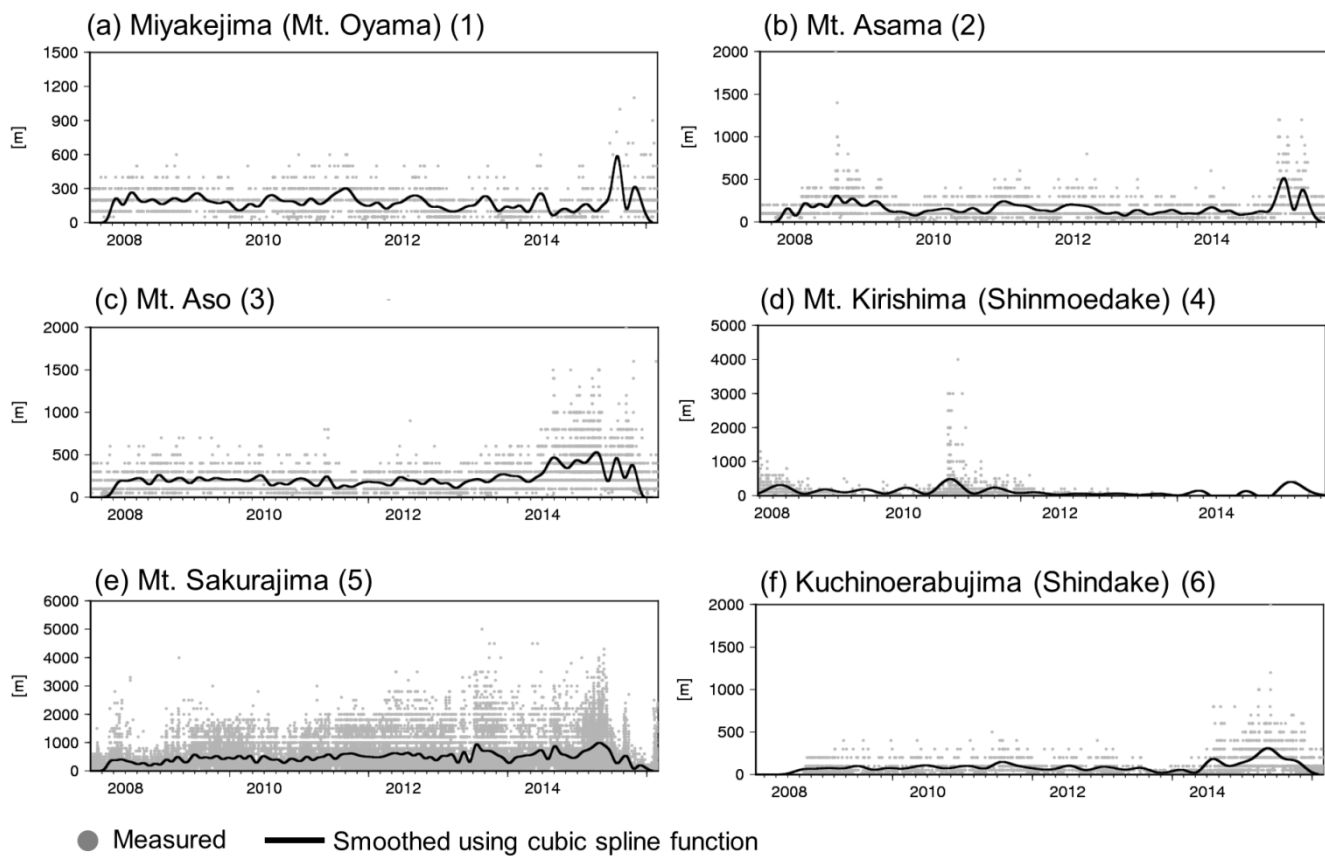
Figure S2-3: The time series of temporally smoothed data (solid line), with the raw data (gray dots) of the observed smoke height measured by the JMA and used in the NHM-Chem model.

Supplement 3

Supplement 3 summarizes comparisons between the simulated and observed variables used for the discussion in Sect. 6, together with the relevant variables, such as O_3 and its precursor gas NO_x, dust extinction coefficient (Ext_D) and PM_{10} ~~during~~ including the dust events of April 2006 (as defined in Sect. 6.2), $PM_{2.5}$, wet deposition amounts of SO_4^{2-}, NO_3^-, and NH_4^+, AOT, SSA, total (dust and spherical) extinction coefficient (Ext_T), $NC_{0.3}$, and PM_{10} during the period when the OPC data were available. Statistical measures for the comparisons are listed in Table 4.

The simulated seasonal mean surface O_3 concentration over China was highest in the summer but that in Japan was highest in the spring due to the long-range transport associated with traveling disturbances (Fig. 3, Fig. S3-1). Figure S3-1 compares the observed and simulated daily O_3 concentrations with the precursor gas NO_x concentrations at the Japanese EANET stations, and the statistical scores are shown in Table 4. The simulated medians agreed well with those observed medians (*Sim:Obs* of O_3 and NO_x are approximately 0.9), although the correlation coefficients were not very large (approximately 0.6 and 0.4 for O_3 and NO_x, respectively). The low correlation coefficients of O_3 were due mainly to the locations of the observation sites: *R* at remote island sites (Rishiri, Sado, Oki, Ogasawara, and Hedo in Fig. 2) was 0.76-0.91, whereas *R* at rural inland sites (Happo and Yusuhara in Fig. 2) was low (0.24-0.49) due to the complex topography that cannot be resolved by the crude resolution of the current simulation. Low correlations of NO_x were obtained mainly because it is difficult to simulate primary short-lived species for the crude resolution models. The unresolvable heterogeneity of emission sources near the sites degraded the model performance of the primary species results more than they did for the secondary species such as O_3.

Figure S3-2 presents the observed and simulated hourly PM_{10} and Ext_D at Oki/Matsue and Hedo in April 2006, when mineral dust transport events were observed. Hedo (CHAAMS) includes EANET and AD-Net, whereas Oki (Matsue) is the only EANET (AD-Net) site. The distance between Oki and Matsue is 50-60 km and there are two model grids between the nearest grids to the sites. The dust events are defined for the period in April 2006, when Ext_D and PM_{10} are greater than 0.1 km^{-1} and 300 µg m^{-3} at the Oki/Matsue stations and 0.06 km^{-1} and 150 µg m^{-3} at the Hedo station. Table 4 compares the observed and simulated Ext_D and PM_{10}_D during the dust events in the month. The *R* values for Ext_D and PM_{10}_D are particularly low, mainly because the values are the comparisons of hourly concentrations during the limited period (totally 69 data). The *R* values for the daily concentrations of Ext_D and PM_{10} at all stations for the whole period are available in Table 4 of Kajino et al. (2019a). The *R* value for Ext_D was still low (0.25) but that for PM_{10} were 0.57-0.58, comparable with other variables such as $PM_{2.5}$ and O_3. There are no data for Ext_D of the 3-category method because sea salt and dust particles are completely internally mixed so that the extinction coefficient of dust particles cannot be isolated from the extinction coefficient of COR, which includes abundant sea salt particles at these near-the-coast sites.
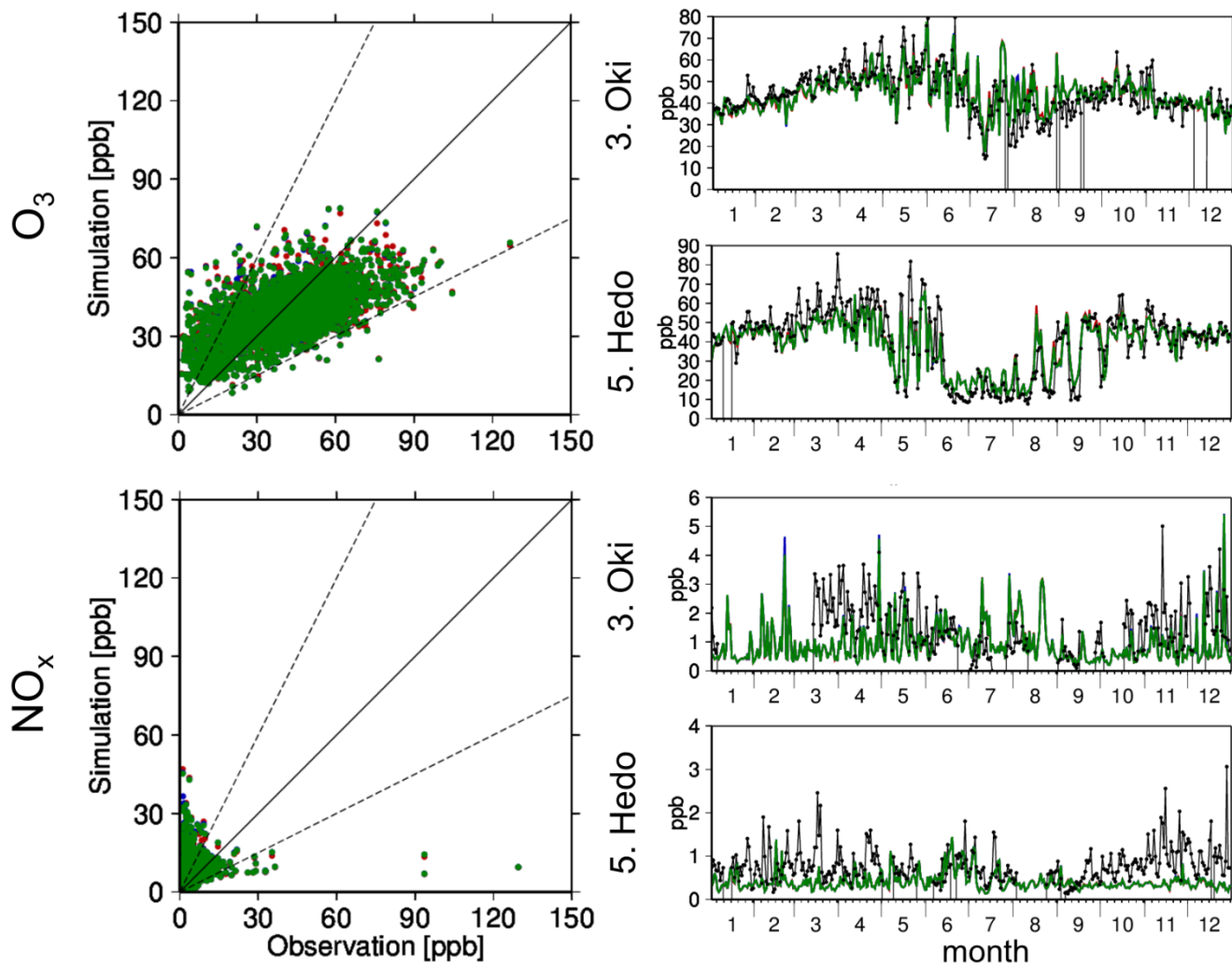
Figure S3-1. (left) Scatter diagrams and (right) time series of the simulated (red: bulk method, blue: 3-category method, green: 5-category method) and observed (black) daily mean surface concentrations of (top) O₃ and (bottom) NOₓ at all Japanese EANET stations for the scatter diagrams and (above) Oki and (below) Hedo for the time series data in 2006.
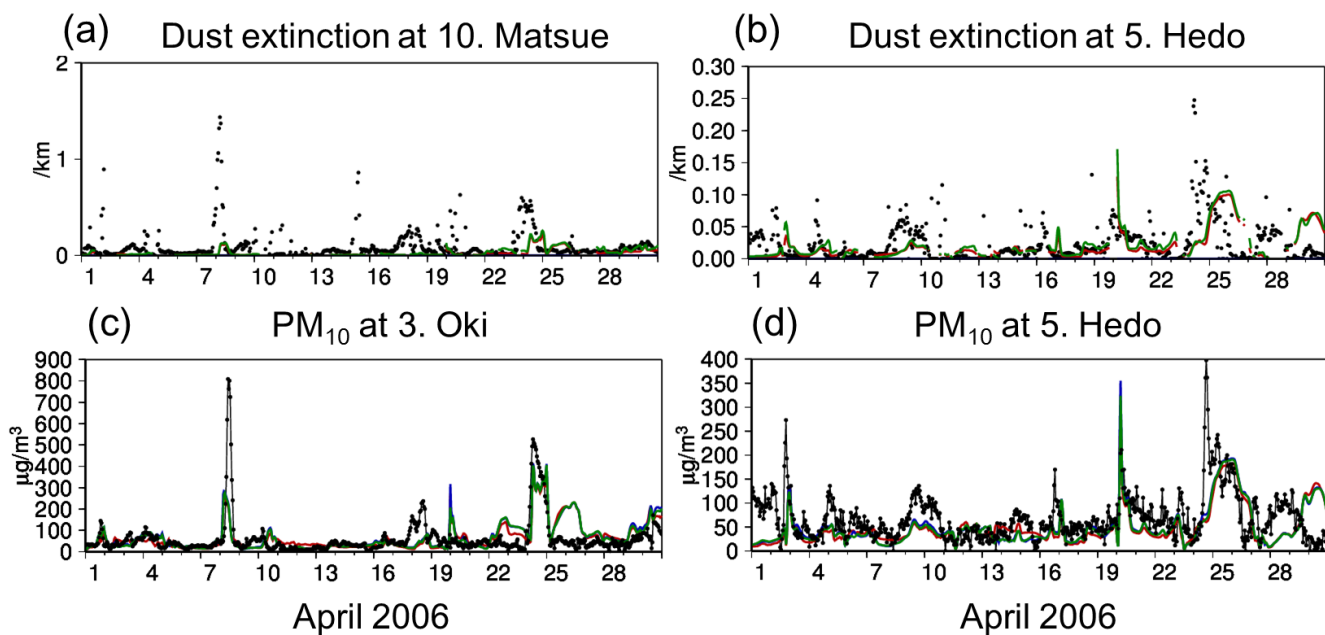
Figure S3-2. Time series of the simulated (red: bulk, blue: 3-category, green: 5-category) and observed (black) daily mean surface (top) dust extinction coefficient at the AD-Net stations and (bottom) PM_{10} at the EANET stations, (left) Matsue and Oki, (right) Hedo in 2006. Note that the observed dust extinction coefficient is the median value below 300 m above ground level (AGL).

The comparison between the simulated and observed $PM_{2.5}$ and $PM_{2.5}$ (pile-up) is shown in Fig. S3-3 and listed in Table 4. The performances of simulated $PM_{2.5}$ were comparable or slightly better than those of $PM_{2.5}$ (pile-up), indicating consistent prediction of the aerosol size distributions. The R values of $PM_{2.5}$ and $PM_{2.5}$ (pile-up) were similar. The *Sim:Obs* of the 3-category $PM_{2.5}$ (1.22) was larger than those of the other two methods due to the complete internal mixing assumption of the sea salt and dust particles in the 3-category method as mentioned in Sect. 6.2. Table 4 shows that the *Sim:Obs* of $PM_{2.5}$ was greater than that of $PM_{2.5}$ (pile-up), indicating that approximately 20% of the sea salt (and 40% of the dust/sea salt mixture) contributed to the $PM_{2.5}$ at Oki and Rishiri. Although they have not yet been discussed, there are still large discrepancies in the simulated and observed $PM_{2.5}$ chemical compositions in Japan. Because the uncertainties in both the simulated chemical compositions and their size distributions contribute to the simulated $PM_{2.5}$, it is not necessary for the 5-category method to yield the best prediction of $PM_{2.5}$. In fact, the R value of $PM_{2.5}$ (0.62) predicted by the bulk method was slightly higher than those of both the $PM_{2.5}$ and $PM_{2.5}$ (pile-up) of the 3- and 5-category methods (0.57-0.58) (Table 4). However, the current analysis is insufficient because the simulated $PM_{2.5}$ was compared with observations obtained at only two stations on remote islands. Currently, evaluation of predicted $PM_{2.5}$ at various locations is ongoing under the framework of a multimodel intercomparison study in Japan called J-STREAM (Chatani et al., 2018).
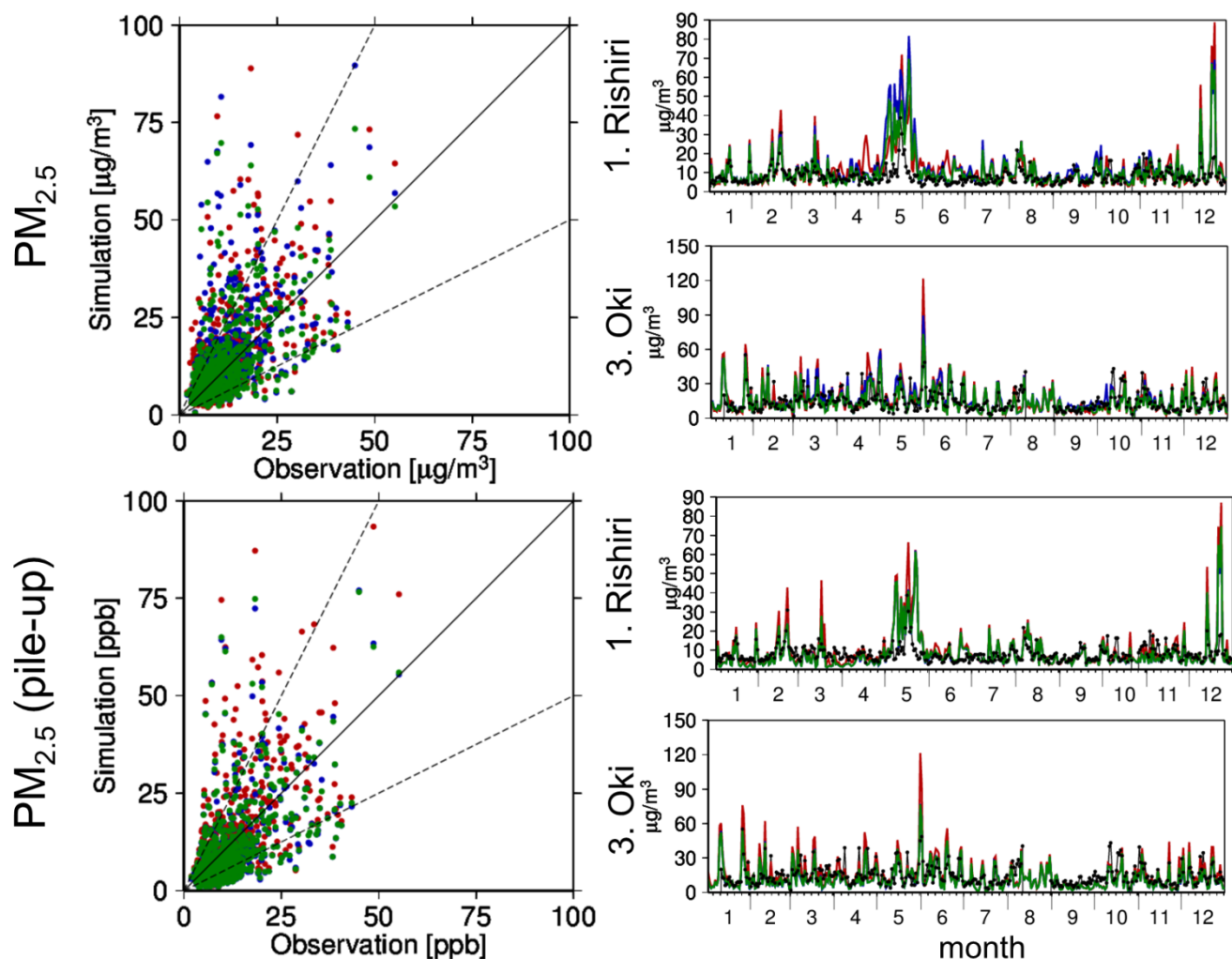
Figure S3-3. (left) Scatter diagrams and (right) time series of the simulated (red: bulk method, blue: 3-category method, green: 5-category method) and observed (black) daily mean surface concentrations of (top) PM$_{2.5}$ and (bottom) PM$_{2.5}$ (pile-up) at the EANET stations, (above) Rishiri and (below) Oki in 2006. The scatter diagrams include Oki and Rishiri data because PM$_{2.5}$ data are available at only these two stations in 2006.

Figure S3-4 shows wet deposition amounts of SO$_4^{2-}$, NO$_3^-$, and NH$_4^+$ and precipitation amounts at Oki and Hedo. As shown in Table 4, the model precipitation predictions by NHM and the wet deposition amounts predicted by Chem are similar: 10-15% underestimation, approximately 0.7 of R, and 0.6 of $Fa2$, except 0.5 of R for wet deposition of nss-SO$_4^{2-}$). A similar feature, underestimation of the wet deposition amounts, is found in Fig. S3-4. Certainly, this is not likely the only reason for the lower R for nss-SO$_4^{2-}$, which could also be due to the effect of short-lived large sea salt particles, as discussed in Kajino et al. (2012b). Because the Japanese EANET stations are located near the coasts (150-700 m from the coastline),

the observed amount of W-Na$^+$ could be substantially affected by the short-lived (traveling distance is approximately 1 km) large sea salt particles ($D > 10$ μm), which is not considered in the model. As a result, the simulated W-Na$^+$ substantially underestimated the observation (*Sim:Obs* = 0.26-0.27). This discrepancy in Na$^+$ slightly lowered the *R* of nss-SO$_4^{2-}$ compared to those of the other chemical components and precipitation (*Sim:Obs* of total (non-sea salt plus sea salt)-SO$_4^{2-}$ = 0.42-0.44). SO$_4^{2-}$ from dimethyl sulfide (DMS), which was not considered in the simulation, could be a reason for the discrepancy, but the contribution may not be large for the region of the simulation (e.g., Kajino et al., 2004).
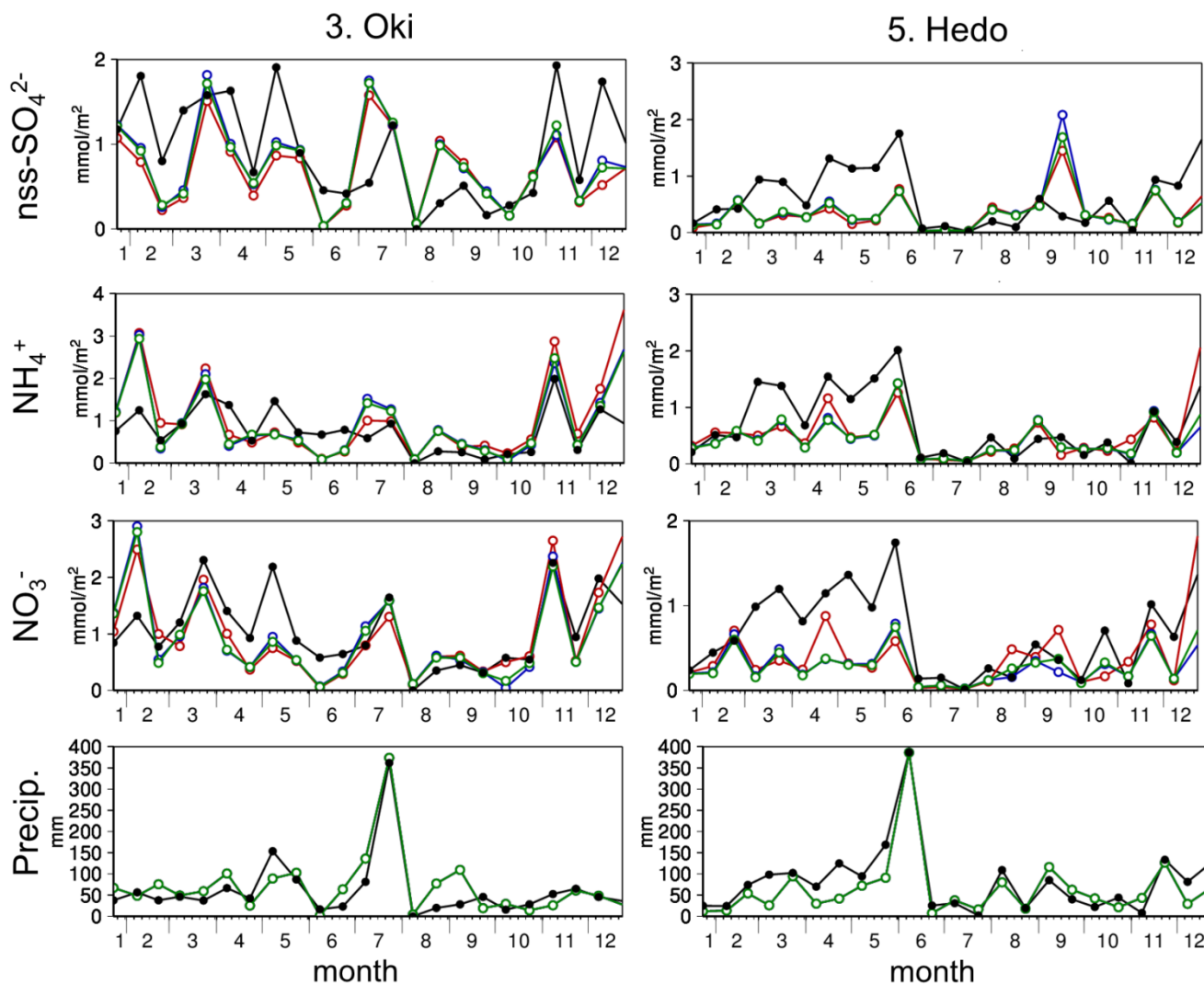
Figure S3-4. The simulated (red: bulk method, blue: 3-category method, green: 5-category method) and observed (black) half-monthly mean (top to bottom) wet deposition amounts of nss-SO$_4^{2-}$, NH$_4^+$, and NO$_3^-$ and precipitation at (left) Oki and (right) Hedo in 2006.
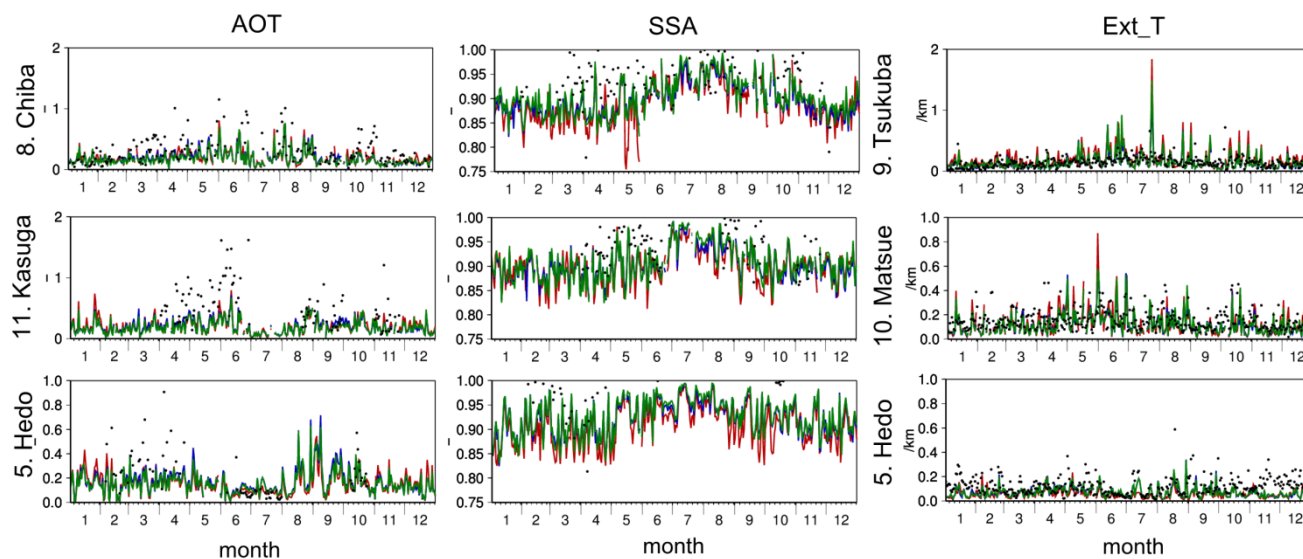
Figure S3-5. The simulated (red: bulk method, blue: 3-category method, green: 5-category method) and observed (black) daily mean (left to right) AOT and SSA of SKYNET and Ext_T of AD-Net at (top) Chiba and Tsukuba, (middle) Kasuga and Matsue, and (bottom) Hedo in 2006. Note that the observed Ext_T is the median value below 300 m AGL, while that simulated is the surface value.

The Fig. S3-5 compares the simulated and observe daily variations of AOT, SSA, and Ext_T and the statistical scores are listed in Table 4. The simulated AOT was underestimated by 50-60% (Table 4). There may be two reasons for this underestimation: the underestimation of upper atmospheric aerosol concentrations or the overestimation of the ratios of mass concentration to extinction coefficient (MEF: the mass/extinction conversion factor, as defined in Sugimoto et al., 2011). Considering that the simulated mass ($PM_{2.5}$, $PM_{2.5}$ (pile-up), and PM_{10}) quantitatively agreed with the observed mass ($PM_{2.5}$) or slightly underestimated the observed mass by 20-30% ($PM_{2.5}$ (pile-up) and PM_{10}) and that the degrees of underestimations of AOT and Ext_T were similar (50-60% and 45-50%, respectively), the underestimation of Ext_T could be due to the overestimation of MEF. The simulated SSA was underestimated by 5-10%, with an observed median of 0.96 (Table 4). Therefore, the values in Fig. 8 (AOT within 1 km) could be underestimated by approximately 50%, whereas the values in Fig. 9 (AAOT within 1 km) could be overestimated by 50-100%. One of the main purposes of the development of the 5-category method was to more realistically simulate the physical and chemical properties of BC-containing particles. The statistical scores of SSA predicted by the 5-category method are better than those predicted by the other two methods, which could support consistent implementation of the 5-category method.
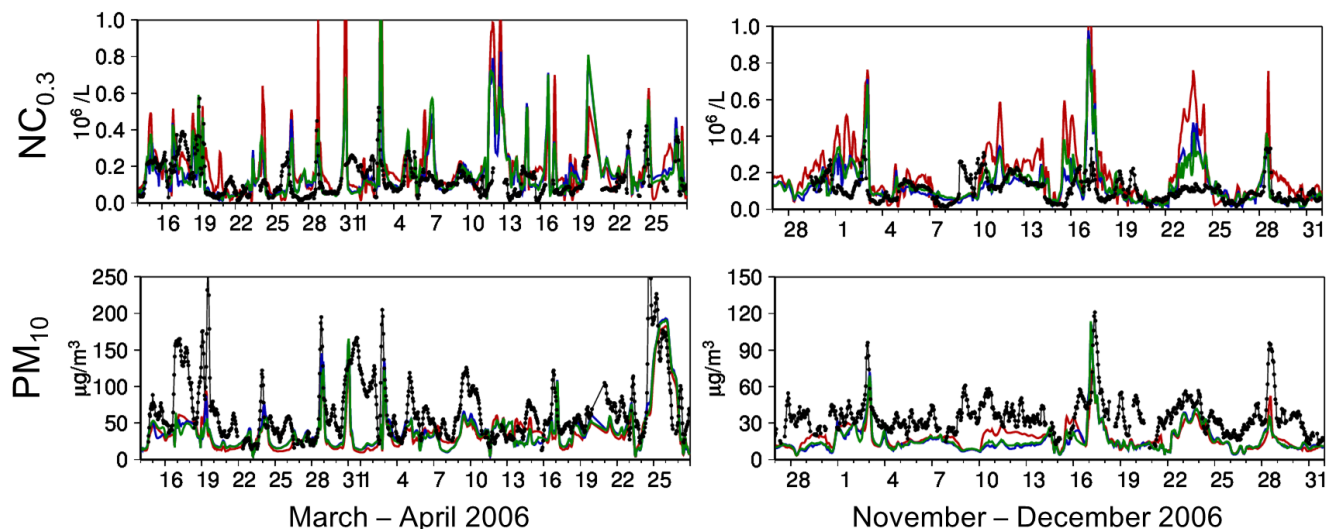
Figure S3-6. The simulated (red: bulk method, blue: 3-category method, green: 5-category method) and observed (black) hourly (top) $NC_{0.3}$ and (bottom) PM_{10} at Hedo, when the OPC data are available, namely, (left) March 14 to 27 and (right) November 27 to December 31 of 2006. A 5-hour running mean is used to draw the lines of the observed PM_{10}, as the raw data fluctuate. Hourly values are used for the statistical comparison in Table 4.

There are no CCN observation data available for the year, but the $NC_{0.3}$ observed by OPC was used alternatively for the model evaluations of simulated CCN. The critical diameter of 0.3 μm corresponds to 0.035-0.041% of the critical supersaturations for κ of 0.3-0.4 (Petters and Kreidenweis, 2007). The OPC data are only available from March to April and November to December 2006 at Hedo. The statistical scores for $NC_{0.3}$ are listed in Table 4. Those of PM_{10} for the same period are also shown in Table 4 to compare the model performance for the prediction of number concentration against that of mass concentrations. The time series data are presented in Fig. S3-6. The simulated $NC_{0.3}$ overestimated the observation by 20-50%, especially for the peak concentrations (Fig. S3-6). The 3-category and 5-category methods successfully avoided the significant overestimations of the peak concentrations predicted by the bulk method, which indicates consistent implementations of aerosol dynamic processes of the 3-category and 5-category methods. PM_{10} at Hedo could be substantially affected by sea salt particles, whereas $NC_{0.3}$ could be controlled by the number of submicron particles. Thus, it is hard to evaluate the number-mass consistency with the available data, but we can safely conclude that the prediction of number concentration was more difficult than that of mass concentration, as the R results of 0.29-0.36 for number concentration was smaller than those for mass concentration (0.52-0.55) (Table 4).

Supplement 4

Supplement 4 shows the seasonal mean surface air concentration of PM$_{2.5}$ (pile-up) predicted by the 5-category, 3-category, and bulk methods. Discussion regarding the figure is made in the main text.
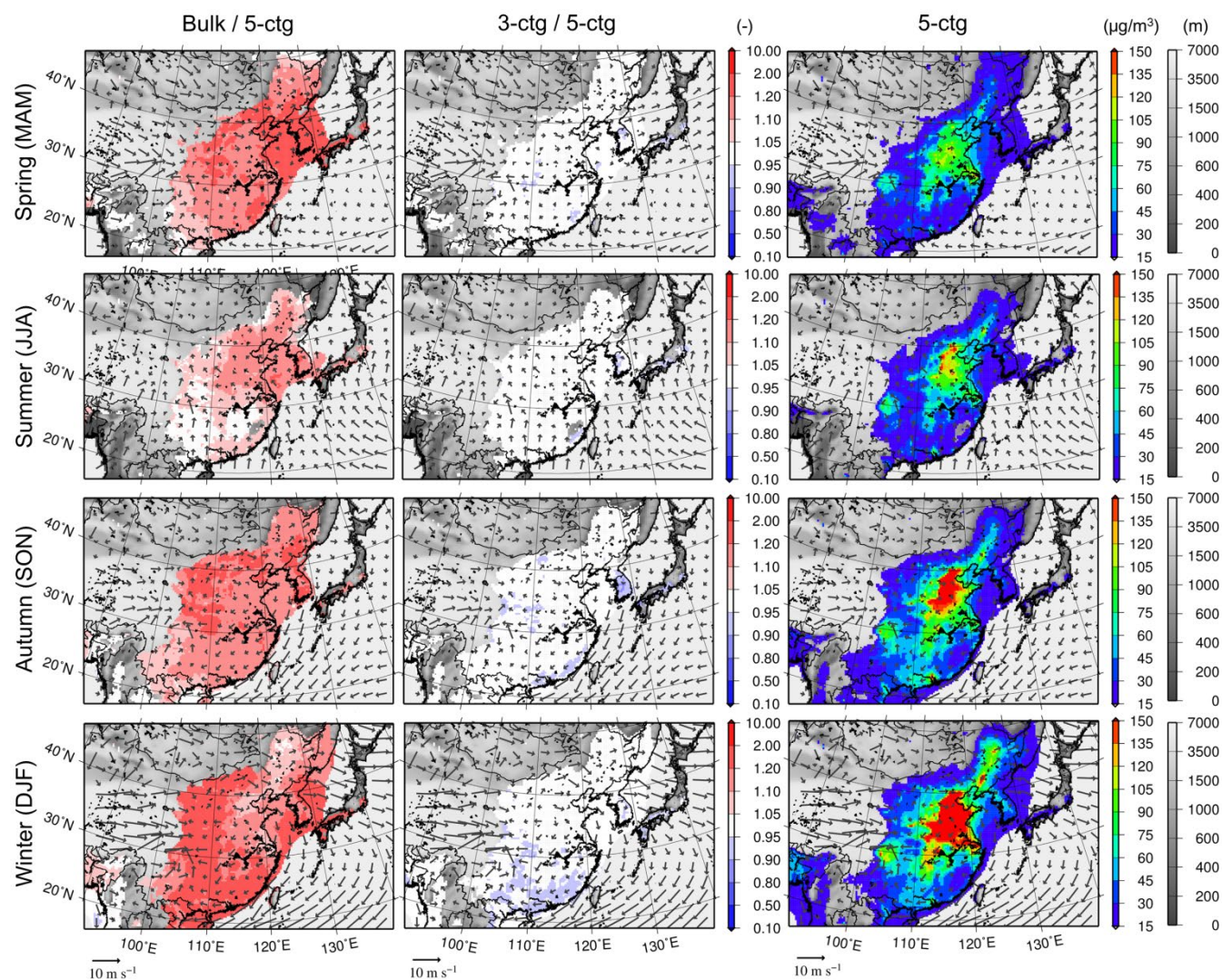
Figure S4-1. Same as Fig. 5 but for PM$_{2.5}$ (pile-up).

Figure S5-1 shows the fog deposition amounts of sum of nss-SO_4^{2-}, T-NH_4^+, and T-NO_3^-, predicted by the 5-category, 3-category, and bulk methods. The fog deposition amounts were generally 1-2 orders of magnitude smaller than those of the dry and wet depositions. The fog deposition amounts of the bulk method are remarkably smaller than those of the other nonequilibrium methods. This is simply because submicron aerosols are smaller in the bulk method because the aerosol microphysical processes are not taken into account. Thus, a major proportion of the submicron aerosols of the bulk method cannot be activated as fog droplets with such low supersaturation conditions for fog formation. The fog occurrence was higher in the colder seasons, and thus, the deposition areas were smallest in the summer, except in Taiwan. In Taiwan, fog deposition was highest in the summer. Larger deposition areas are found over the high topography with highly vegetated regions in the spring, autumn, and winter. The largest deposition areas are observed over the North China Plain in the winter, associated with the increase in the radiation fog frequency and air pollution levels in winter.

Figure S5-1. Seasonal mean fog depositions of sum of nss-SO_4^{2-}, T-NH_4^+, and T-NO_3^- in (top to bottom) spring, summer, autumn, and winter of 2006 for (left to right) the bulk, the 3-category, and the 5-category methods.

References

Abdul-Razzak, H. and Ghan, S. J.: A parameterization of aerosol activation. 2. Multiple aerosol types. J. Geophys. Res., 105, 6837-6844, 2000.

Andres R. J. and Kasgnoc, A. D.: A time-averaged inventory of subaerial volcanic sulfur emissions. J. Geophys. Res., 103(D19), 25,251-25,261, 1998

Andronache, C., Grönholm, T., Laakso, L., Phillips, V., and Venäläinen, A.: Scavenging of ultrafine particles by rainfall at a boreal site: observations and model estimations. Atmos. Chem. Phys., 6, 4739-4754, 2006.

Aranami, K., Hara, T., Ikuta, Y., Kawano, K., Matsubayashi, K., Kusabiraki, H., Ito, T., Egawa, T., Yaashita, K., Ota, Y., Ishikawa, Y. Fujita, T., and Ishida, J.: A new operational regional model for convection-permitting numerical weather prediction at JMA, CAS/JSC WGNE Research Activities in Atmospheric and Oceanic Modelling, 5, 5-6, 2015.

Byun, D., and Schere K.: Review of the governing equations, computational algorithms, and other components of the Models-3 Community Multiscale Air Quality (CMAQ) modeling system. Appl. Mech. Rev., 59, 51-77, 2006.

Carlton, A. G., Turpin, B. J., Altieri, K. E., Seitzinger, S., Reff, A., Lim, H.-J., and Ervens, B.: Atmospheric oxalic acid and SOA production from glyoxal: Results of aqueous photooxidation experiment. Atmos. Environ., 41, 7588-7602, 2007.

Carter, W.: Documentation of the SAPRC-99 chemical mechanism for VOC reactivity assessment. Final report to California Air Resources Board, Rep. 92-329, Univ. of Calif., Riverside, 8 May, 569 pp, 2000.

Chapman, E. G., Gustafson Jr. W. I., Easter, R. C., Barnard, J. C., Ghan, S. J., Pekour, M. S., and Fast, J. D.: Coupling aerosol-cloud-radiative processes in the WRF-Chem model: Investigating the radiative impact of elevated point sources. Atmos. Chem. Phys., 9, 945-964, 2009.

Chatani, S., Yamaji, K., Sakurai, T., Itahashi, S., Shimadera, H., Kitayama, K., and Hayami, H.: Overview of Model Inter-Comparison in Japan's Study for Reference Air Quality Modeling (J-STREAM). Atmosphere, 9(1), 19, 14 pp, 2018.

Chen, L., Gao, Y., Zhang, M., Fu, J. S., Zhu, J., Liao, H., Li, J., Huang, K., Ge, B., Wang, X., Lam, Y. F., Lin, C.-Y., Itahashi, S., Nagashima, T., Kajino, M., Yamaji, K., Wang, Z., and Kurokawa, J.: MICS-Asia III: multi-model comparison and evaluation of aerosol over East Asia, Atmos. Chem. Phys., 19, 11911–11937, https://doi.org/10.5194/acp-19-11911-2019, 2019.

Clarke, A. D., Owens, S. R., and Zhou, J.: An ultrafine sea-salt flux from breaking waves: Implications for cloud condensation nuclei in the remote marine atmosphere. J. Geophys. Res., 111, D06202, 14 pp, 2006.

Deushi, M. and Shibata, K.: Development of an MRI Chemistry-Climate Model ver.2 for the study of tropospheric and stratospheric chemistry. Papers in Meteor. Geophys., 62, 1-46, 2011.

Donahue, N. M., Robinson, A. L., Stanier, C. O., and Pandis, S. N.: Coupled partitioning, dilution, and chemical aging of semivolatile organics. Environ. Sci. Technol., 40, 2635-2643, 2006.

Edney, E. O., Kleindienst, T. E., Lewandowski, M., and Offenberg, J. H.: Updated SOA chemical mechanism for the Community Multiscale Air Quality model. EPA 600/X-07/025, US Environ. Prot. Agency, Durham, NC, 2007.

Fountoukis, C. and Nenes, A.: ISORROPIA II: a computationally efficient thermodynamic equilibrium model for K^+-Ca^{2+}-Mg^{2+}-NH_4^+-Na^+-SO_4^{2-}-NO_3^--Cl^--H_2O aerosols. Atmos. Chem. Phys., 7, 4639-4659, 2007.

Fukui, T., Kokuryo, K., Baba, T., and Kannari, A.: Updating EAGrid2000-Japan emissions inventory based on the recent emission trends. J. Jpn. Soc. Atmos. Environ., 49(2), 117-125, 2014 (in Japanese).

Ge, B., Itahashi, S., Sato, K., Xu, D., Wang, J., Fan, F., Tan, Q., Fu, J. S., Wang, X., Yamaji, K., Nagashima, T., Li, J., Kajino, M., Liao, H., Zhang, M., Wang, Z., Li, M., Woo, J.-H., Kurokawa, J., Pan, Y., Wu, Q., Liu, X., and Wang, Z.: MICS-Asia III: Multi-model comparison of reactive Nitrogen deposition over China, Atmos. Chem. Phys. Discuss., https://doi.org/10.5194/acp-2019-1083, in review, 2020.

Giglio, L., Randerson, J. T., van der Werf, G. R., Kasibhatla, P. S., Collatz, G. J., Morton, D. C., and DeFries, R. S.: Assessing variability and long-term trends in burned area by merging multiple satellite fire products. Biogeosciences, 7, 1171-1186, 2010.

Grell, G. A., Peckham, S. E., Schmitz, R., McKeen, S. A., Frost, G., Skamarock, W. C., and Eder, B.: Fully coupled "online" chemistry within the WRF model. Atmos. Environ., 39, 6957-6975, 2005.

Guenther, A., Karl, T., Harley, P., Wiedinmyer, C., Palmer, P. I., and Geron, C.: Estimates of global terrestrial isoprene emissions using MEGAN (Model of Emissions of Gases and Aerosols from Nature). Atmos. Chem. Phys., 6, 3181-3210, 2006.

Han, Z., Ueda, H., Matsuda, K., Zhang, R.., Arao, K., Kanai, Y., and Hasome, H.: Model study on particle size segregation and deposition during Asian dust events in March 2002. J. Geophys. Res., 109, D19205, 22 pp, 2004.

Ishikawa, H.: Mass-consistent wind model as a meteorological preprocessor for tracer transport models. J. Appl. Meteorol., 33, 733-743, 1994.

Itahashi, S., Ge, B., Sato, K., Fu, J. S., Wang, X., Yamaji, K., Nagashima, T., Li, J., Kajino, M., Liao, H., Zhang, M., Wang, Z., Li, M., Kurokawa, J., Carmichael, G. R., and Wang, Z.: MICS-Asia III: overview of model intercomparison and evaluation of acid deposition over Asia, Atmos. Chem. Phys., 20, 2667–2693, https://doi.org/10.5194/acp-20-2667-2020, 2020.

Jacob, D. J.: Heterogeneous chemistry and tropospheric ozone. Atmos. Environ., 34, 2131-2159, 2000.

JMA: The next generation non-hydrostatic model ASUCA. Suuchi Yohoka Hokoku Bessatsu (Additonal Volume to Report of Numerical Prediction Division) 60, 151 pp., 2014 (in Japanese)

Kajino, M., Ueda, H., Satsumabayashi, H., and An, J.: Impacts of the eruption of Miyakejima Volcano on air quality over far east Asia. J. Geophys. Res., 109, D21204, 11 pp, 2004.

Kajino, M.: MADMS: Modal Aerosol Dynamics model for multiple Modes and fractal Shapes in the free-molecular and near-continuum regimes. J. Aerosol Sci., 42, 224-248, 2011.

Kajino, M. and Kondo, Y.: EMTACS: Development and regional-scale simulation of a size, chemical, mixing type, and soot shape resolved atmospheric particle model. J. Geophys. Res., 116, D02303, 28 pp, 2011.

Kajino, M., Inomata, Y., Sato, K., Ueda, H., Han, Z., An, J., Katata, G., Deushi, M., Maki, T., Oshima, N., Kurokawa, J., Ohara, T., Takami, A., and Hatakeyama, S.: Development of the RAQM2 aerosol chemical transport model and predictions of the Northeast Asian aerosol mass, size, chemistry, and mixing type. Atmos. Chem. Phys., 12, 11833-11856, 2012a.

Kajino, M., Deushi, M., Maki, T., Oshima, N., Inomata, Y., Sato, K., Ohizumi, T., and Ueda, H.: Modeling wet deposition and concentration of inorganics over Northeast Asia with MRI-PM/c. Geosci. Model Dev., 5, 1363-1375, 2012b.

Kajino, M., Deushi, M., Sekiyama, T. T., Oshima, N., Yumimoto, K., Tanaka, T. Y., Ching, J., Hashimoto, A., Yamamoto, T., Ikegami, M., Kamada, A., Miyashita, M., Inomata Y., Shima S., Adachi, K., Zaizen, Y., Igarashi, Y., Ueda, H., Maki, T., and Mikami, M.: NHM-Chem , the Japan Meteorological Agency's regional meteorology-chemistry model (v1.0): model description and aerosol representations, Geosci. Model Dev. Discuss., https://doi.org/10.5194/gmd-2018-128, 2018.

Kajino, M., Sekiyama, T. T., Igarashi, Y., Katata, G., Sawada, M., Adachi, K., Zaizen, Y., Tsuruta, H., Nakajima, T.: Deposition and dispersion of radio-cesium released due to the Fukushima nuclear accident: Sensitivity to meteorological models and physical modules, J. Geophys. Res., 124, 1823-1845, doi:10.1029/2018JD028998, 2019.

Kannari, A., Tonooka, Y., Baba, T., and Murano, K.: Development of multiple-species 1 km × 1 km resolution hourly basis emissions inventory for Japan. Atmos. Environ., 41, 3428-3439, 2007.

Katata, G., Nagai, H., Wrzesinsky, T., Klemm, O., Eugster, W., and Burkard, R.: Development of a land surface model including cloud water deposition on vegetation. J. Appl. Meteo. Clim., 47, 2129-2146, 2008.

Katata, G., Nagai, H., Zhang, L., Held, A., Serça, D., and Klemm, O.: Development of an atmosphere-soil-vegetation model for investigation of radioactive materials transport in the terrestrial biosphere. P. Nucl. Sci. Technol., 2, 530-537, 2011a.

Katata, G., Kajino, M., Hiraki, T., Aikawa, M., Kobayashi, T., and Nagai, H.: A method for simple and accurate estimation of fog deposition in a mountain forest using a meteorological model. J. Geophys. Res., 116, D20102, 2011b.

Katata, G., Chino, M., Kobayashi, T., Terada, H., Ota, M., Nagai, H., Kajino, M., Draxler, R., Hort, M. C., Malo, A., Torii, T., and Sanada. Y.: Detailed source term estimation of the atmospheric release for the Fukushima Daiichi Nuclear Power Station accident by coupling simulations of an atmospheric dispersion model with an improved deposition scheme and oceanic dispersion model. Atmos. Chem. Phys., 15, 1029-1070, 2015.

Kong, L., Tang, X., Zhu, J., Wang, Z., Fu, J. S., Wang, X., Itahashi, S., Yamaji, K., Nagashima, T., Lee, H.-J., Kim, C.-H., Lin, C.-Y., Chen, L., Zhang, M., Tao, Z., Li, J., Kajino, M., Liao, H., Wang, Z., Sudo, K., Wang, Y., Pan, Y., Tang, G., Li, M., Wu, Q., Ge, B., and Carmichael, G. R.: Evaluation and uncertainty investigation of the NO2, CO and NH3 modeling over China under the framework of MICS-Asia III, Atmos. Chem. Phys., 20, 181–202, https://doi.org/10.5194/acp-20-181-2020, 2020.

Kuang, C., McMurry, P. H., McCormick, A. V., and Eisele, F. L.: Dependence of nucleation rates on sulfuric acid vapor concentration in diverse atmospheric locations. J. Geophys. Res., 113, D10209, 9 pp, 2008.

Kunii, M.: Mesoscale data assimilation for a local severe rainfall event with the NHM-LETKF system. Wea. Forecasting, 29, 1093-1105, 2014.

Kurokawa, J., Ohara, T, Morikawa, T., Hanayama, S., Janssens-Maenhout, G., Fukui, T., Kawashima, K., and Akimoto, H.: Emissions of air pollutants and greenhouse gases over Asian regions during 2000-2008: Regional Emission inventory in ASia (REAS) version 2. Atmos. Chem. Phys., 13, 11019-11058, 2013.

Li, J., Nagashima, T., Kong, L., Ge, B., Yamaji, K., Fu, J. S., Wang, X., Fan, Q., Itahashi, S., Lee, H.-J., Kim, C.-H., Lin, C.-Y., Zhang, M., Tao, Z., Kajino, M., Liao, H., Li, M., Woo, J.-H., Kurokawa, J., Wu, Q., Akimoto, H., Carmichael, G. R., and Wang, Z.: Model evaluation and inter-comparison of surface-level ozone and relevant species in East Asia in the context of MICS-Asia phase III Part I: overview.. Atmos. Chem. Phys., 19, 12993-13015, doi:10.5194/acp-19-12993-2019, 2019.

Lin, Y.-L., Farley, R. D., and Orville, H. D.: Bulk parameterization of the snow field in a cloud model. J. Appl. Meteo. Clim., 22, 1065-1092, 1983.

Lohmann, U. and Diehl, K.: Sensitivity studies of the importance of dust ice nuclei for the indirect aerosol effect on stratiform mixedphase clouds. J. Atmos. Sci., 63, 968-982, 2006.

Madronich, S.: Photodissociation in the atmosphere: 1. Actinic flux and the effects of ground reflections and clouds. J. Geophys. Res., 92, 9740-9752, 1987.

Murakami, M., Magono, C., and Kikuchi, K.: Experiments on aerosol scavenging by natural snow crystals, Part III: The effect of snow crystal charge on collection efficiency. J. Meteorol. Soc. Jpn., 63, 1127-1137, 1985.

Nishizawa, S., Yashiro, H., Sato, Y., Miyamoto, Y., and Tomita, H.: Influence of grid aspect ratio on planetary boundary layer turbulence in large-eddy simulations, Geosci. Model Dev., 8, 3393-3419, doi:10.5194/gmd-8-3393-2015, 2015.

Oshima, N., Koike, M., Zhang, Y., Kondo, Y., Moteki, N., Takegawa, N., and Miyazaki, Y.: Aging of black carbon in outflow from anthropogenic sources using a mixing state resolved model: Model development and evaluation. J. Geophys. Res., 114, D06210, 2009a.

Petters, M. D. and Kreidenweis, S. M.: A single parameter representation of hygroscopic growth and cloud condensation nucleus activity. Atmos. Chem. Phys., 7, 1961-1971, 2007.

Pleim, J. E. and Chang, J. S.: A non-local closure model for vertical mixing in the convective boundary layer. Atmos. Environ., 26A, 965-981, 1992.

Saito, K., Fujita, T., Yamada, Y., Ishida, J., Kumagai, Y., Aranami, K., Ohmori, S., Nagasawa, R., Kumagai, S., Muroi, C., Kato, T., Eito, H., and Yamazaki, Y.: The operational JMA nonhydrostatic mesoscale model. Mon. Wea. Rev., 134, 1266-1298, 2006.

Saito, K., Ishida, J., Aranami, K., Hara, T., Segawa, T., Narita, M., and Honda, Y.: Nonhydrostatic atmospheric models operational development at JMA. J. Meteor. Soc. Japan, 85B, 271-304, 2007.

Saito, K.: Chapter 5. The JMA nonhydrostatic model and its application to operation and research. *Atmospheric Model Applications*, Ed. Ismail Yucel, InTech Open Access Publisher, 85-110, 2012.

Sato, Y., Nishizawa, S., Yashiro, H., Miyamoto, Y., Kajikawa, Y., and Tomita, H.: Impacts of cloud microphysics on trade wind cumulus: which cloud microphysics processes contribute to the diversity in a large eddy simulation?, Prog. Earth Planet. Sci., 2, 23, doi:10.1186/s40645-015-0053-6, 2015.

Sekiyama, T. T., Kunii, M., Kajino, M., and Shimbori, T.: Horizontal resolution dependence of atmospheric simulations of the Fukushima nuclear accident using 15-km, 3-km, and 500-m Grid Models. J. Meteor. Soc. Japan, 93, 49-64, 2015.

Skamarock, W. C., Klemp, J. B., Dudhia, J., Gill, D. O., Barker, D. M., Duda, M. G., Huang, X. Y., Wang, W., and Powers, J. G.: A description of the advanced research WRF version 3. Tech. Note, NCAR/TN~475+STR, 125 pp., Natl. Cent. for Atmos. Res., Boulder, Colo, 2008.

Slinn, W. G. N.: Precipitation scavenging, in: Atmospheric Science and Power Production. Chap. 11, edited by: Randerson, D., No. DOE/TIC-27601, US Department of Energy, Washington, DC, 466-532, 1984.

Sugimoto, N., Hara, Y., Shimizu, A., Yumimoto, K., Uno, I., and Nishikawa, M. Comparison of surface observations and a regional dust transport model assimilated with lidar network data in Asian dust event of March 29 to April 2, 2007. *SOLA*, 7A, 13-16, 2011.

Wong, D. C, Pleim, J., Mathur, R., Binkowski, F., Otte, T., Gilliam, R., Pouliot, G., Xiu, A., Young, J. O., and Kang, D.: WRF-CMAQ two-way coupled system with aerosol feedback: software development and preliminary results. Geosci. Model Dev., 5, 299-312, 2012.

Woo, J.-H., Streets, D. G., Carmichael, G. R., Tang, Y., Yoo, B., Lee, W.-C., Thongboonchoo, N., Pinnock, S., Kurata, G., Uno, I., Fu, Q., Vay, S., Sachse, G. W., Clake, D. R., Fried, A., and Thornton, D. C.: Contribution of biomass and biofuel emissions to trace gas distributions in Asia during the TRACE-P experiment. J. Geophys. Res., 108(D21), 8812, 2003.

Yumimoto, K. Tanaka, T. Y., Oshima, N., and Maki, T.: JRAero: the Japanese Reanalysis for Aerosol v1.0. Geosci. Model Dev., 10, 3225-3253, 2017.

Yumimoto, K., Kajino, M., Tanaka, T. Y., and Uno, I.: Dust vortex in the Taklimakan desert by Himawari-8 high frequency and resolution observation, Sci. Rep., 9:1209, 7 pp., doi:10.1038/s41598-018-37861-4, 2019.

Zaveri, R. A., Barnard, J. C., Easter, R. C., Riemer, N., and West, M.: Particle-resolved simulation of aerosol size, composition, mixing state, and the associated optical and cloud condensation nuclei activation properties in an evolving urban plume. J. Geophys. Res., 115, D17210, 2010.

Zhang, D., and Iwasaka, Y.: Size change of Asian dust particles caused by sea salt interaction: Measurements in southwestern Japan. Geophys. Res. Lett., 31, L15102, 4 pp, 2004.

Zhang, K., O'Donnell, D., Kazil, J., Stier, P., Kinne, S., Lohmann, U., Ferrachat, S., Croft, B., Quaas, J., Wan, H., Rast, S., and Feichter, J.: The global aerosol-climate model ECHAM-HAM, version 2: sensitivity to improvements in process representations, Atmos. Chem Phys. 12, 8911-8949, 2012.

Zhang, L., Gong, S., Padro, J., and Barrie, L.: A size-segregated particle dry deposition scheme for an atmospheric aerosol module. Atmos. Environ., 35, 549-560, 2001.

Zhang, L., Brook, J. R., and Vet, R.: A revised parameterization for gaseous dry deposition in air-quality models. Atmos. Chem. Phys., 3, 2067-2082, 2003.

Zhang, L., Wang, X., Moran, M. D., and Feng, J.: Review and uncertainty assessment of size-resolved scavenging coefficient formulations for below-cloud snow scavenging of atmospheric aerosols. Atmos. Chem. Phys., 13, 10005-10025, 2013.

Zhang, Y., Pan, B., Vijayaraghavan, K., Wu, S.-Y., Seigneur, C., Pandis, S. N., Jacobson, M. Z., Nenes, A., and Seinfeld, J. H.: Development and application of the Model of Aerosol Dynamics, Reaction, Ionization, and Dissolution (MADRID). J. Geophys. Res., 109, D01202, 2004.

Zhang, Y., Pan, Y., Wang, K., Fast, J. D., and Grell, G. A.: WRF/Chem-MADRID: Incorporation of an aerosol module into WRF/Chem and its initial application to the TexAQS20000 episode. J. Geophys. Res., 115, D18202, 2010.